Motion Compensation and Other Advanced CT Techniques

Marc Kachelrieß

German Cancer Research Center (DKFZ)
Heidelberg, Germany
www.dkfz.de/ct

DEUTSCHES
KREBSFORSCHUNGSZENTRUM
IN DER HELMHOLTZ-GEMEINSCHAFT

Contents

- Motion compensation
- Photon counting CT
- Deep learning

Motion Compensation

for CT Systems Rotating Slow Compared to the Organ Motion Frequency

Motion Management for CBCT in IGRT

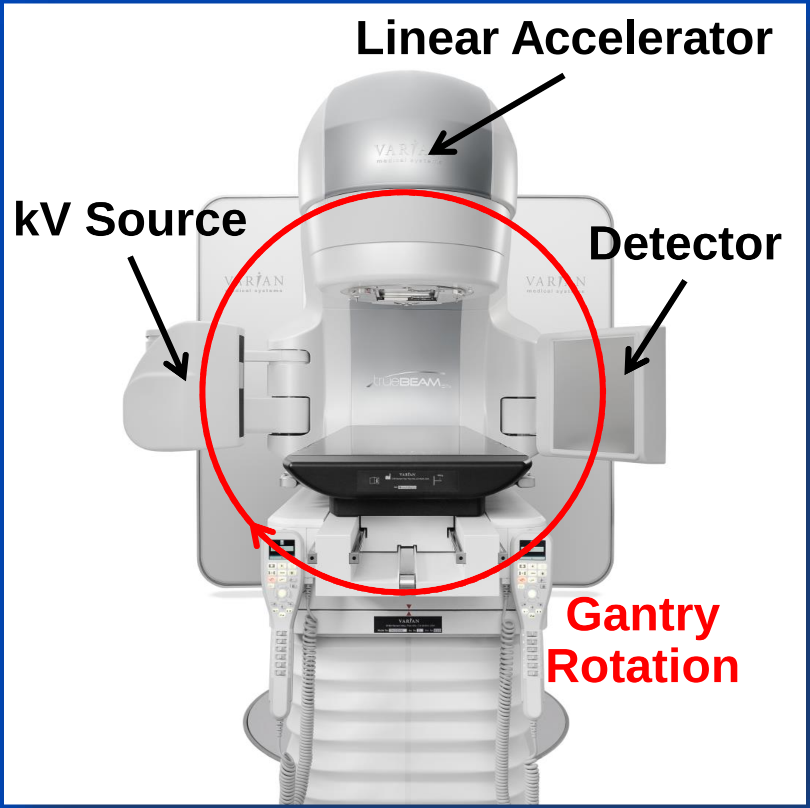

4D CBCT Scan
with Retrospective Gating

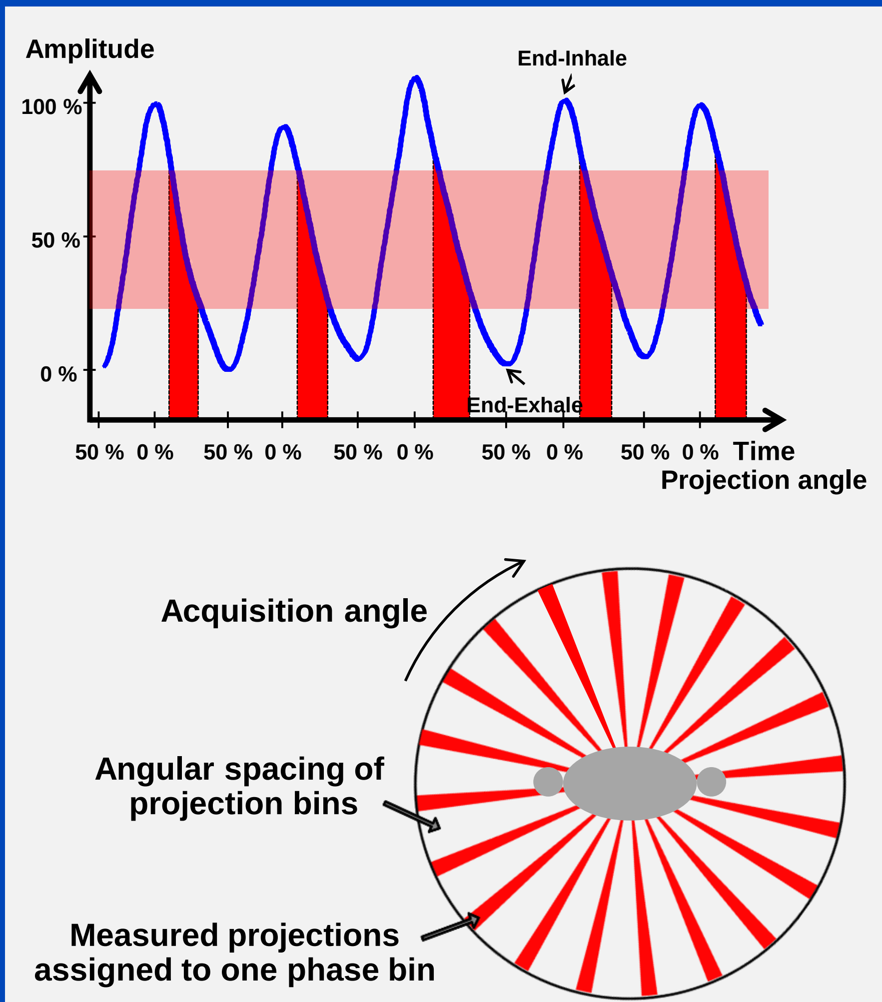

Without gating (3D): Motion artifacts

With gating (4D): Sparse-view artifacts

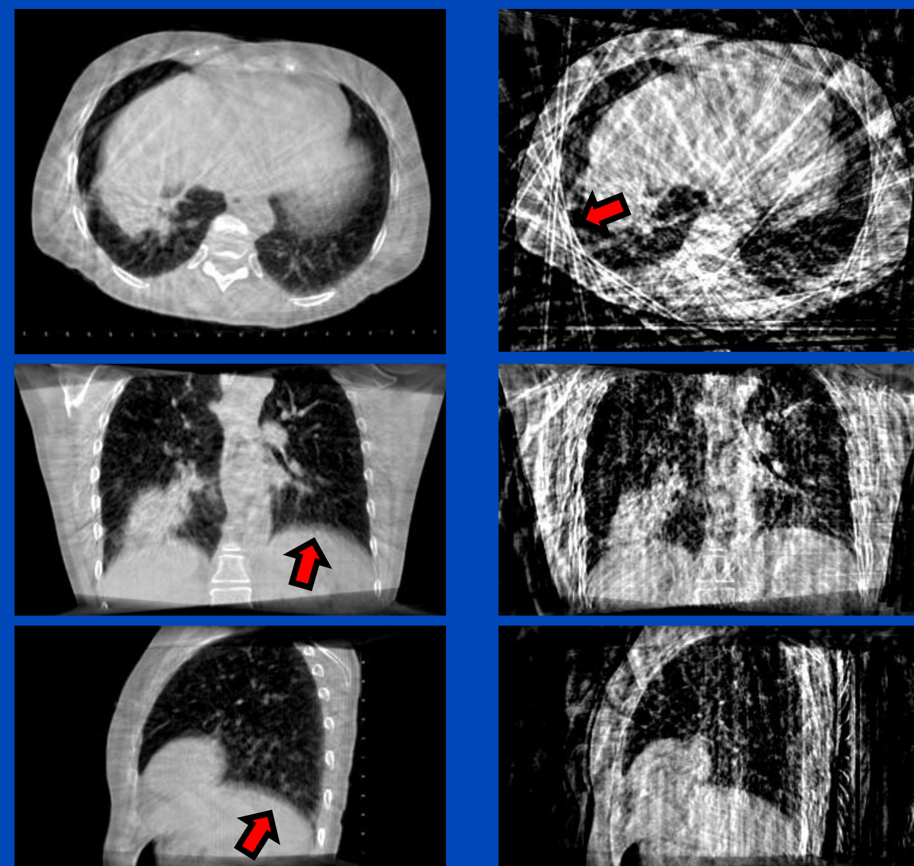

A Standard Motion Estimation and Compensation Approach (sMoCo)

- Motion estimation via standard 3D-3D registration

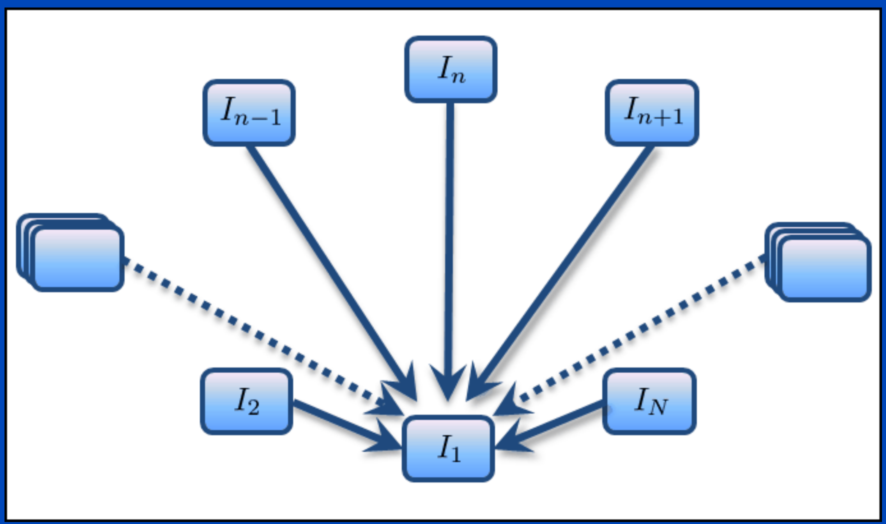

- Has to be repeated for each reconstructed phase

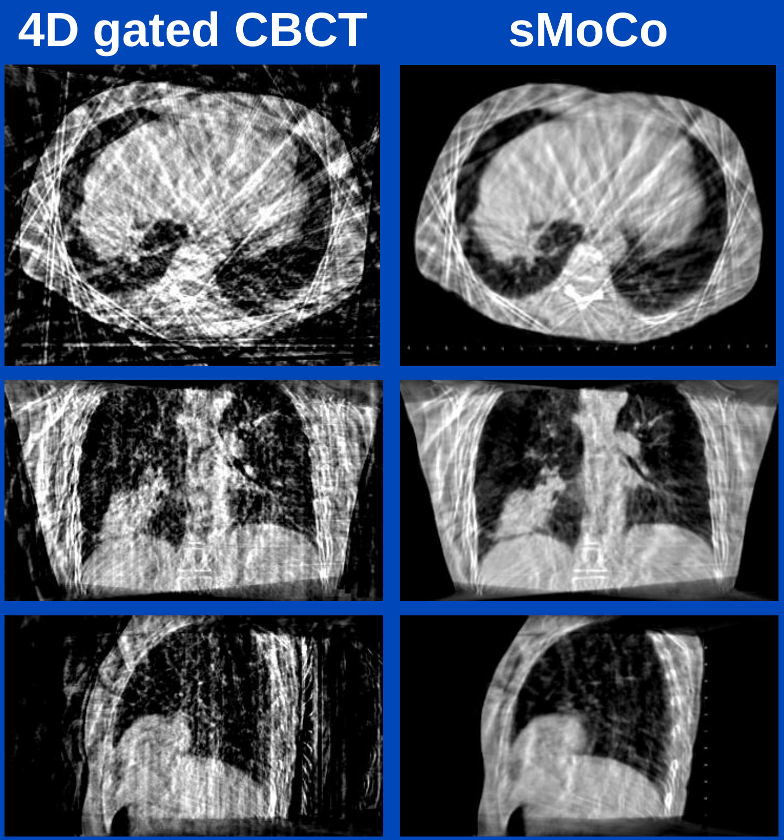

- Streak artifacts from gated reconstructions propagate into sMoCo results

Li, Koong, and Xing, “Enhanced 4D cone–beam CT with inter–phase motion model,” Med. Phys. 51(9), 3688–3695 (2007).

The Cyclic Motion Estimation and Compensation Approach (cMoCo)

- Motion estimation only between adjacent phases
- Incorporate additional knowledge
  - A priori knowledge of quasi periodic breathing pattern
  - Non-cyclic motion is penalized
  - Error propagation due to concatenation is reduced

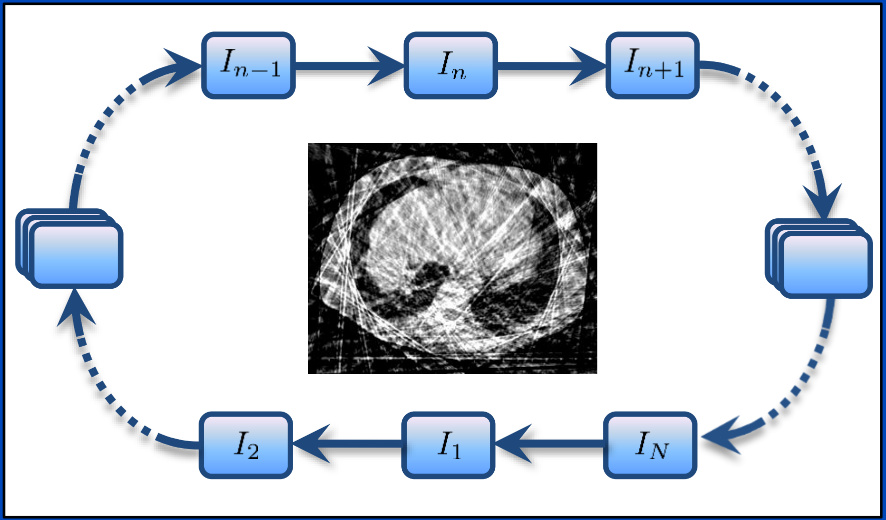

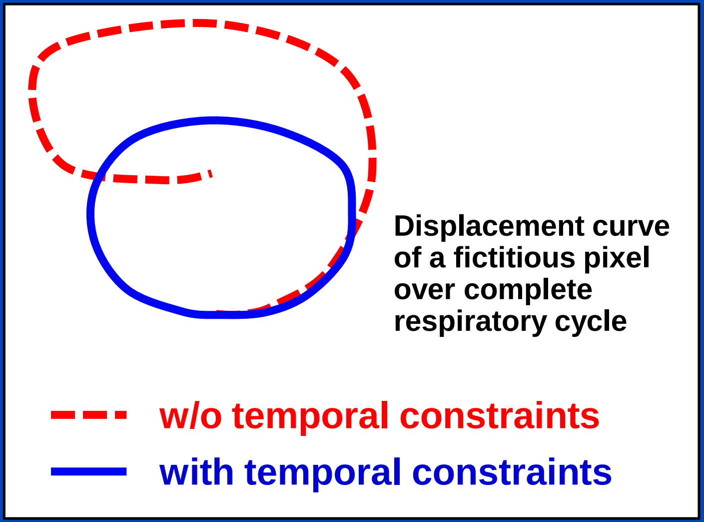

Brehm, Paysan, Oelhafen, Kunz, and Kachelrieß, “Self-adapting cyclic registration for motion-compensated cone-beam CT in image-guided radiation therapy,” Med. Phys. 39(12):7603-7618, 2012.

Artifact Model-Based MoCo (aMoCo)

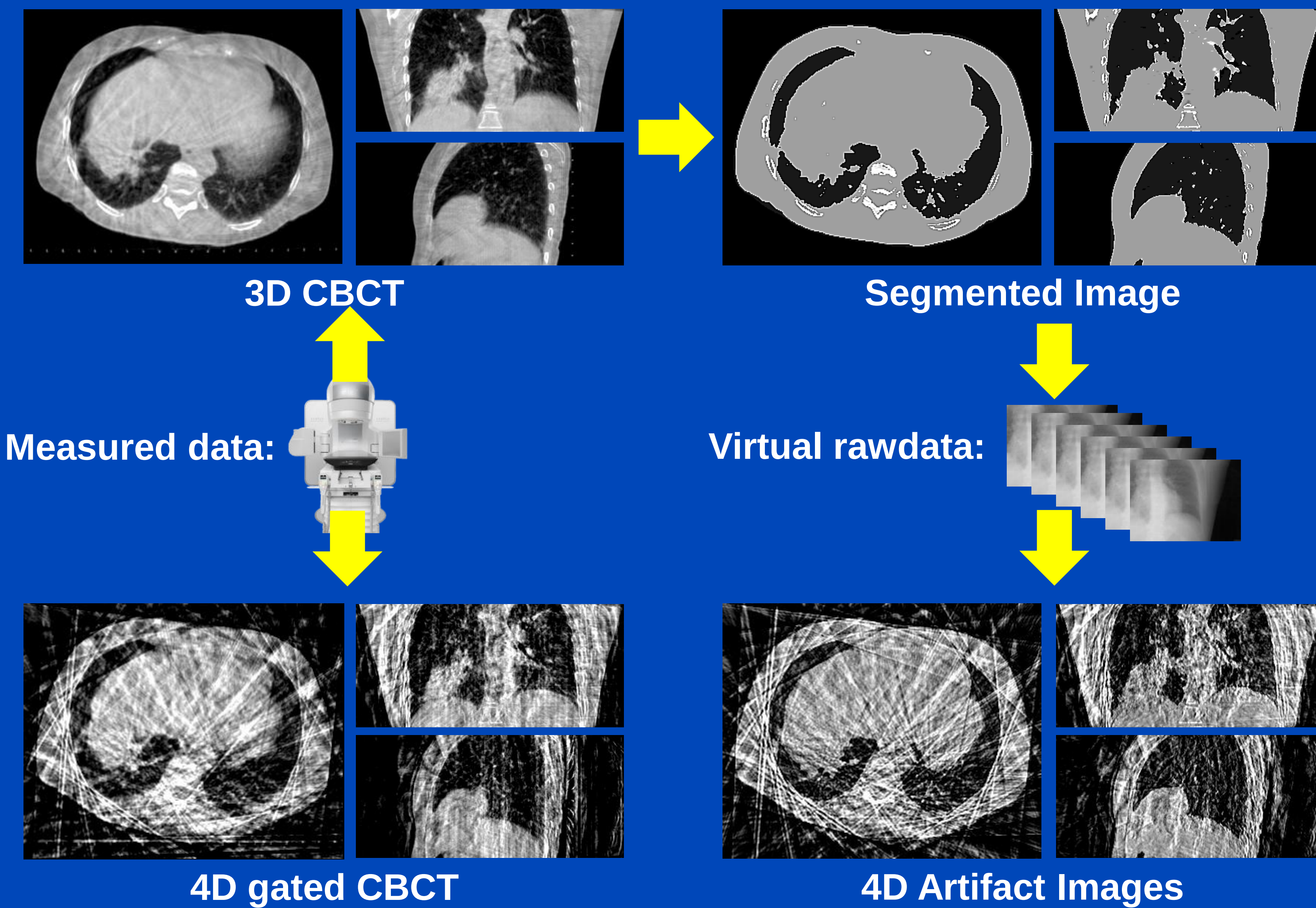

varian

Brehm, Paysan, Oelhafen, and Kachelrieß, “Artifact-resistant motion estimation with a patient-specific artifact model for motion-compensated cone-beam CT” Med. Phys. 40(10):101913, 2013.

dkfz.

Motion Estimation using a Patient-Specific Artifact Model

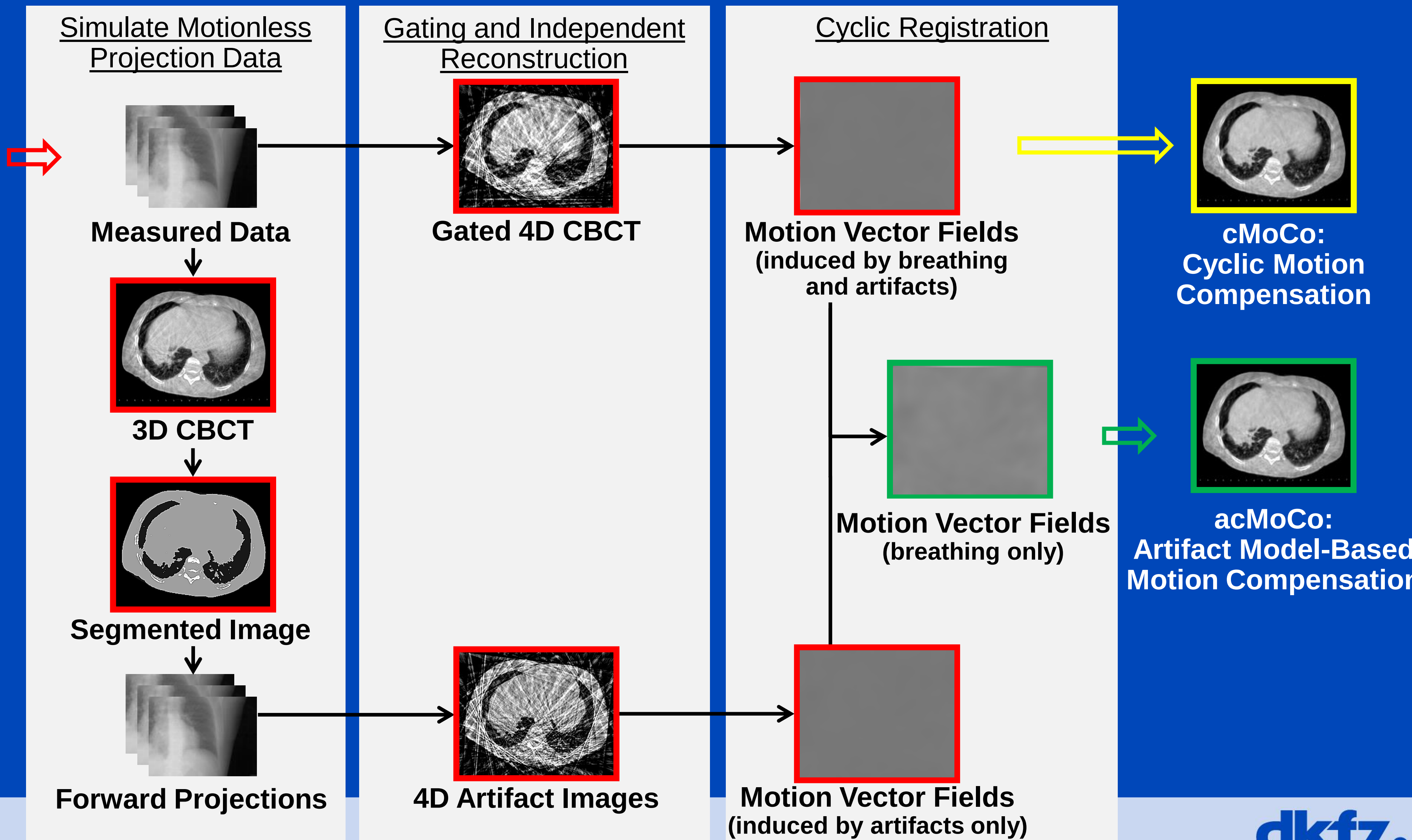

dkfz.

Patient Data – Results

3D CBCT Standard	4D gated CBCT Conventional Phase-Correlated	sMoCo Standard Motion Compensation	acMoCo Artifact Model-Based Motion Compensation

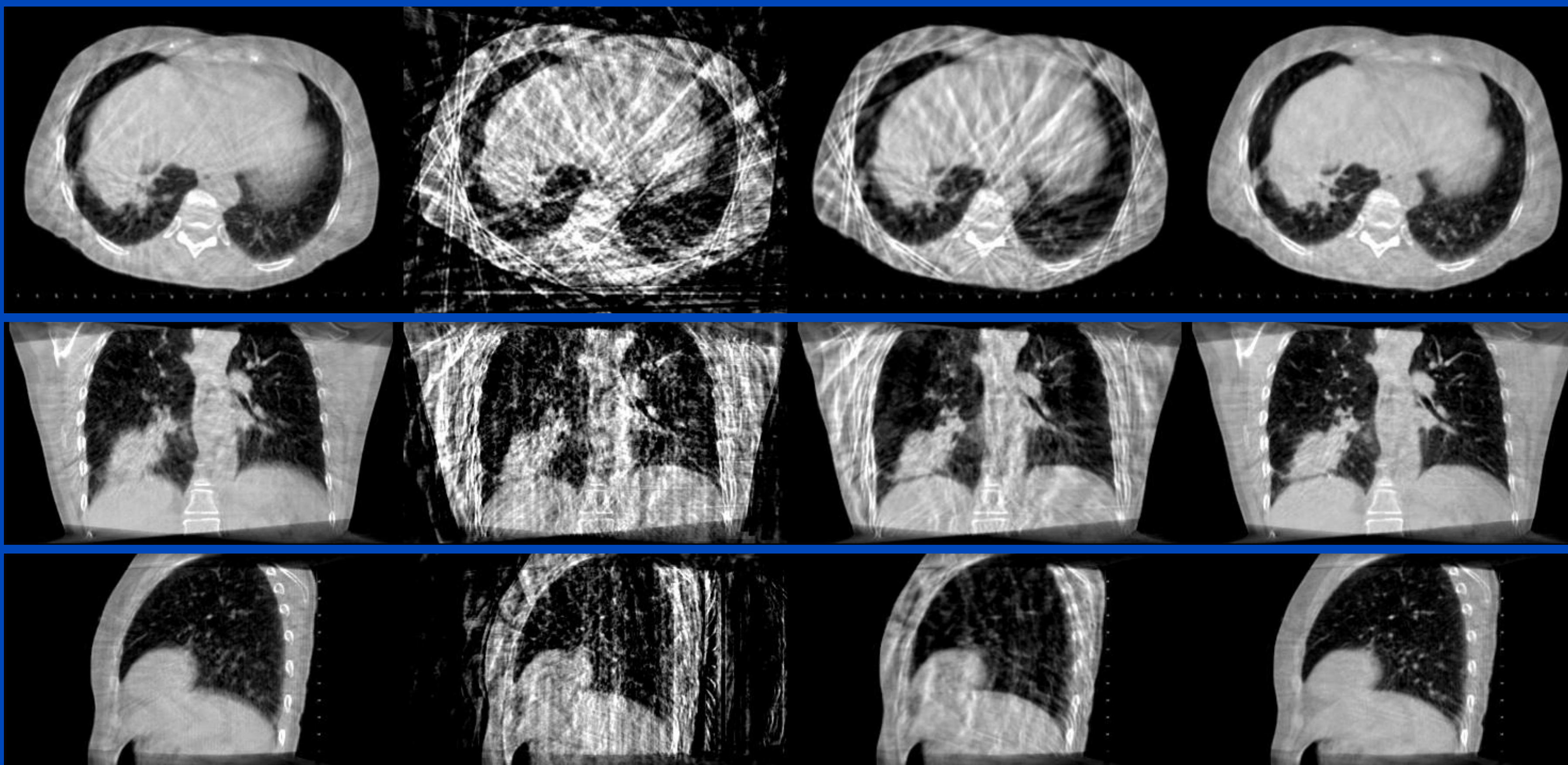

varian

C = -200 HU, *W* = 1400 HU, displayed with 30 rpm.
Patient data provided by Memorial Sloan–Kettering Cancer Center, New York, NY.

dkfz.

Spin-Off Effects?

4D PET/MR Motion Compensation

MR Results Patient s04

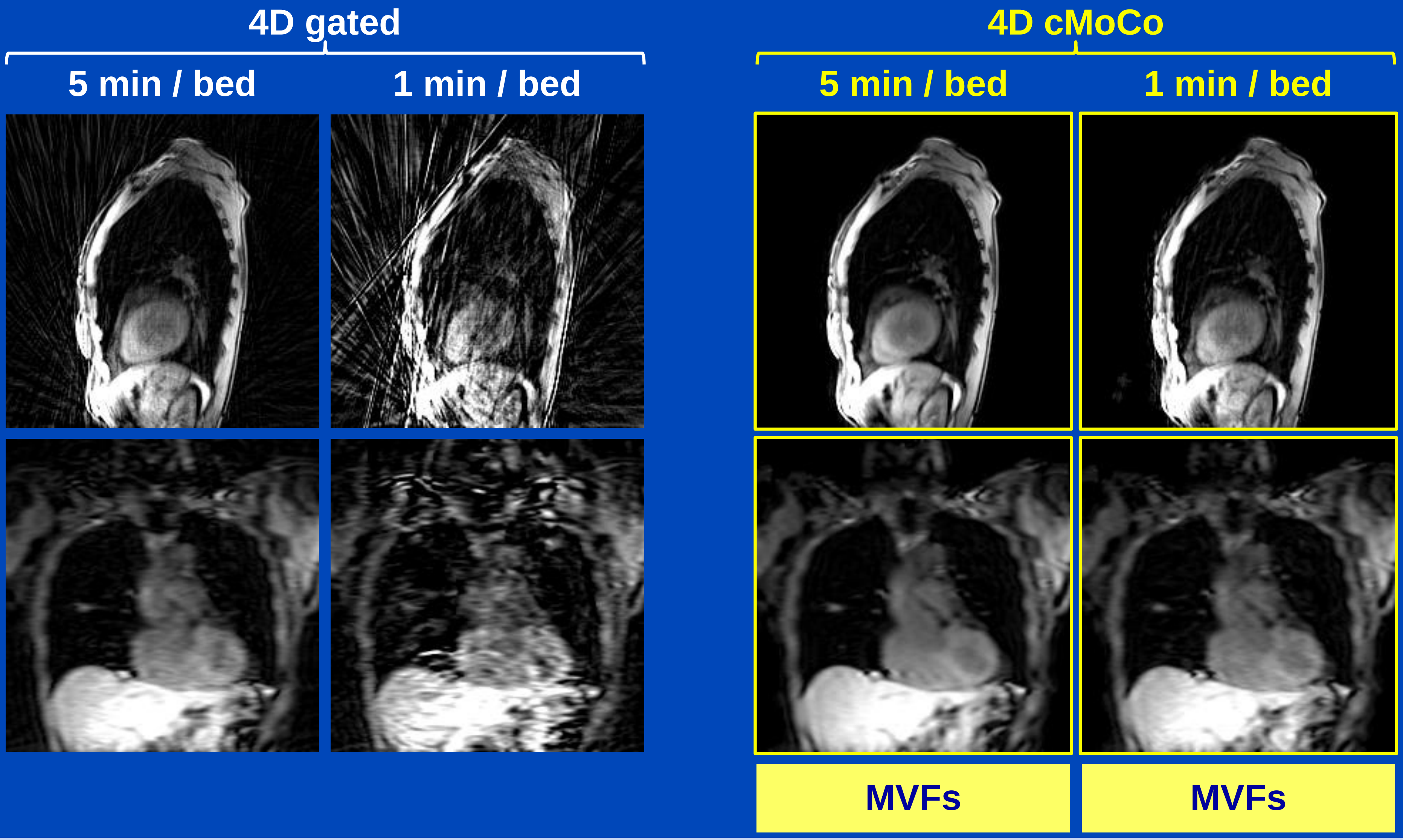

Rank, Heußer, Buzan, Wetscherek, Freitag, Dinkel, Kachelrieß. 4D respiratory motion-compensated image reconstruction of free-breathing radial MR data with very high undersampling. Magn Reson Med 77(3):1170-1183, 2017.

4D PET/MR Motion Compensation

PET Results Patient s01

4D cMoCo

3D | 4D gated | MR: 5 min / bed | MR: 1 min / bed

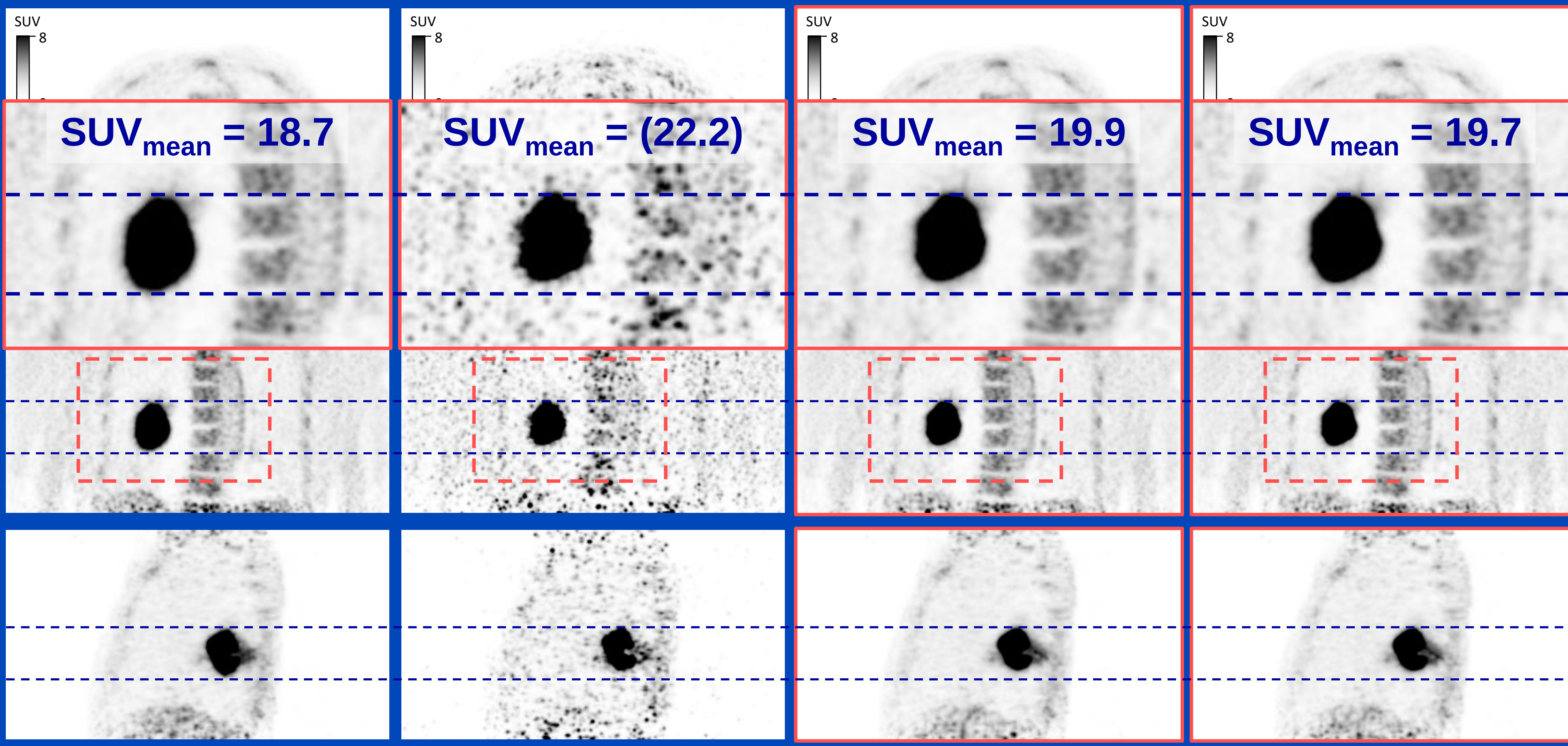

due to the high noise level of 4D gated PET, SUV$_{mean}$ was systematically overestimated

C. Rank, T. Heußer, A. Wetscherek, M. Freitag, O. Sedlaczek, H.-P. Schlemmer, and M. Kachelrieß. Respiratory motion compensation for simultaneous PET/MR based on highly undersampled MR data. Med. Phys. 43(12):6234-6245, December 2016.

Is There More?

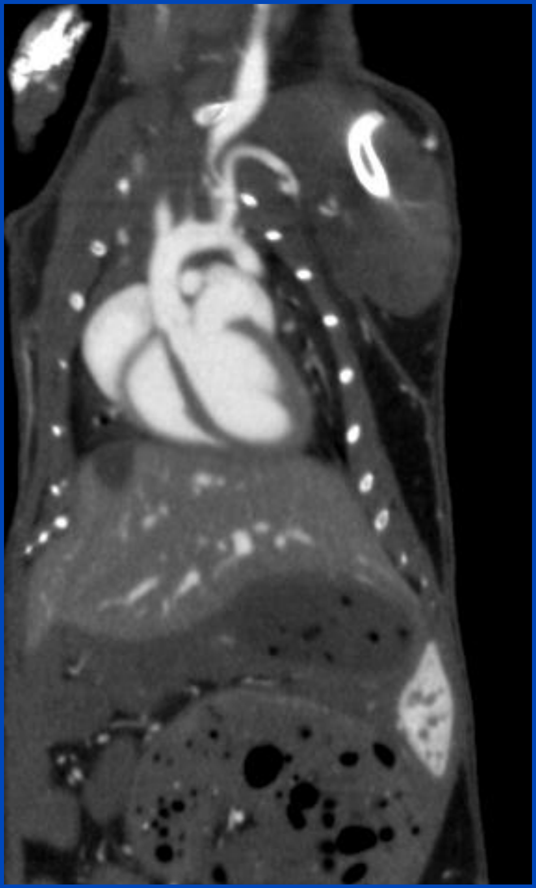

Data displayed as:

Heart: 280 bpm

Lung: 150 rpm

Mouse with 150 rpm and 280 bpm.

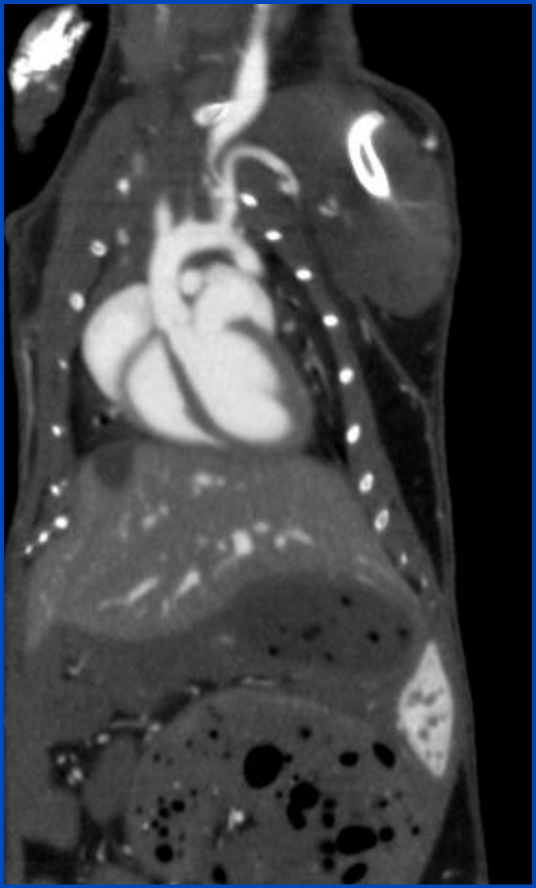

<u>Data displayed as:</u>

Heart: 180 bpm

Lung: 90 rpm

Mouse with 180 rpm and 240 bpm.

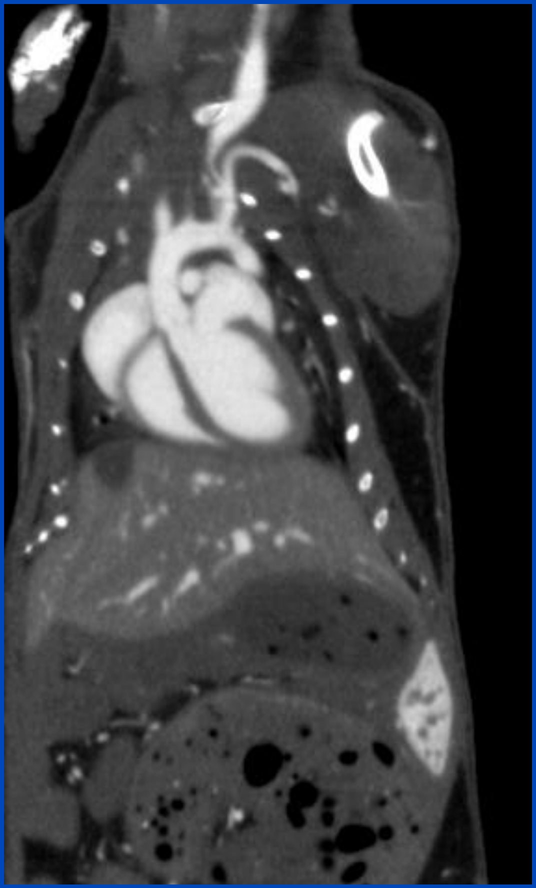

Data displayed as:

Heart: 90 bpm

Lung: 90 rpm

Mouse with 180 rpm and 240 bpm.

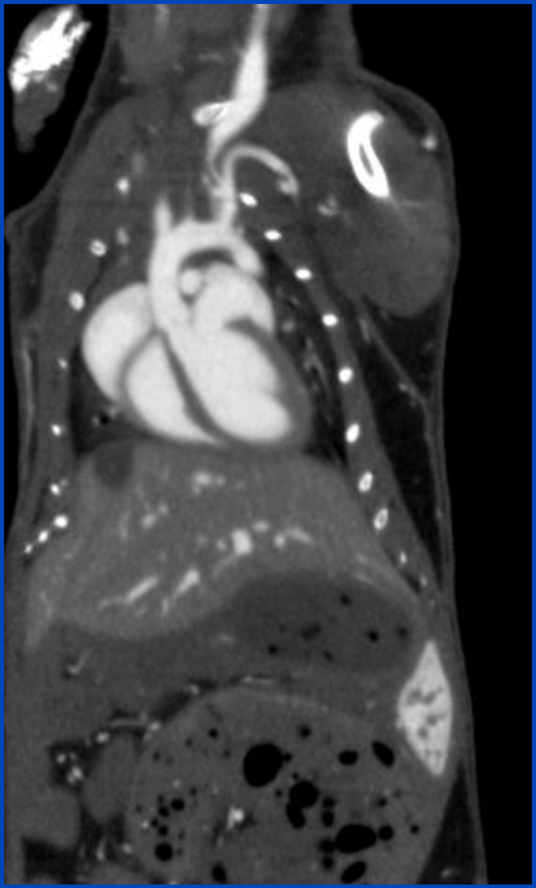

<u>Data displayed as:</u>

Heart: 0 bpm

Lung: 90 rpm

Mouse with 180 rpm and 240 bpm.

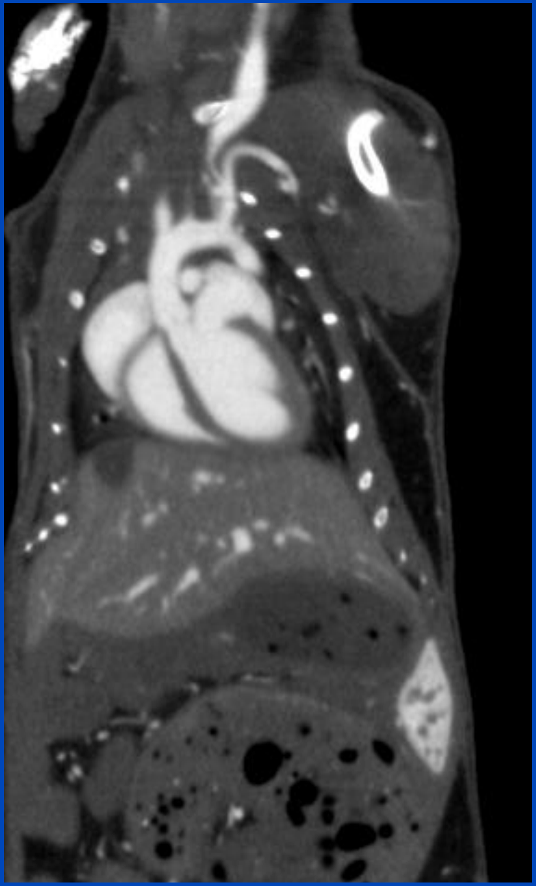

<u>Data displayed as:</u>

Heart: 90 bpm

Lung: 0 rpm

Mouse with 180 rpm and 240 bpm.

5D with Double Gating?

Double gating example:

• Cardiac window width: 20%
• Respiratory window width: 10%
• Only 2% of all projections per reconstructed volume

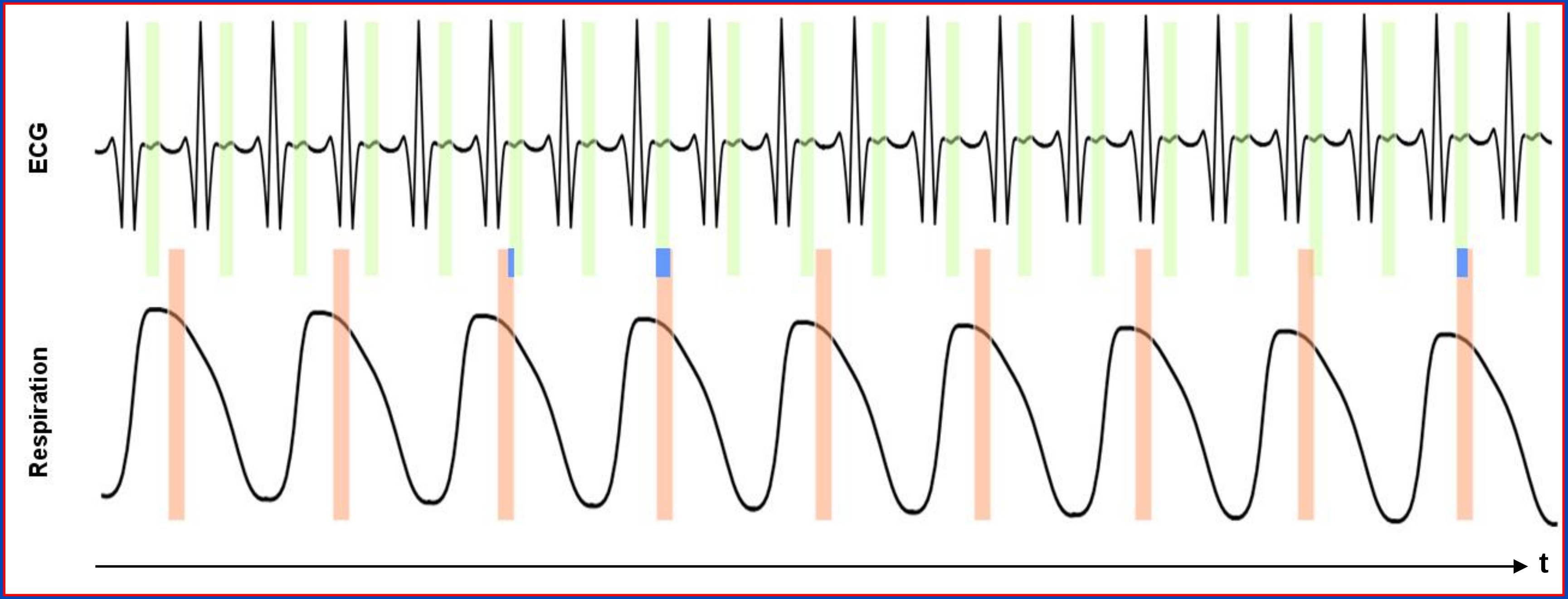

Injection Techniques[1]

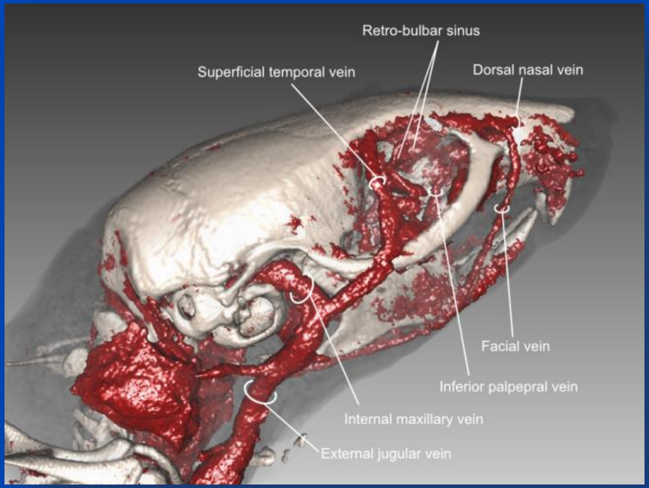

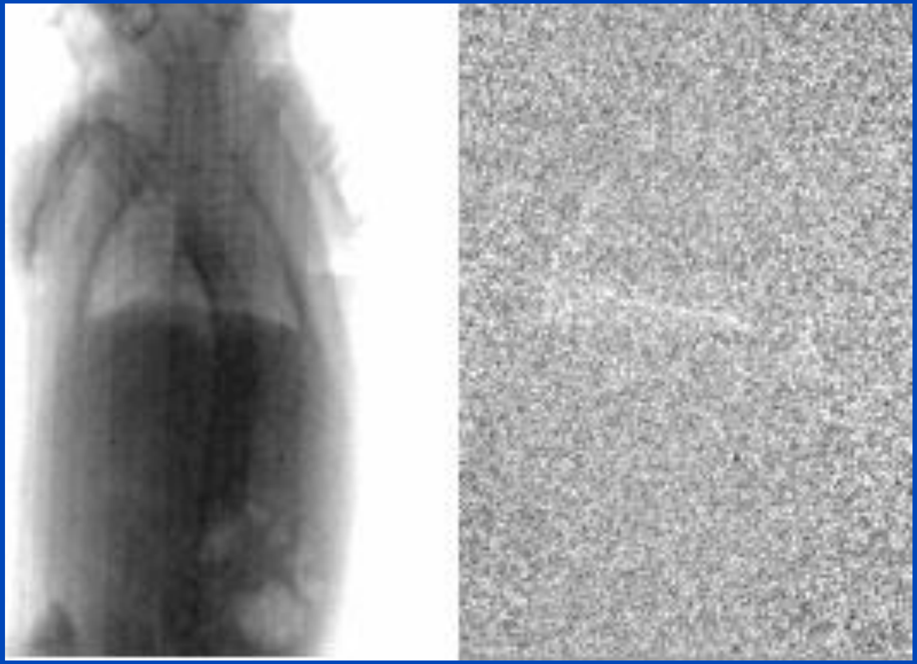

Tail Vein Injection

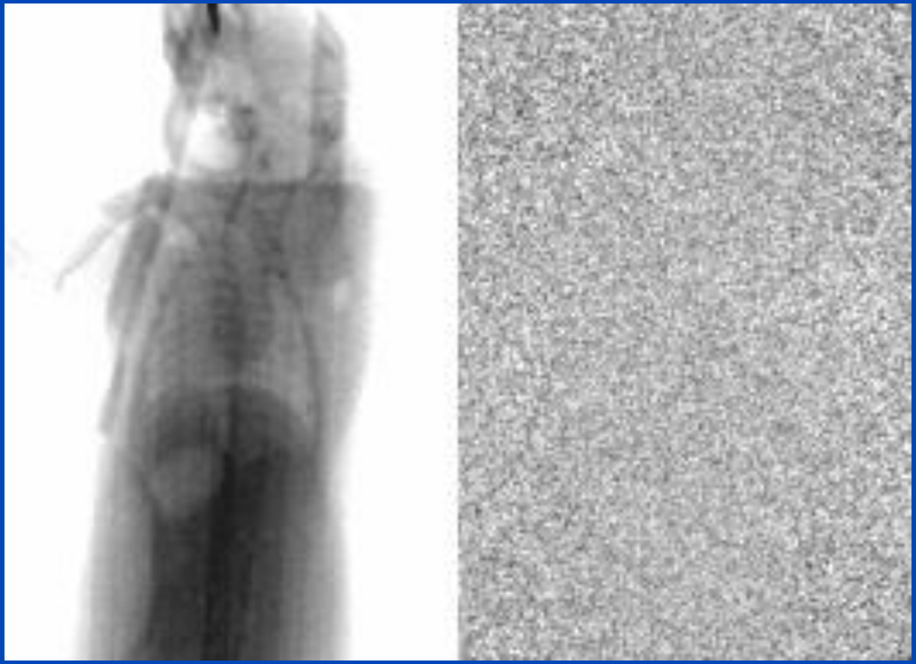

Retro Bulbar Injection

[1] M. Socher, J. Kuntz, S. Sawall, S. Bartling, and M. Kachelrieß. The retrobulbar sinus is superior to the lateral tail vein for the injection of contrast media in small animal cardiac imaging. Lab. Anim. 48(2), pp. 105-113, February 2014.

dkfz.

5D Motion Compensation

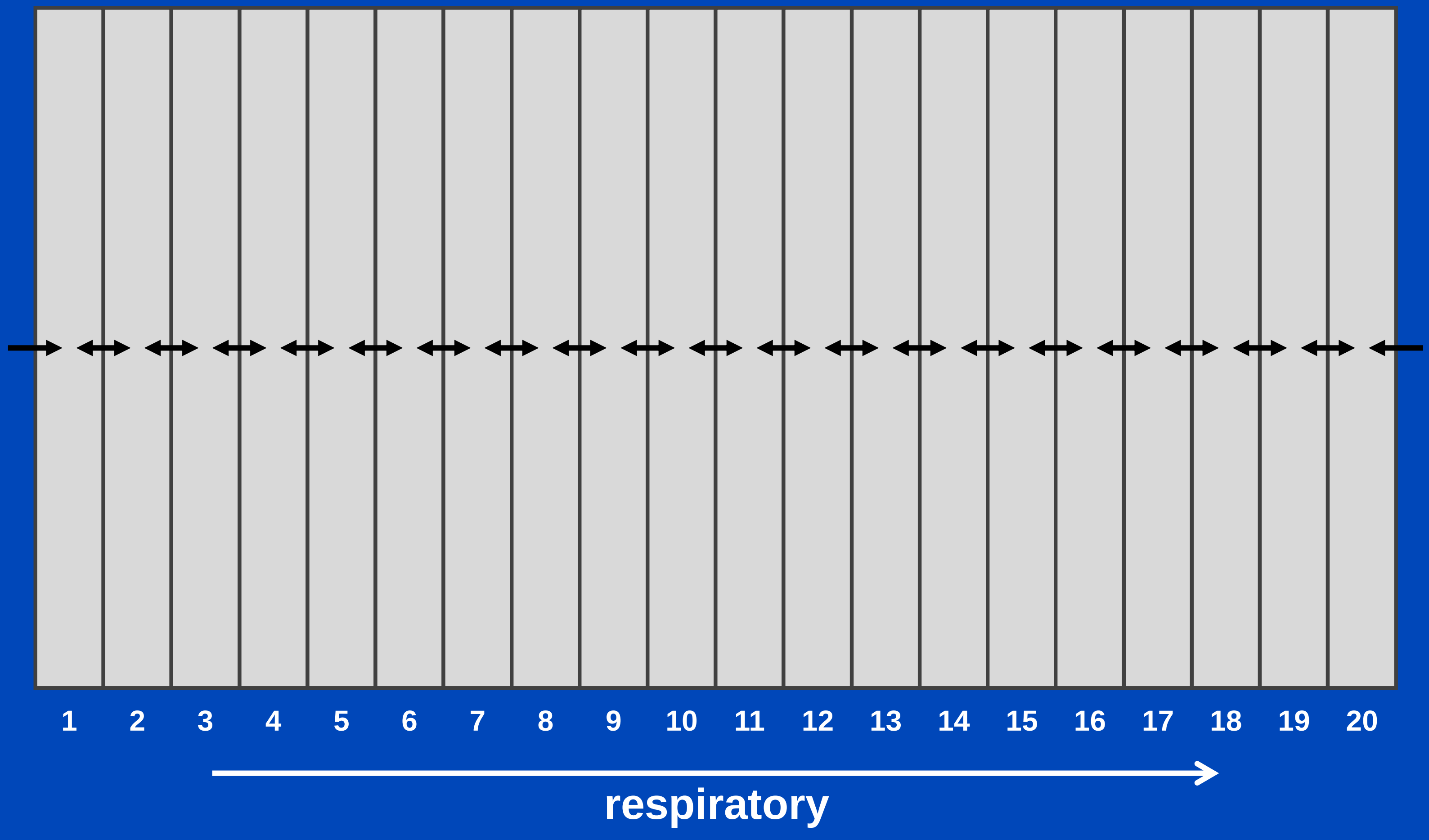

Brehm, Sawall, Maier, and Kachelrieß, “Cardio-respiratory motion-compensated micro-CT image reconstruction using an artifact model-based motion estimation” Med. Phys. 42(4):1948-1958, 2015.

5D Motion Compensation

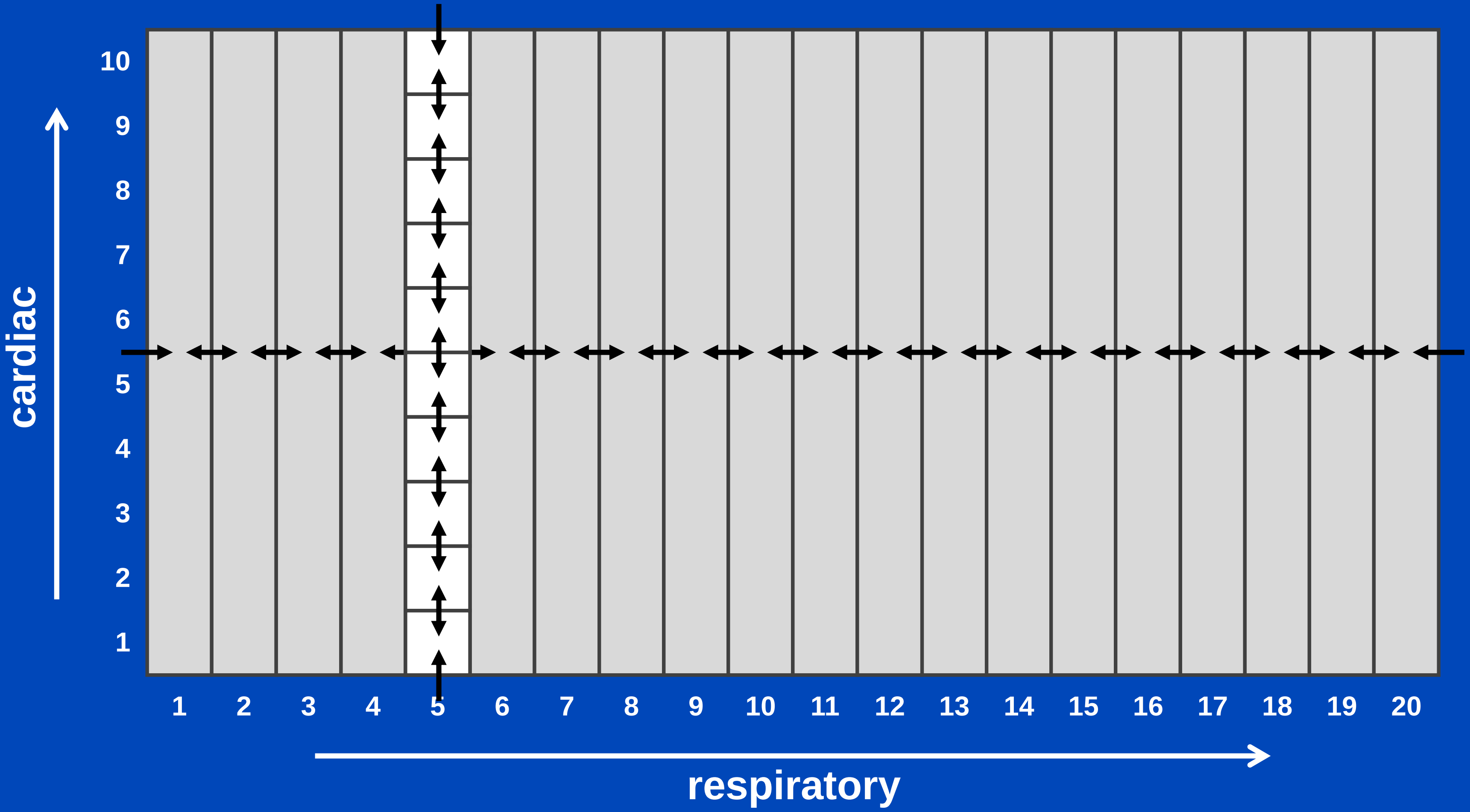

Brehm, Sawall, Maier, and Kachelrieß, "Cardio-respiratory motion-compensated micro-CT image reconstruction using an artifact model-based motion estimation" Med. Phys. 42(4):1948-1958, 2015.

5D Motion Compensation

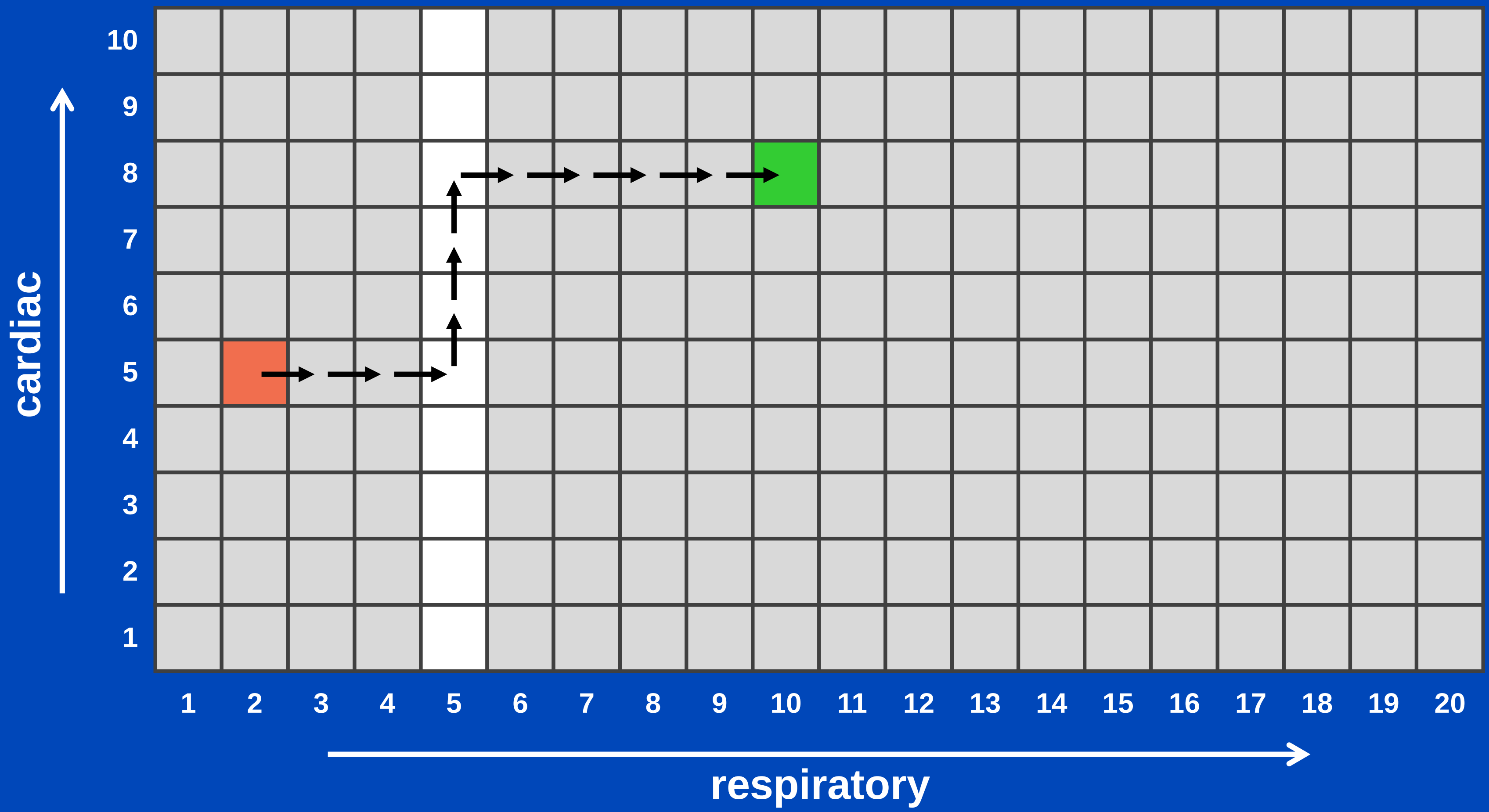

Brehm, Sawall, Maier, and Kachelrieß, “Cardio-respiratory motion-compensated micro-CT image reconstruction using an artifact model-based motion estimation” Med. Phys. 42(4):1948-1958, 2015.

5D Motion Compensation

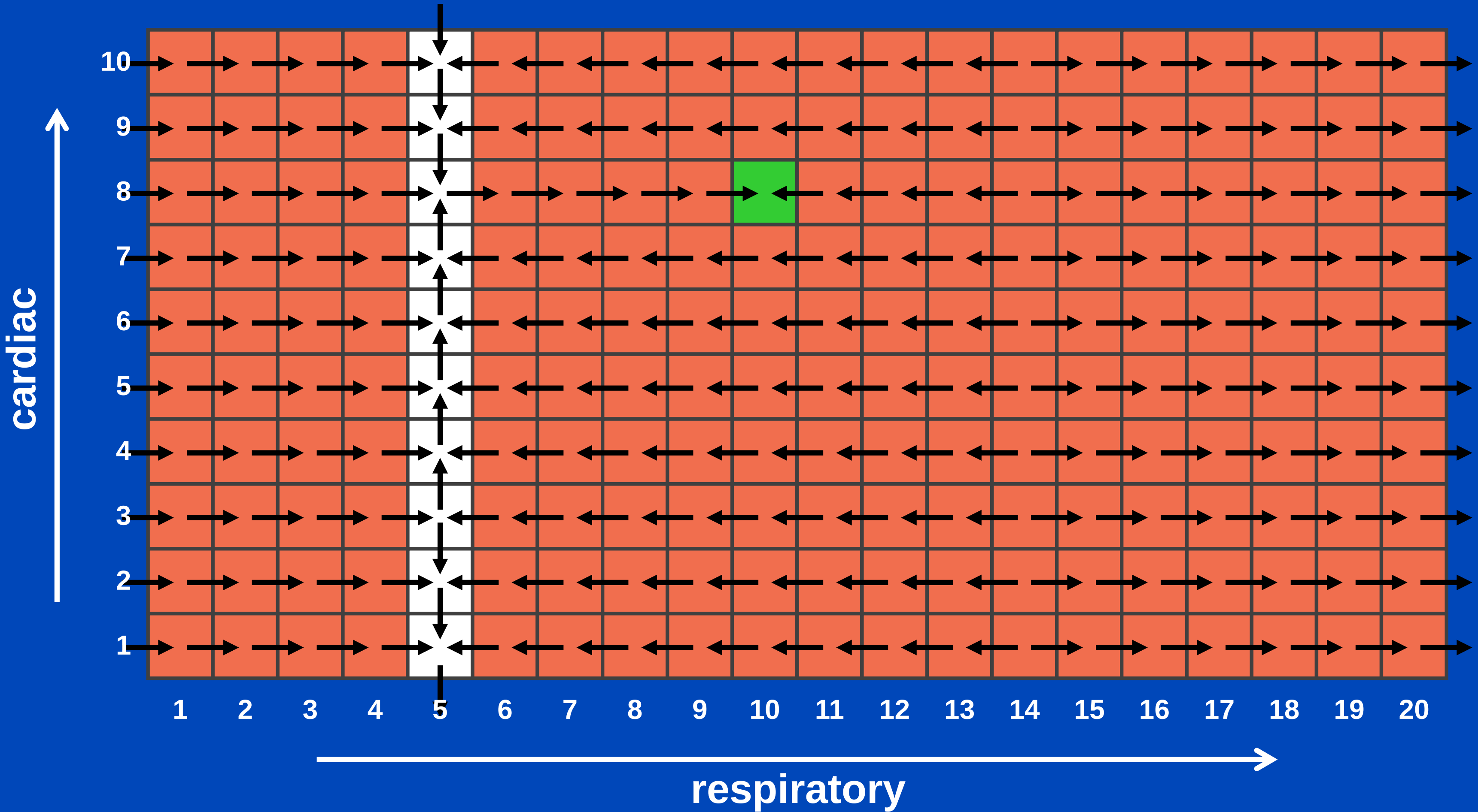

Brehm, Sawall, Maier, and Kachelrieß, "Cardio-respiratory motion-compensated micro-CT image reconstruction using an artifact model-based motion estimation" Med. Phys. 42(4):1948-1958, 2015.

7200 Projections

3D CBCT | 5D double-gated CBCT | 5D Motion Compensation

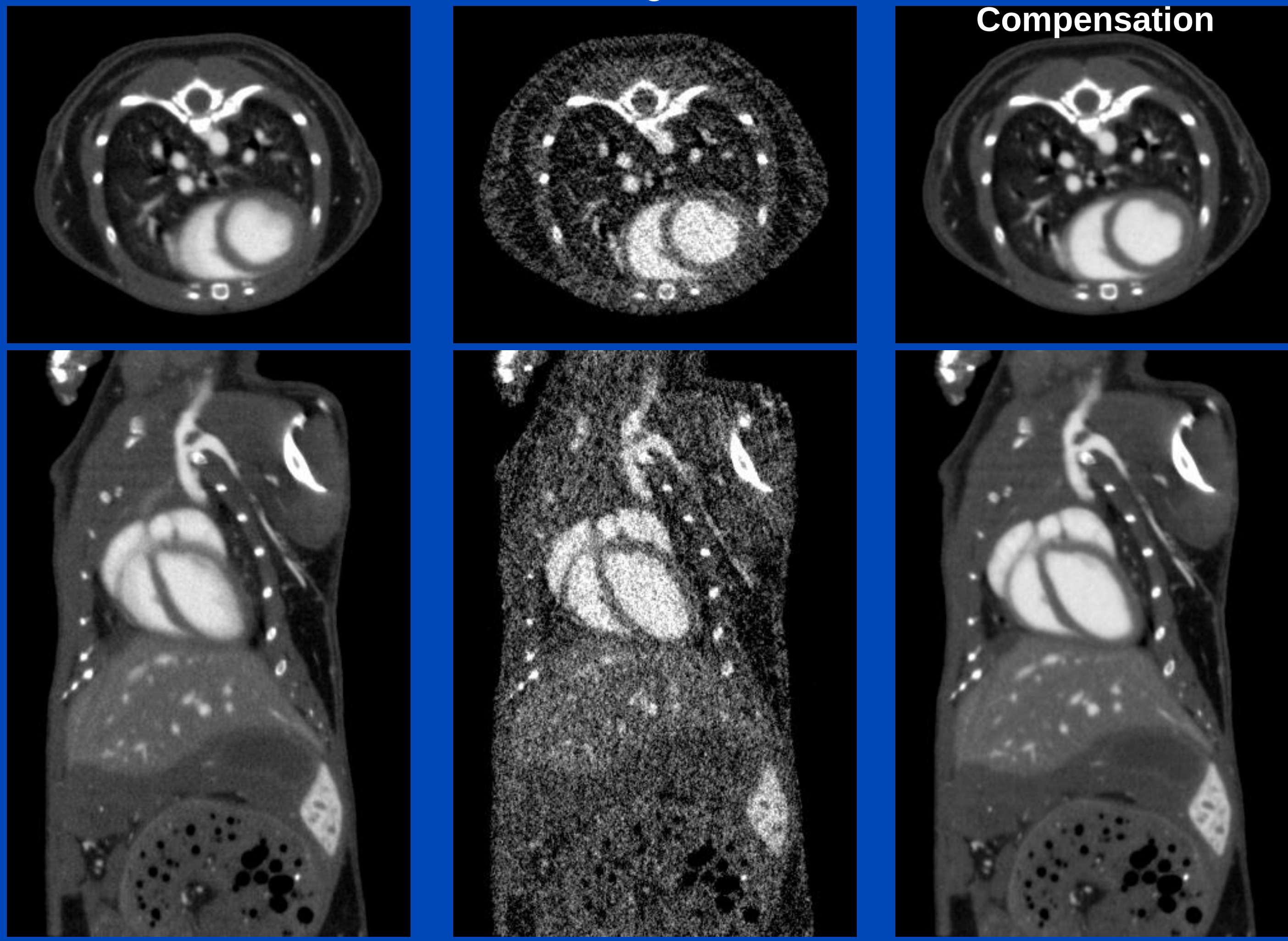

The images show a fixed respiratory and cardiac phase.

Brehm, Sawall, Maier, and Kachelrieß, “Cardio-respiratory motion-compensated micro-CT image reconstruction using an artifact model-based motion estimation” Med. Phys. 42(4):1948-1958, 2015.

3600 Projections

3D CBCT | **5D double-gated CBCT** | **5D Motion Compensation**

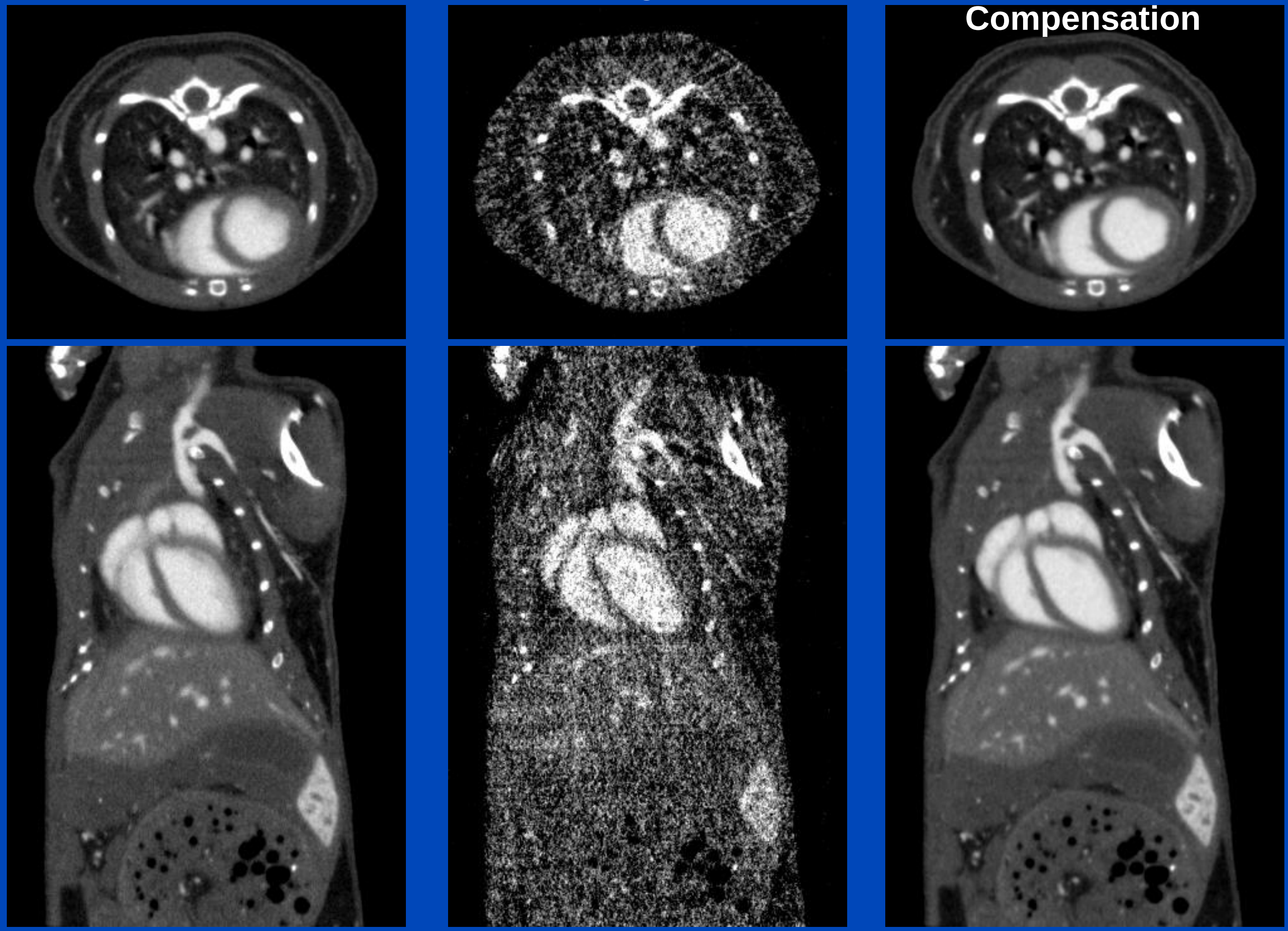

The images show a fixed respiratory and cardiac phase.

Brehm, Sawall, Maier, and Kachelrieß, "Cardio-respiratory motion-compensated micro-CT image reconstruction using an artifact model-based motion estimation" Med. Phys. 42(4):1948-1958, 2015.

720 Projections

3D CBCT | **5D double-gated CBCT** | **5D Motion Compensation**

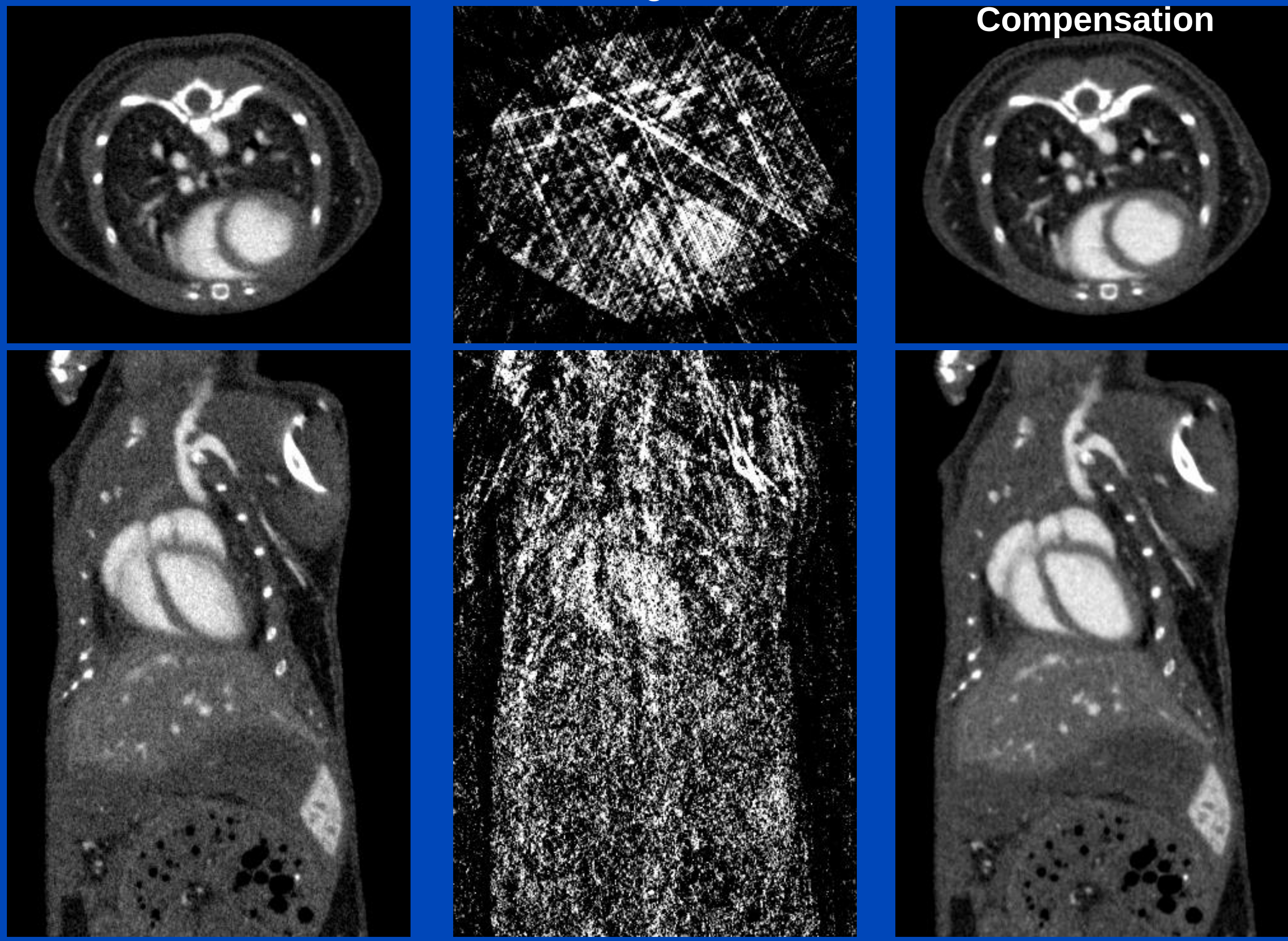

The images show a fixed respiratory and cardiac phase.

Brehm, Sawall, Maier, and Kachelrieß, "Cardio-respiratory motion-compensated micro-CT image reconstruction using an artifact model-based motion estimation" Med. Phys. 42(4):1948-1958, 2015.

Spin-Off Effects?

5D MR Motion Compensation

Results Patient c12

3D	5D	5D	5D MoCo
motion average	resp & card gated	resp MoCo & card gated	resp & card MoCo
	r = 1, *c*-loop	*r* = 1, *c*-loop	*r* = 1, *c*-loop

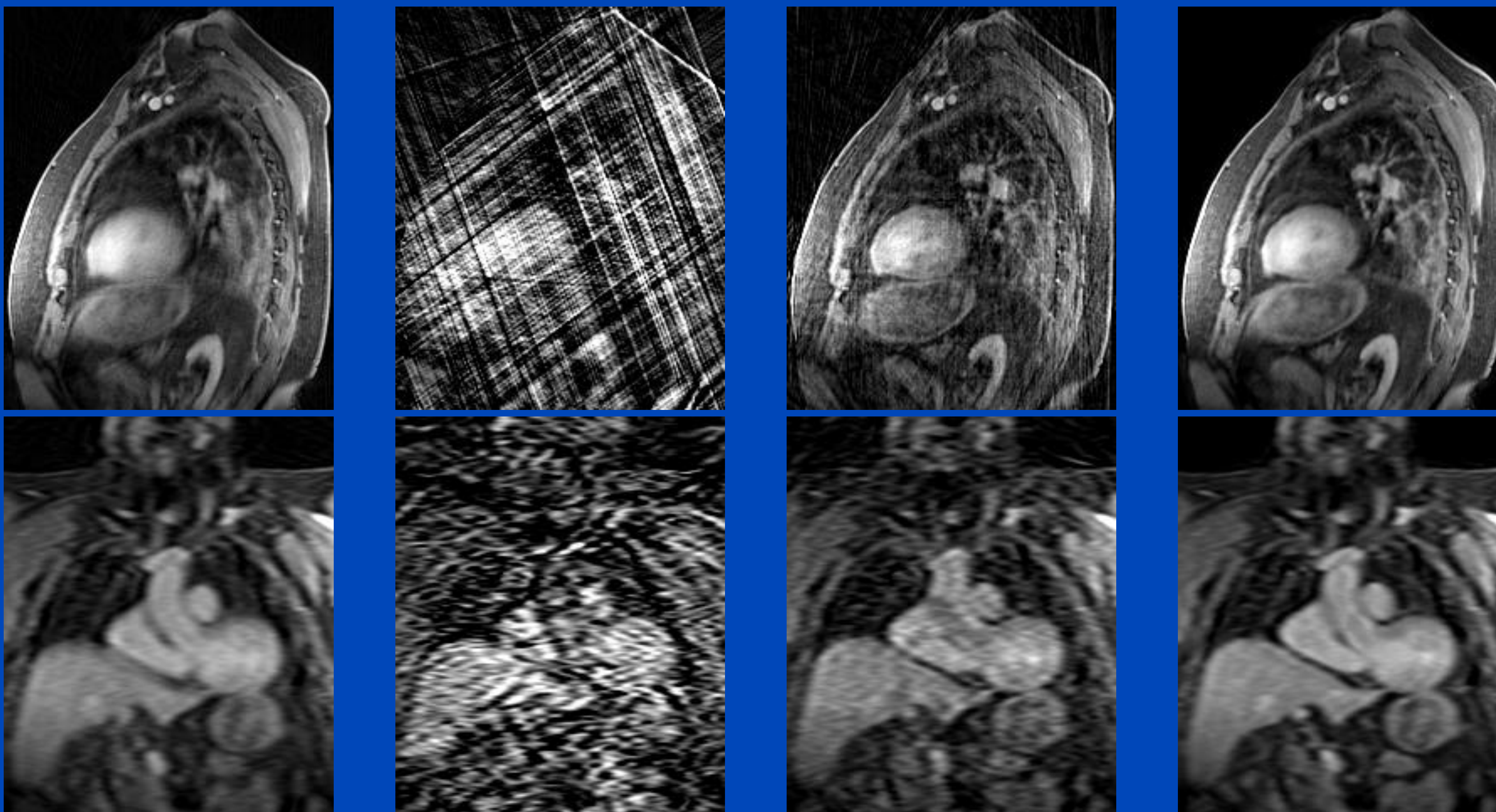

total acquisition time: 1 min 55 s, radial undersampling = 36

5D PET/MR Motion Compensation

Results Patient s04

3D PET	5D double-gated PET	5D MoCo PET	5D MoCo MR
motion average	$r = 1$, c-loop	$r = 1$, c-loop	$r = 1$, c-loop

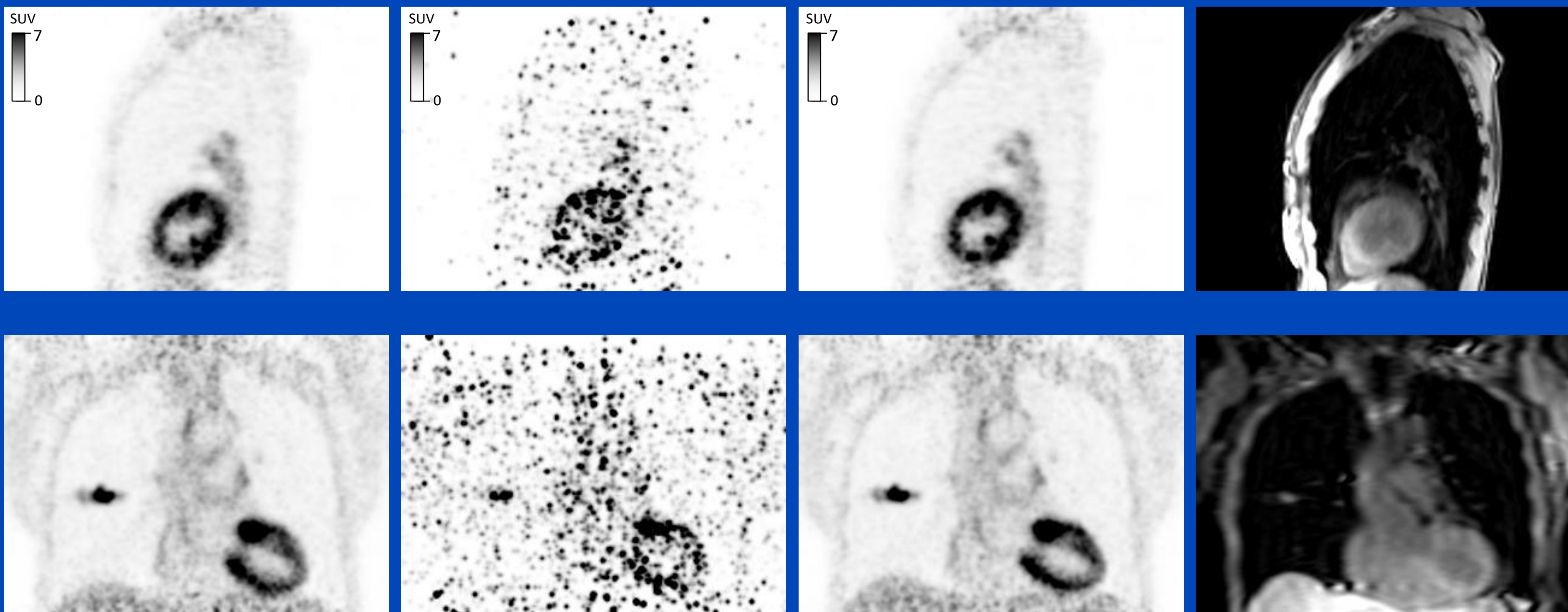

Photon Counting CT

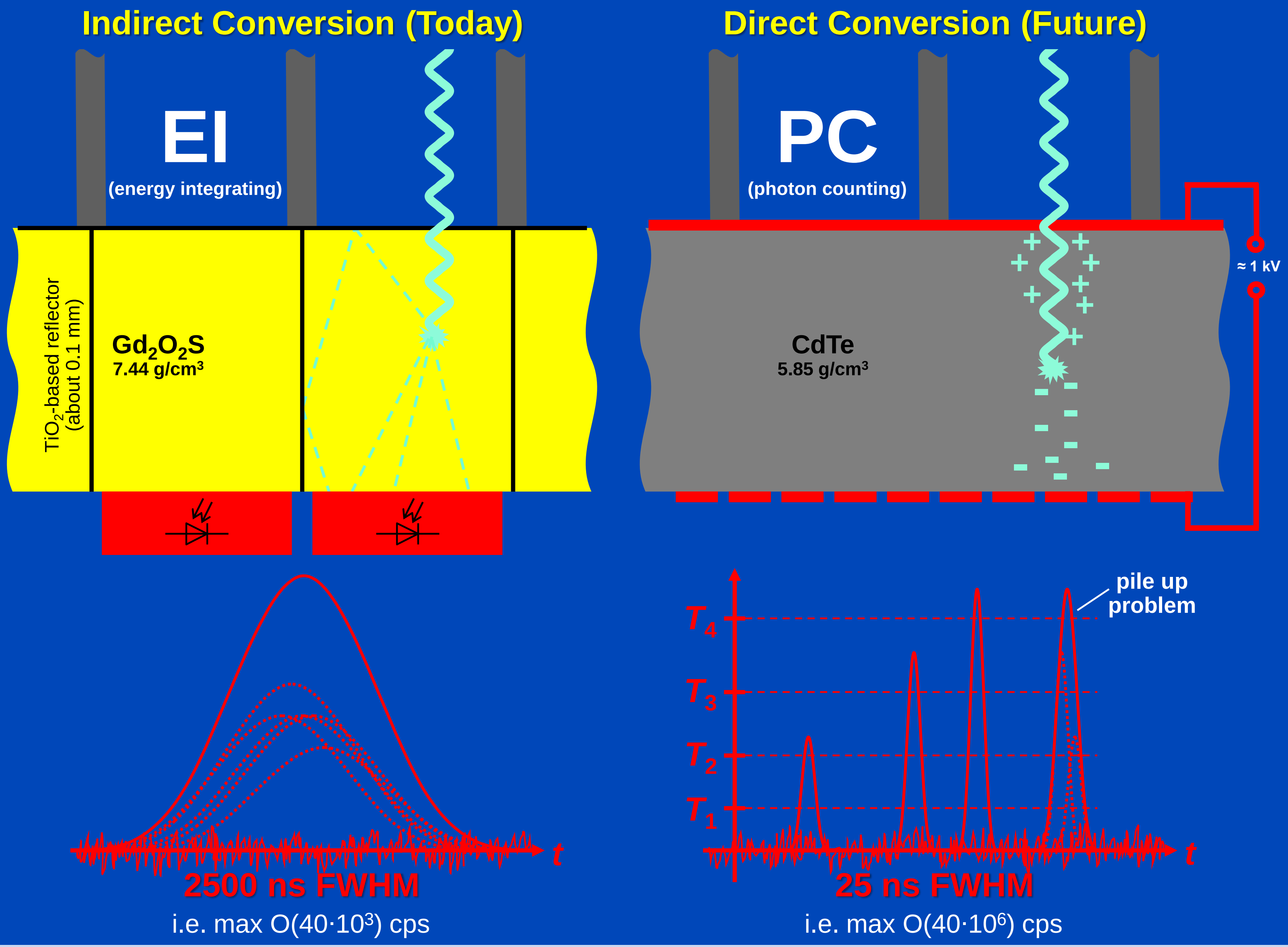

Requirements for CT: up to 10^9 x-ray photon counts per second per mm^2.
Hence, photon counting only achievable for direct converters.

Energy-Selective Detectors: Improved Spectroscopy, Reduced Dose?

Ideally, bin spectra do not overlap, …

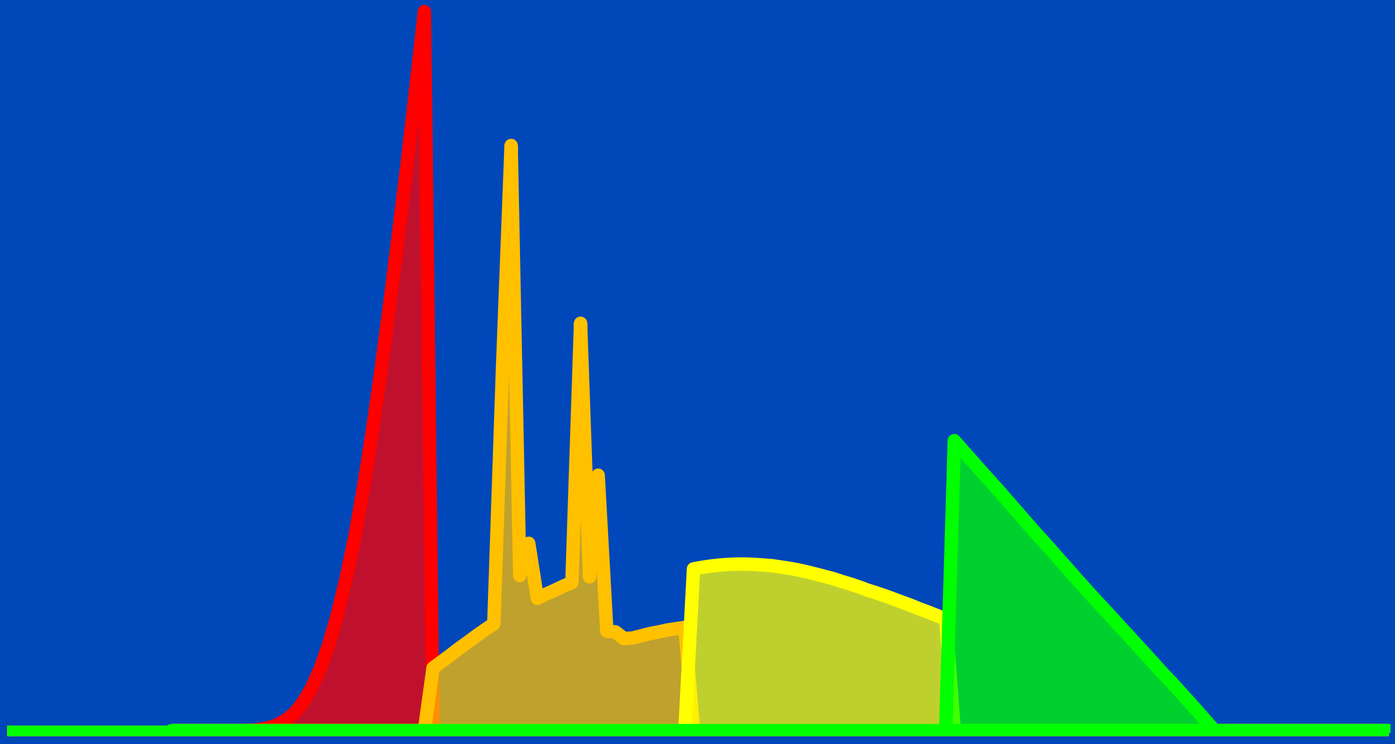

Energy-Selective Detectors: Improved Spectroscopy, Reduced Dose?

… realistically, however they do!

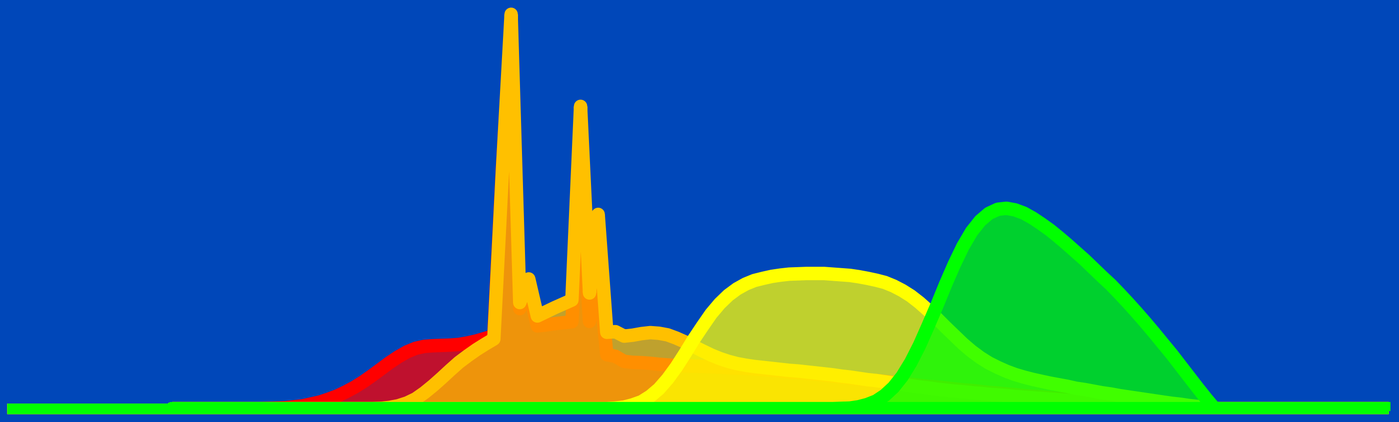

Spectra as seen after having passed a 32 cm water layer.

Existing Systems 2020

	Setup	Detector	Pixel size (mm^2)	FOV	Thresholds	Acquisition	Extra
Philips Healthcare (preclinical) [1, 2, 3]	Preclinical	CdZnTe	0.5 × 0.5	16.8 cm	5 (30-98 keV)	2400 fps	
MARS Bioimaging (preclinical) [4, 5]	Preclinical MARS orthopaedic imaging-cooming soon	2 mm CdZnTe; five medipix3RX chips in a row (70 mm × 14 mm)	0.11 × 0.11	10 cm	8 (10-120 keV)	Scan time: 8 min for a sample with 30 mm diameter and 15 mm length	Charge summing mode
Siemens Somatom CounT [6]	**Clinical, whole body**	Dual-source CT with one PC detector of 1.6 mm CdTe	0.225 × 0.225 or 0.45 × 0.45 or 0.9 × 0.9	**27.5 cm**	4 (20-90 keV)	2304 fps 4608 fps	
KTH Royal Institute of Technology, Stockholm [7]	Table-top Translating detector	30 mm silicon strip	0.4 × 0.5	0.93 cm (need to translate the detector several times)	8	300 $Mcps/mm^2$	Edge-on design
Center for In Vivo Microscopy, Duke University, Durham (preclinical) [8, 9]	Preclinical Table-top	1 mm CdTe	0.15 × 0.15	~6.5 cm	4		
DKFZ (preclinical)	Preclinical	1 mm CdTe	0.15 × 0.15	~15 cm	4 (9-90 keV)	200 fps 100 $Mcps/mm^2$	

Non-Proprietary Relevant PC Detectors

	Sensor	Pixel	Sensor Area	Bins	Acquisition	Features
Medipix3RX[1,2]	Si or CdTe	55 µm	1.4×1.4 cm^2 3-side buttable	2	61 Mcps/mm^2	Charge summing mode: half the number of thresholds, count rate reduced by a factor of 4 to 5
		110 µm		8	15 Mcps/mm^2	
Pixirad Module[3]	CdTe 0.65 mm	55 µm	3.1×2.5 cm^2 2-side buttable	2	200 fps 162 Mcps/mm^2	Hexagonal pixel
Dectris Säntis[4]	CdTe	150 µm	30.8×3.8 cm^2	4	200 fps 100 Mcps/mm^2	
Direct conversion XC Thor[5]	CdTe 0.75 or 2.0 mm	100 µm	up to 5.12×40.0 cm^2	2	300 fps 200 Mcps/mm^2	Charge sharing correction

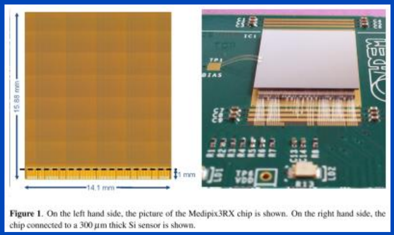

Medipix


Pixirad

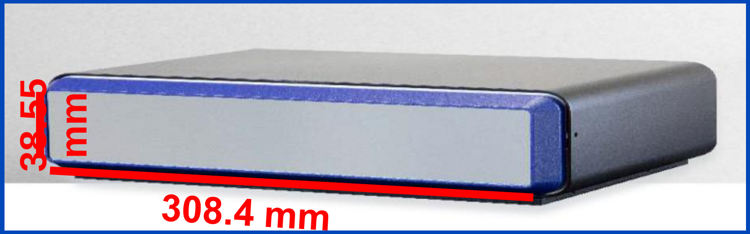

Säntis


XC Thor

[1] Ballabriga, et al. (2013). The medipix3RX: A high resolution, zero dead-time pixel detector readout chip allowing spectroscopic imaging. Journal of Instrumentation.
[2] Frojdh, et al. (2014). Count rate linearity and spectral response of the Medipix3RX chip coupled to a 300µm silicon sensor under high flux conditions. Journal of Instrumentation.
[3] https://indico.cern.ch/event/284070/sessions/53910/attachments/524517/723391/Ravenna_Bellazzini1.pdf
[4] Information provided by Dectris Ltd.
[5] https://directconversion.com/product/xc-thor/

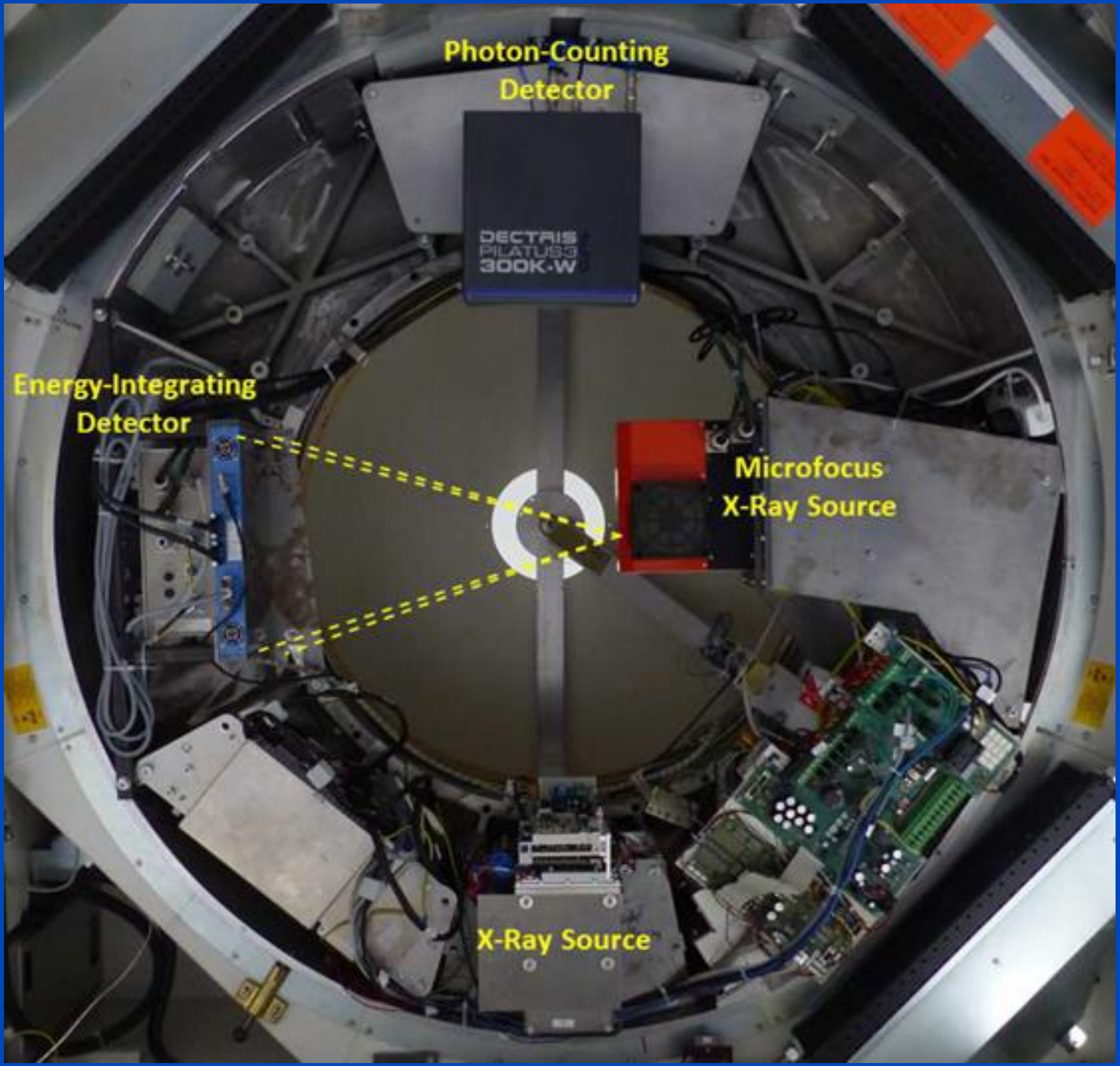

Photon-Counting Detector
DECTRIS PILATUS3 300K-W
Energy-Integrating Detector
Microfocus X-Ray Source
X-Ray Source

Diagnostic CT (Conventional Detector) of a Low Contrast Phantom

Photon Counting Detector CT of a Low Contrast Phantom

EI

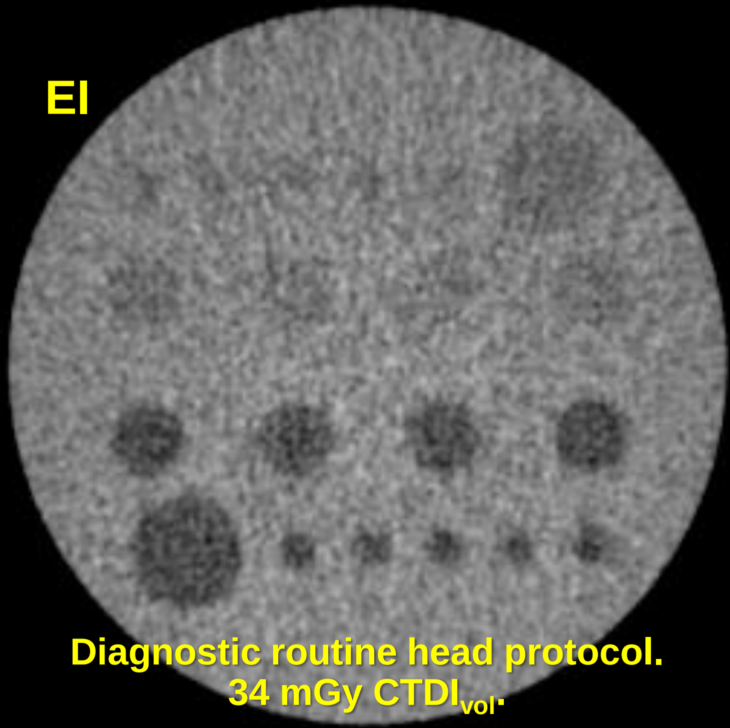

Diagnostic routine head protocol.
34 mGy CTDI_{vol}.

PC

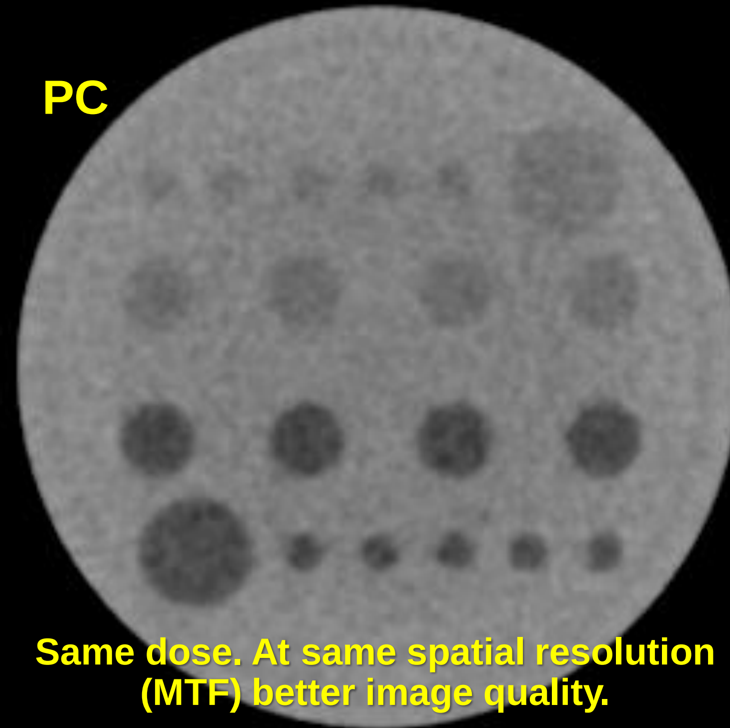

Same dose. At same spatial resolution (MTF) better image quality.

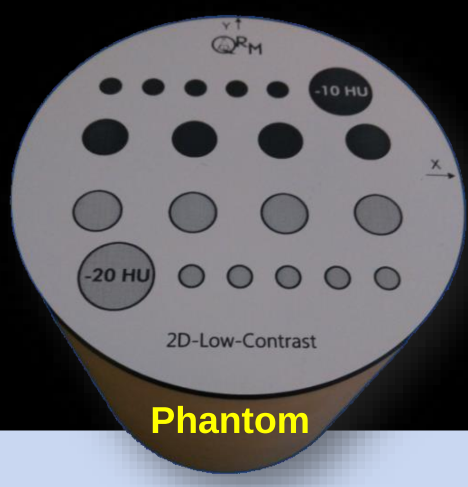

Phantom

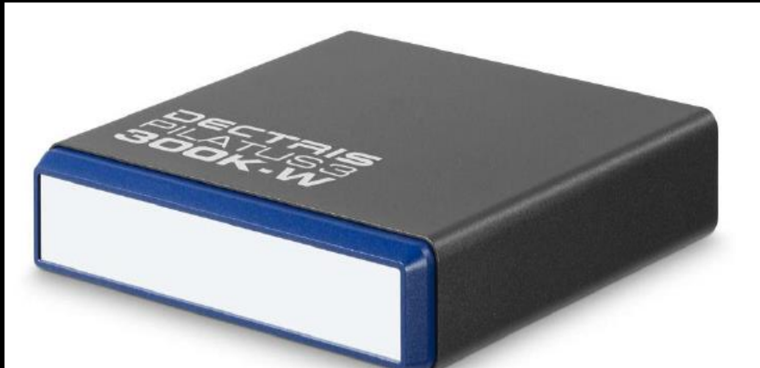

Photon Counting Detector

C = 0 HU, W = 80 HU

SIEMENS
SOMATOM CounT
@ dkfz.

Siemens CounT CT System

Gantry from a clinical dual source scanner

A: conventional CT detector (50.0 cm FOV)

B: Photon counting detector (27.5 cm FOV)

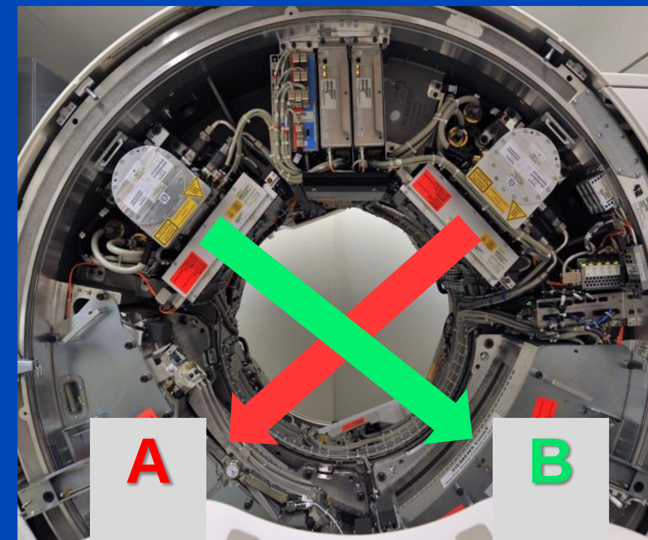

Readout Modes of the CounT

PC-UHR Mode	PC-Macro Mode	EI detector
0.25 mm pixel size	0.50 mm pixel size	0.60 mm pixel size

Experimental CT, not commercially available.

dkfz.

Advantages of Photon Counting CT

- No reflective gap between detector pixels
  - Higher geometrical efficiency
  - Less dose
- No electronic noise
  - Less dose for infants
  - Less noise for obese patients
- Counting
  - Swank factor = 1 = maximal
  - Higher weights on low energies = good for iodine contrast
- Energy bin weighting
  - Lower dose/noise
  - Improved iodine CNR
- Smaller pixels (to avoid pileup)
  - Higher spatial resolution
  - Lower dose/noise at conventional resolution
- Spectral information on demand

Dark Image of Photon Counter Shows Background Radiation

18 frames, 5 min integration time per frame

Events per Frame

Energy Integrating (Dexela)

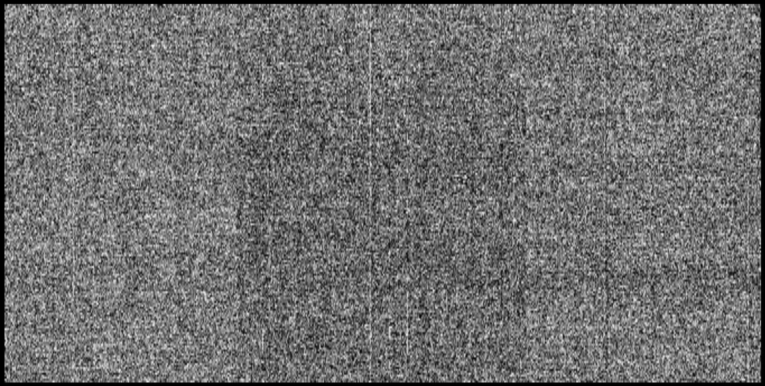

C/W = 0 a.u./70 a.u.

Photon Counting (Dectris Santis)

C/W = 1 cnts/2 cnts

Accumulated Signal

Dark current dominates.
Readout noise only.
Single events hidden!

C/W = 30 a.u./450 a.u.

No dark current.
No readout noise.
Single events visible!

C/W = 3 cnts/8 cnts

Photon Counting used to Maximize CNR

- With PC energy bins can be weighted individually.
- To optimize the CNR the optimal bin weighting factor is given by (weighting after log):

$$w_b \propto \frac{C_b}{V_b}$$

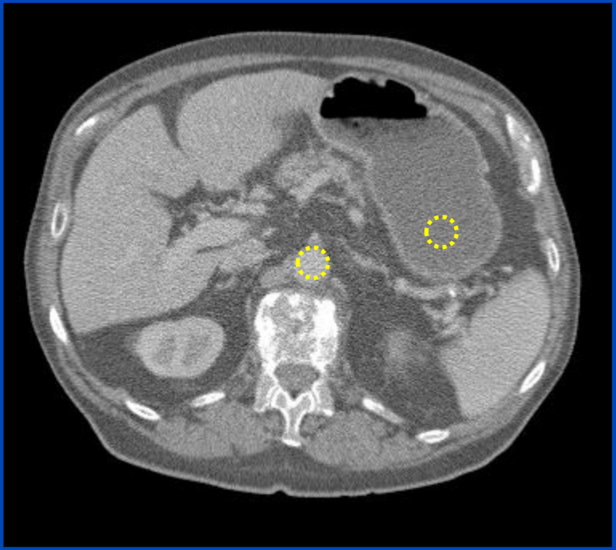

- The resulting CNR is

$$\mathrm{CNR}^2 = \frac{\left(\sum_b w_b C_b\right)^2}{\sum_b w_b^2 V_b}$$

- At the optimum this evaluates to

$$\mathrm{CNR}^2 = \sum_{b=1}^{B} \mathrm{CNR}_b^2$$

Energy Integrating vs. Photon Counting
with 1 bin from 20 to 140 keV

Energy Integrating

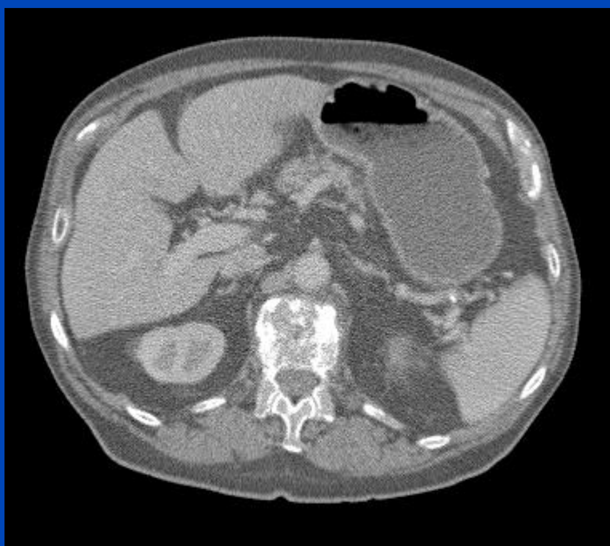

CNR = 2.11

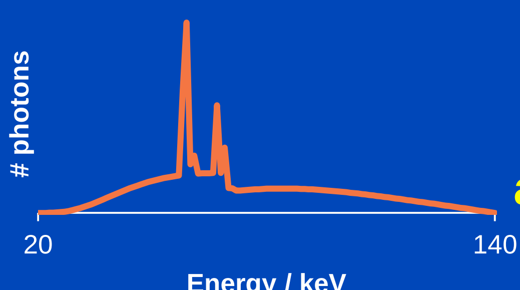

PC minus EI

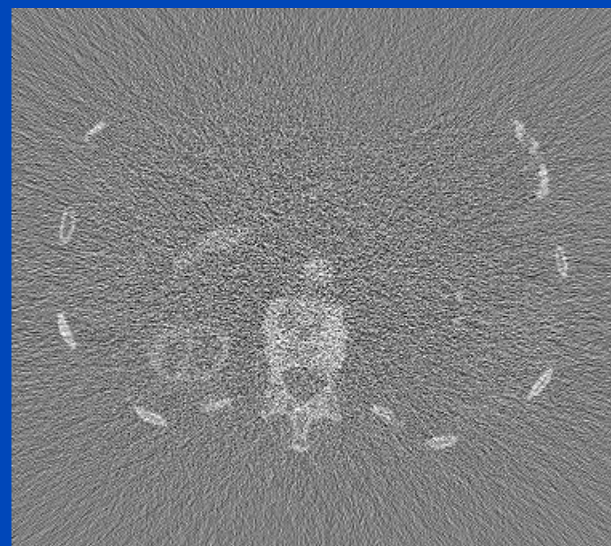

40% CNR improvement or 49% dose reduction achievable due to improved Swank factor and more weight on low energies (iodine contrast benefits).

Photon Counting

CNR = 2.95

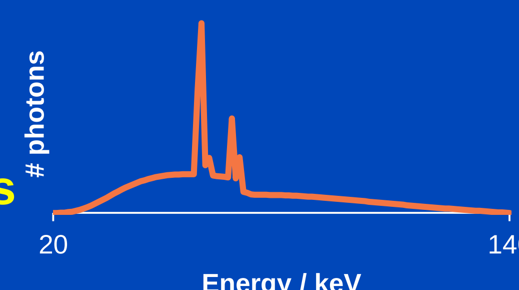

Images: *C* = 0 HU, *W* = 700 HU, difference image: *C* = 0 HU, *W* = 350 HU, bins start at 20 keV

Energy Integrating vs. Photon Counting

with 4 bins from 20 to 140 keV

Energy Integrating

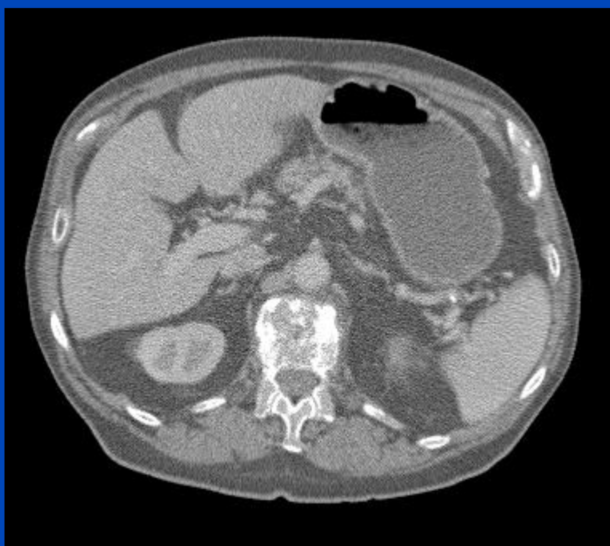

CNR = 2.11

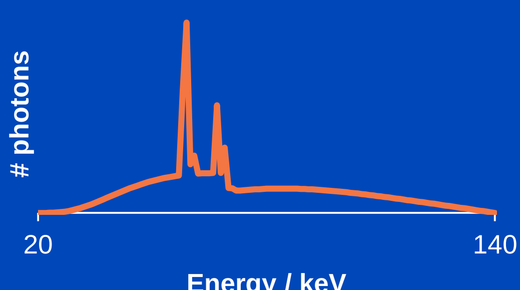

PC minus EI

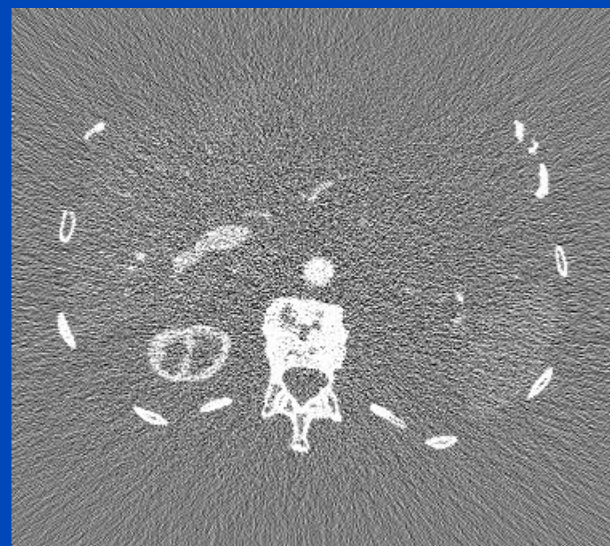

99% CNR improvement or 75% dose reduction achievable due to improved Swank factor and optimized energy weighting.

Photon Counting

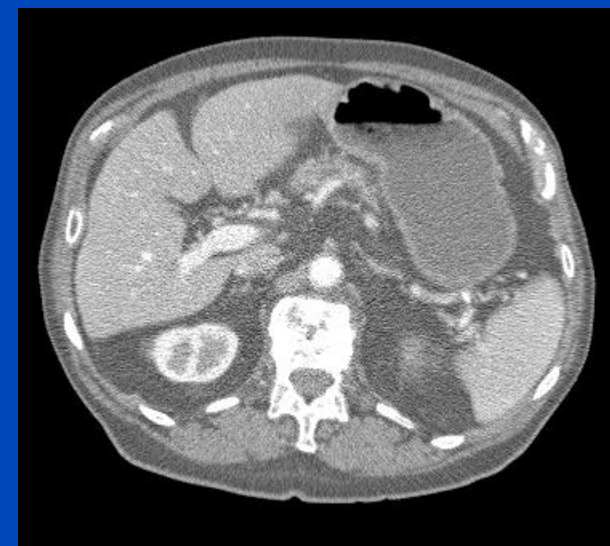

CNR = 4.19

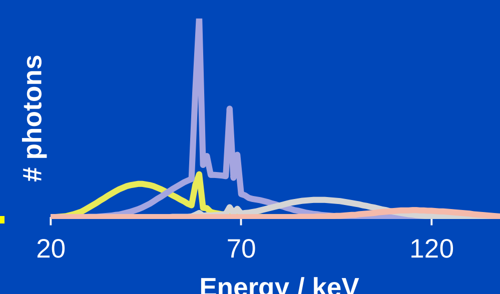

Images: *C* = 0 HU, *W* = 700 HU, difference image: *C* = 0 HU, *W* = 350 HU, bins start at 20 keV

dkfz.

Spatial Resolution

- Small electrodes are necessary to avoid pile-up.
- High bias voltages (around 300 V) limit charge diffusion and thus blurring in the non-structured semiconductor layer.
- Thus, higher spatial resolution is achievable.

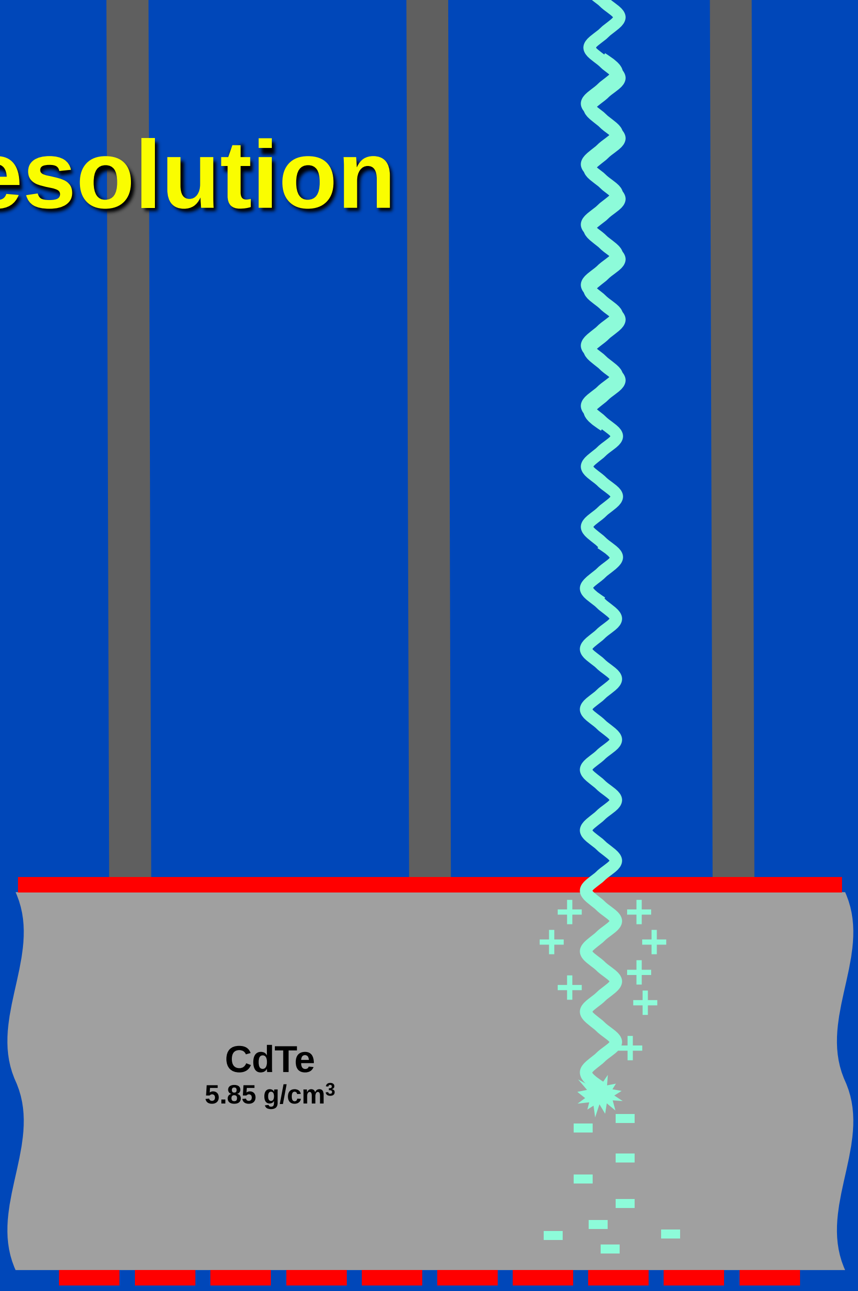

Ultra-High Resolution on Demand

Energy Integrating CT
(Somatom Flash)

Photon Counting CT
(Somatom CounT in UHR-Mode)

MAYO
CLINIC

Courtesy of Cynthia McCollough, Mayo Clinic, Rochester, USA.

The "Small Pixel Effect"

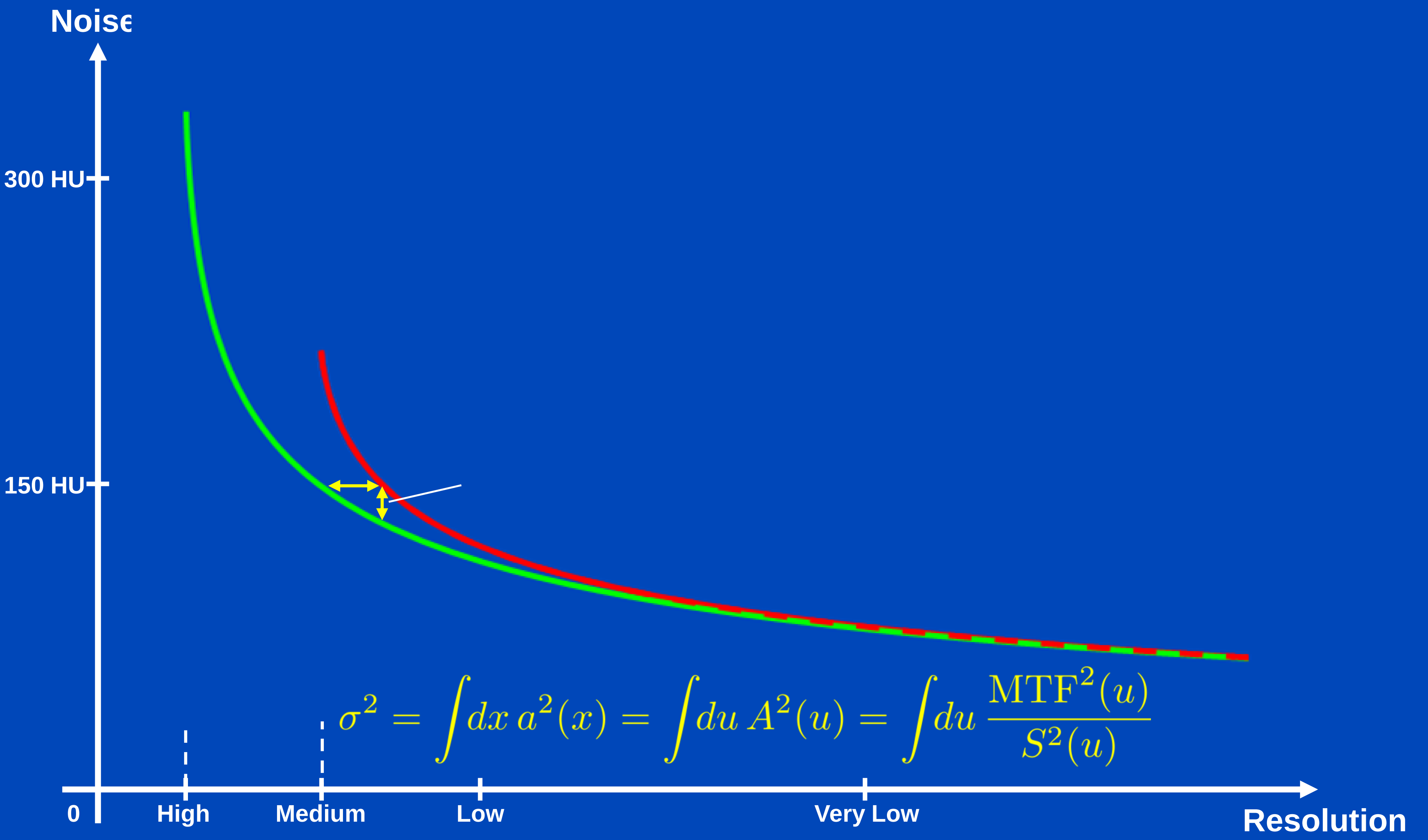

$$\sigma^2 = \int dx\, a^2(x) = \int du\, A^2(u) = \int du\, \frac{\mathrm{MTF}^2(u)}{S^2(u)}$$

All images reconstructed with 1024² matrix and 0.15 mm slice increment.
C = 1000 HU
W = 3500 HU

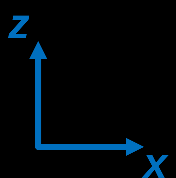

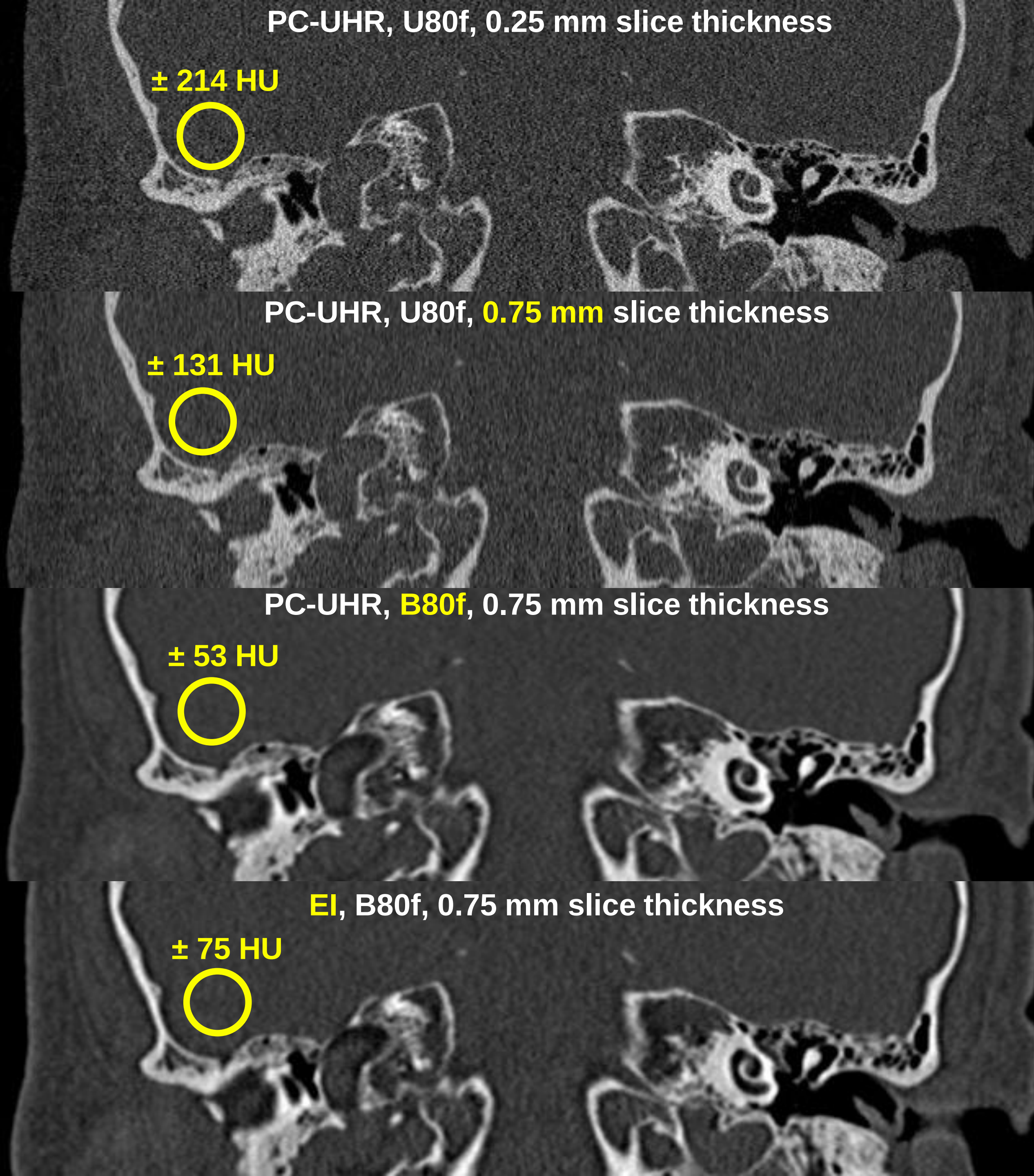

10% MTF: 19.1 lp/cm
10% MTF:17.2 lp/cm
xy FWHM: 0.48 mm
z FWHM: 0.40 mm
$CTDI_{vol}$: 16.0 mGy

10% MTF: 19.1 lp/cm
10% MTF:17.2 lp/cm
xy FWHM: 0.48 mm
z FWHM: 0.67 mm
$CTDI_{vol}$: 16.0 mGy

10% MTF: 9.3 lp/cm
10% MTF:10.5 lp/cm
xy FWHM: 0.71 mm
z FWHM: 0.67 mm
$CTDI_{vol}$: 16.0 mGy

10% MTF: 9.3 lp/cm
10% MTF:10.5 lp/cm
xy FWHM: 0.71 mm
z FWHM: 0.67 mm
$CTDI_{vol}$: 16.0 mGy

Data courtesy of the Institute of Forensic Medicine of the University of Heidelberg and of the Division of Radiology of the German Cancer Research Center (DKFZ)

dkfz.

L. Klein, C. Amato, S. Heinze, M. Uhrig, H.-P. Schlemmer, M. Kachelrieß, and S. Sawall. **Effects of Detector Sampling on Noise Reduction in a Clinical Photon Counting Whole-Body CT**. Investigative Radiology, vol. 55(2), in press, February 2020.

Energy Integrating Detector (B70f)

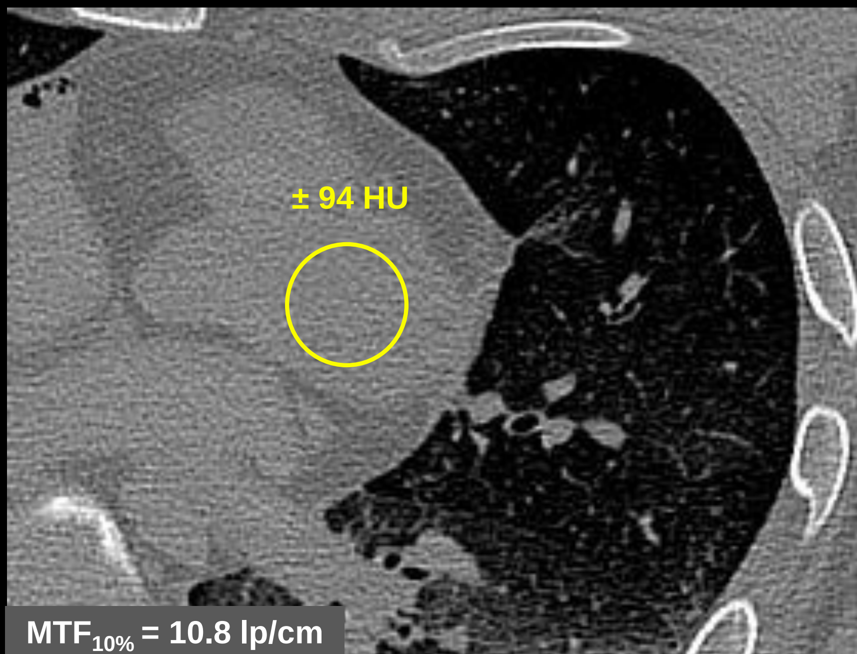

Acquisition with EI:

- Tube voltage of 120 kV
- Tube current of 300 mAs
- Resulting dose of $CTDI_{vol\ 32\ cm}$ = 22.6 mGy

Photon Counting Detector (B70f)

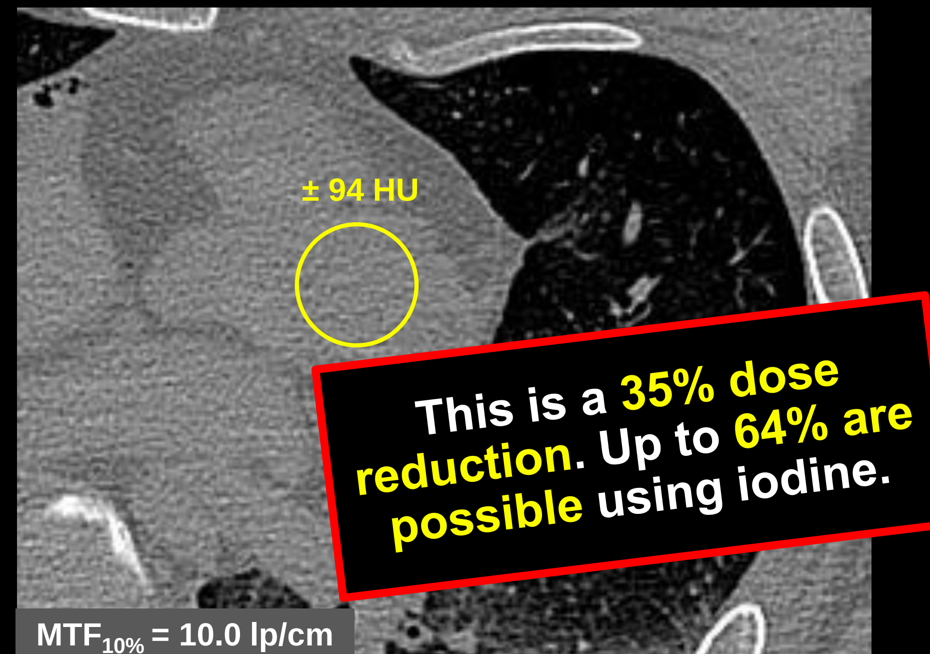

Acquisition with UHR:

- Tube voltage of 120 kV
- Tube current of 180 mAs
- Resulting dose of $CTDI_{vol\ 32\ cm}$ = 14.6 mGy

C = 50 HU, *W* = 1500 HU

MIP of low threshold images (20 keV)

Coronal Sagittal

Scan 1

Scan 2

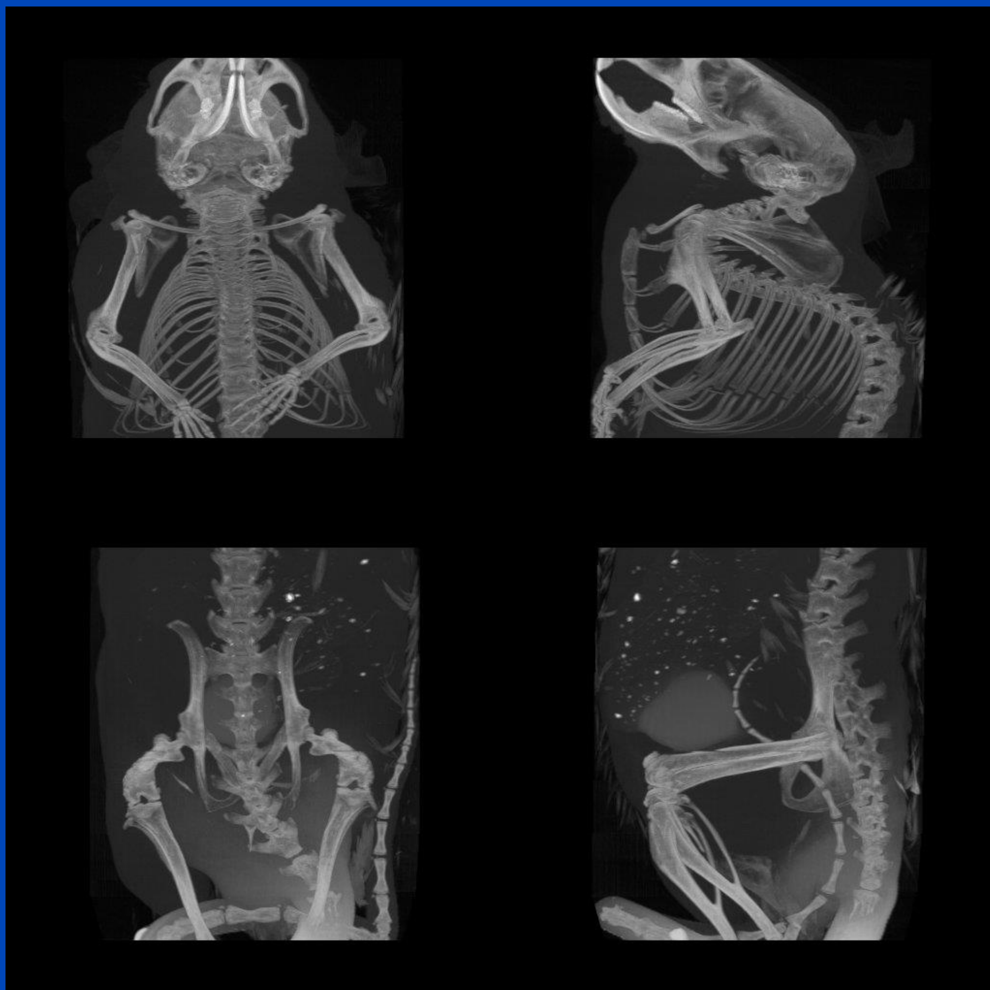

Scan at 60 kV of the late phase of iodine based contrast agent (iodine in the bladder). Part of the contrast agent was injected outside of the vessel (enhancement in the tail).

MIP of iodine and bone

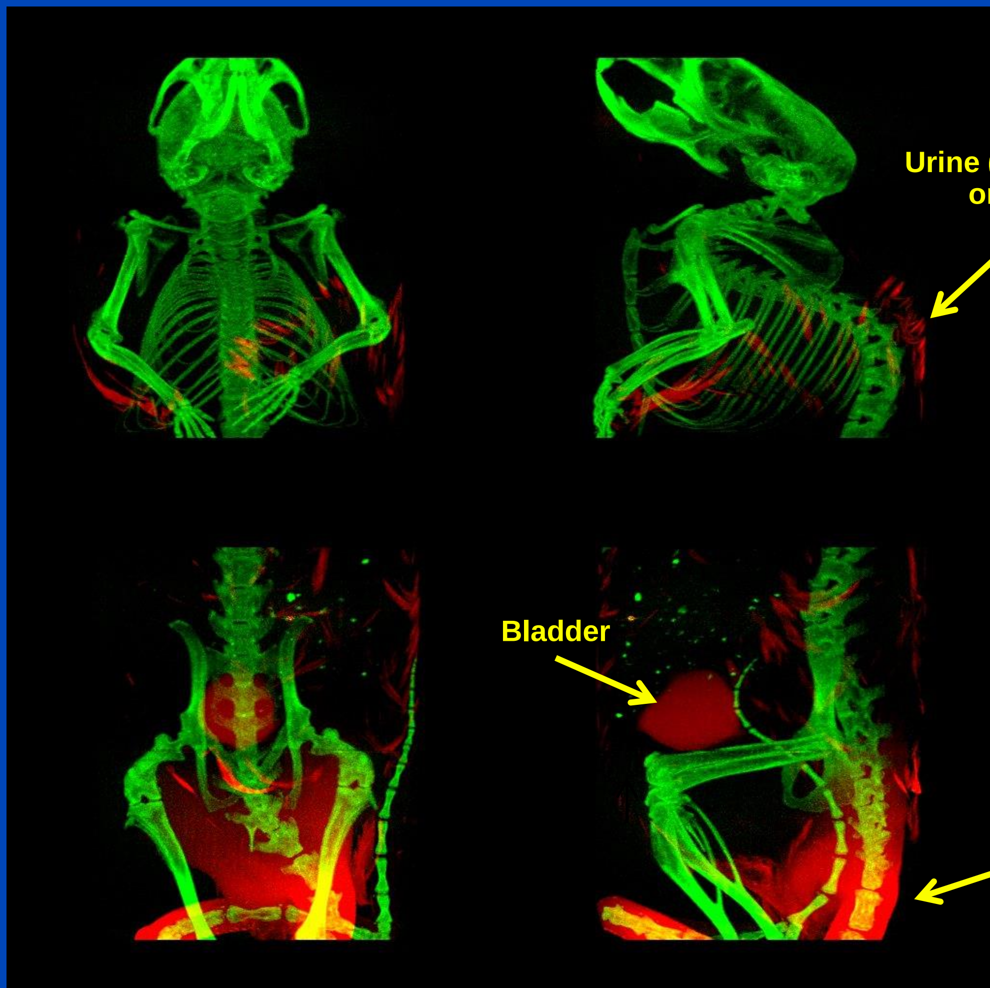

Energy thresholds at 20 and 32 keV.
Iodine k-edge at 33 keV.

Possibility to unambiguously differentiate iodine and bone.

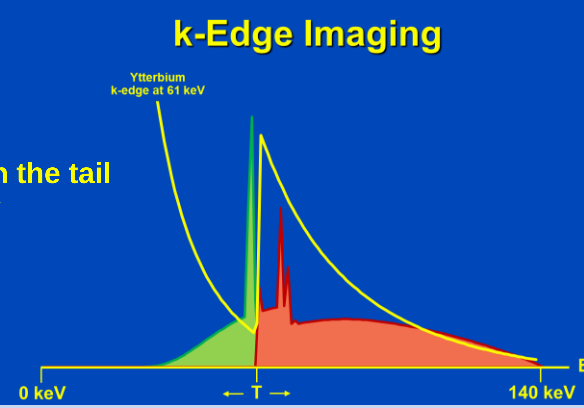

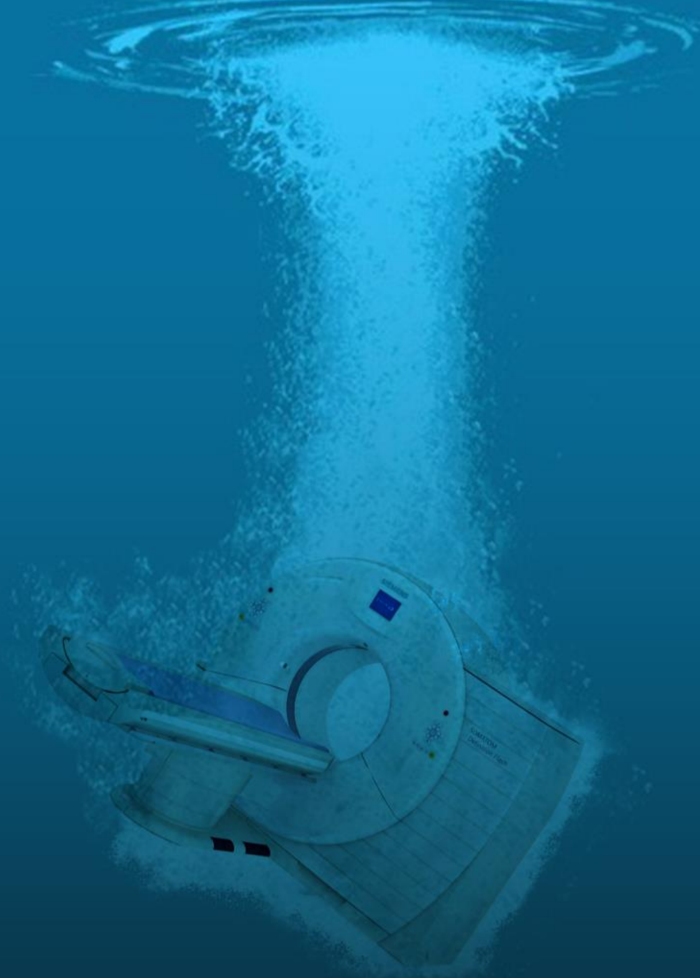

Deep Learning in CT

Fully Connected Neural Network

- Each layer fully connects to previous layer
- Difficult to train (many parameters in *W* and *b*)
- Spatial relations not necessarily preserved

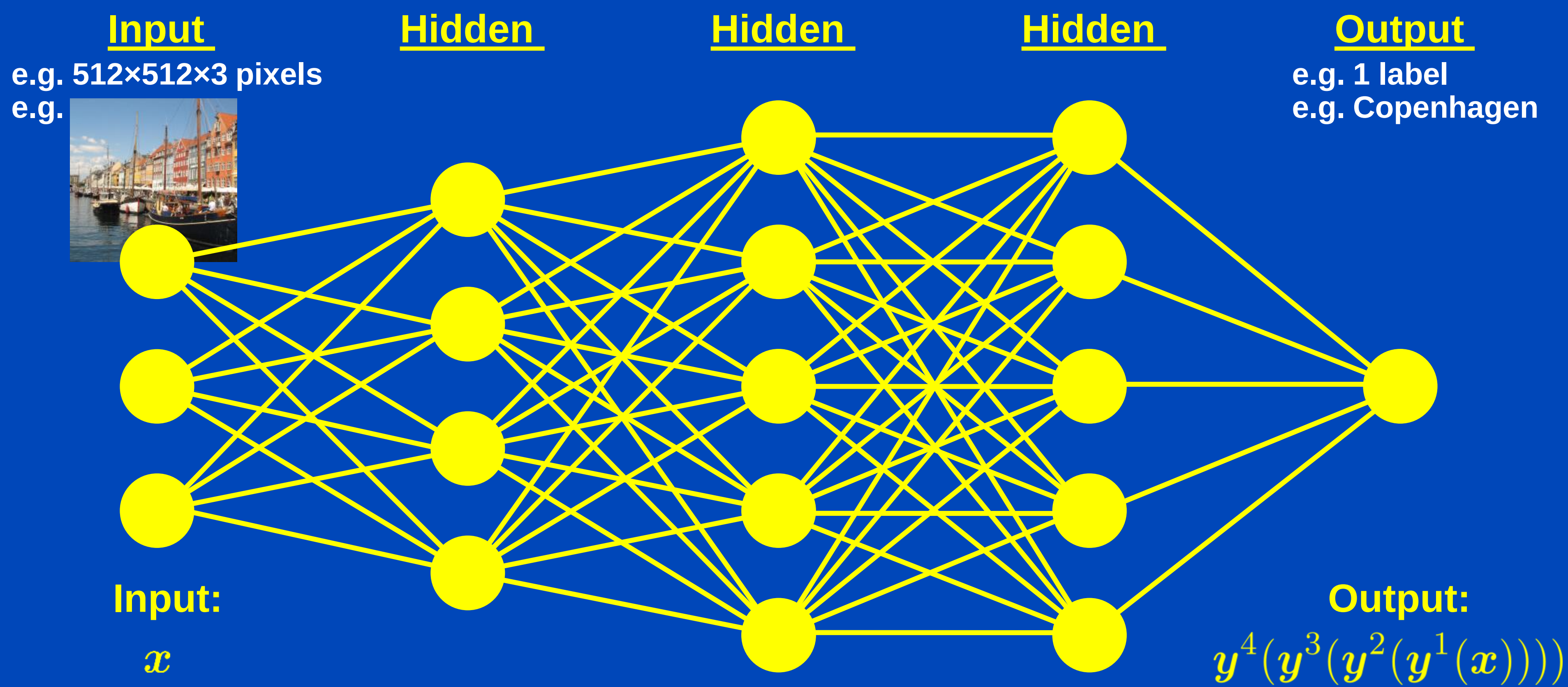

$\boldsymbol{y}(\boldsymbol{x}) = \boldsymbol{f}(\boldsymbol{W}\cdot\boldsymbol{x}+\boldsymbol{b})$ with $\boldsymbol{f}(\boldsymbol{x}) = \big(f(x_1), f(x_2), \ldots\big)$ point-wise scalar, e.g. $f(x) = x \vee 0 = \mathrm{ReLU}$

Convolutional Neural Network (CNN)

- Replace dense *W* in $y(x) = f(W \cdot x + b)$ by a sparse matrix *W* with sparsity being of convolutional type.
- CNNs consist (mainly) of convolutional layers.
- Convolutional layers are not fully connected.
- Convolutional layers are connected by small, say 3×3, convolution kernels whose entries need to be found by training.
- CNNs preserve spatial relations to some extent.

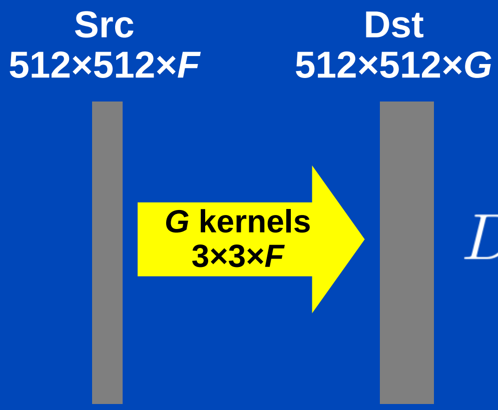

$$D_{i,j,g} = \sum_f S_{i,j,f} * K^g_{i,j,f} = \sum_{a,b,f} S_{i-a,j-b,f} K^g_{a,b,f}$$

Attention: No convolution in depth direction!

U-Net[1]

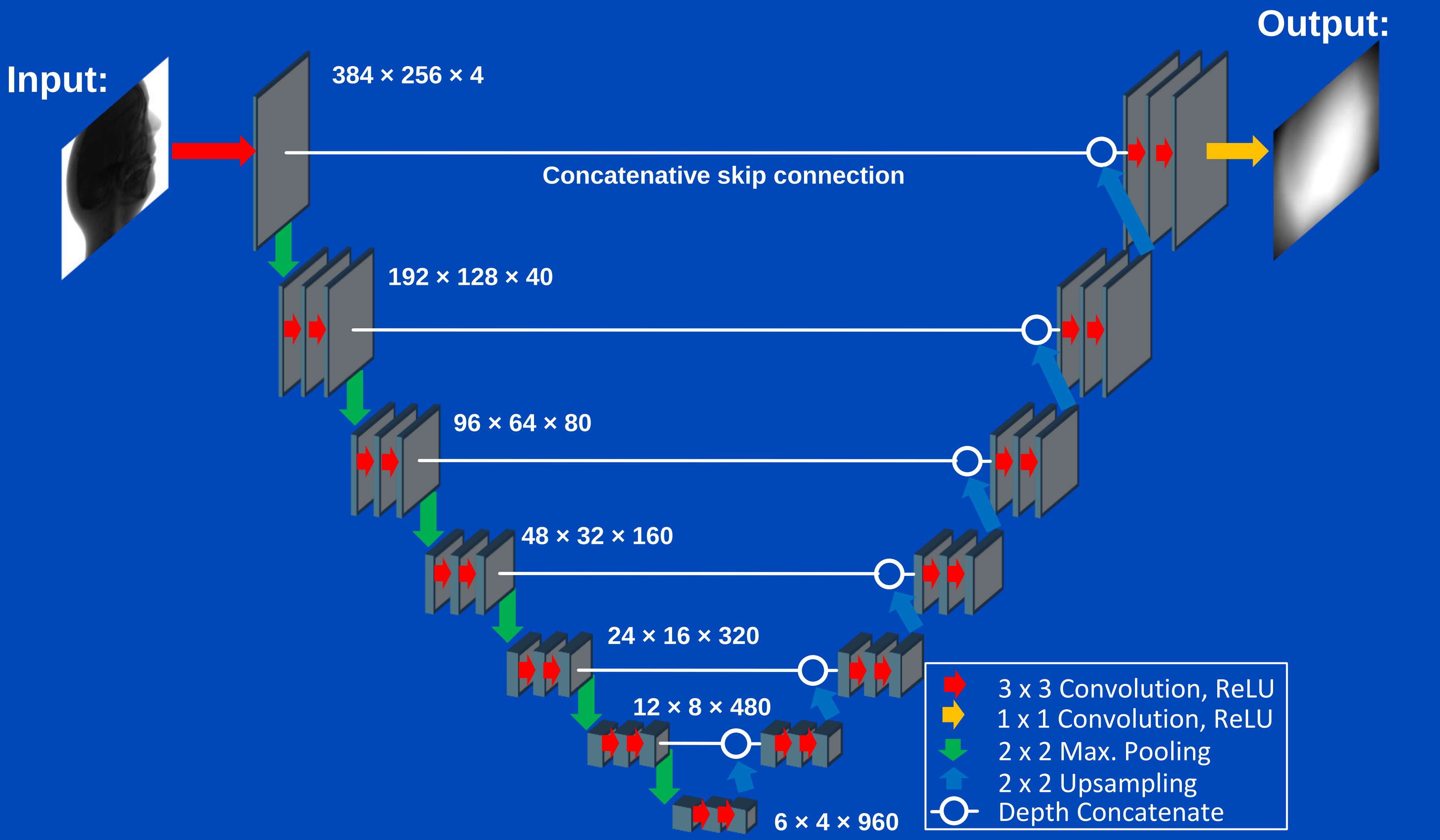

[1]O. Ronneberger, P. Fischer, and T. Brox. U-net: Convolutional networks for biomedical image segmentation. Proc. MICCAI:234-241, 2015.

Generative Adversarial Network[1] (GAN)

- Useful, if no direct ground truth (GT) is available, the training data are unpaired, unsupervised learning

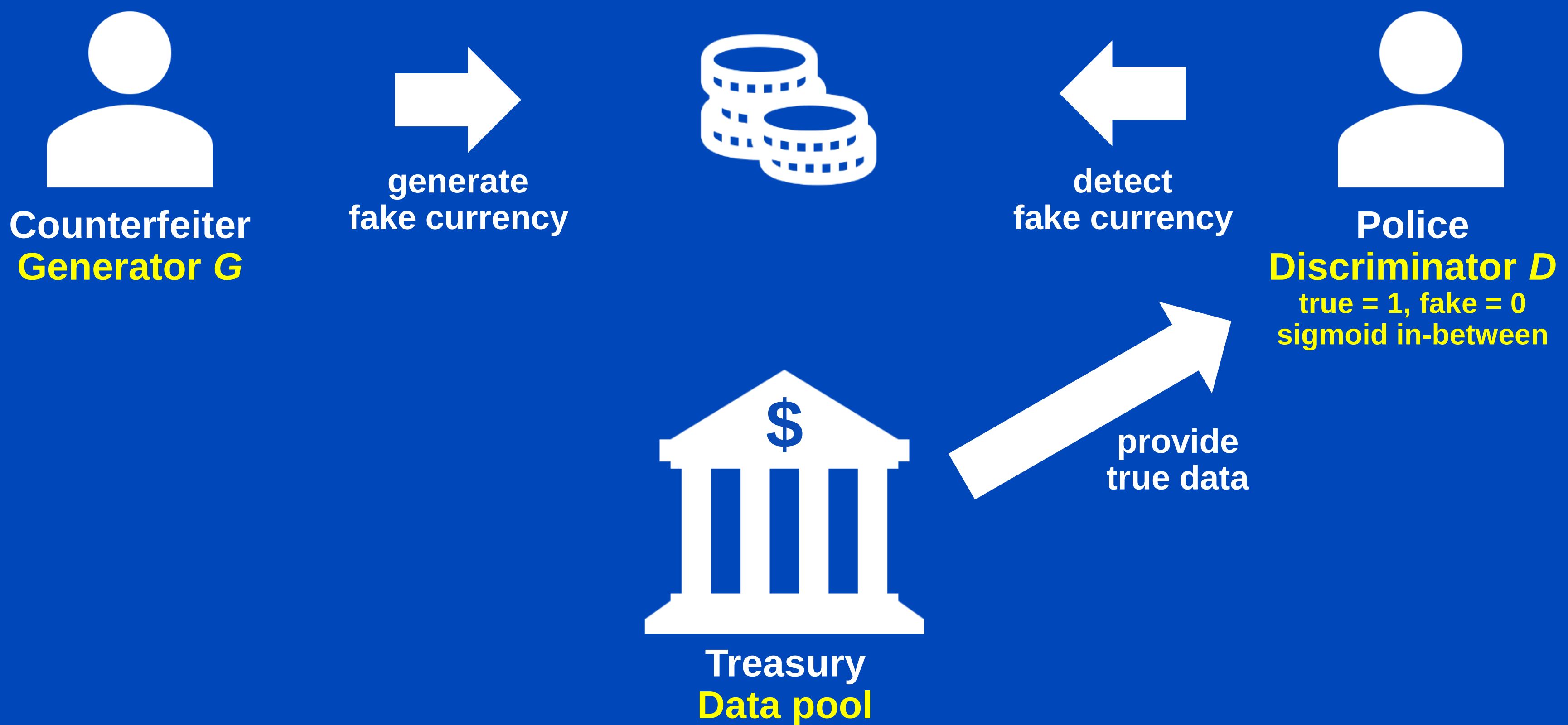

[1] I. Goodfellow et al. Generative Adversarial Nets, arXiv 2014

dkfz.

Metal Artifact Reduction Example

- Deep CNN-driven patch-based combination of the advantages of several MAR methods trained on simulated artifacts

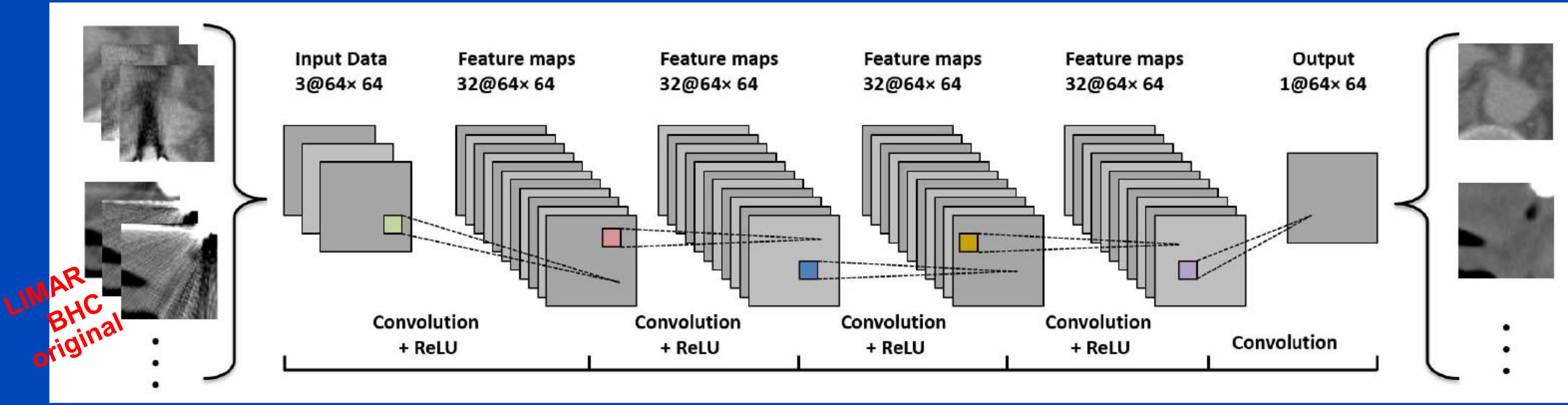

- followed by segmentation into tissue classes
- followed by forward projection of the CNN prior and replacement of metal areas of the original sinogram
- followed by reconstruction

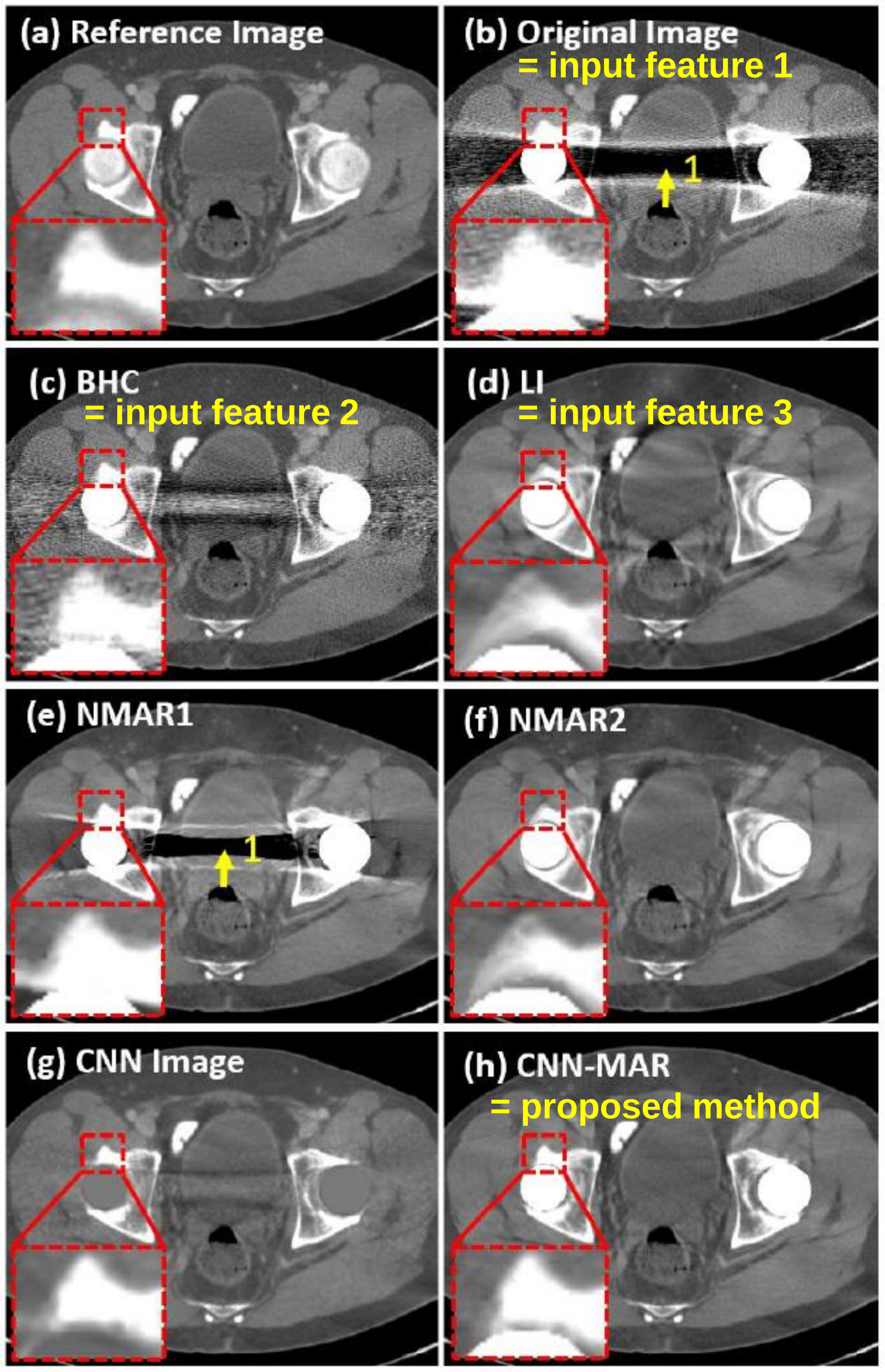
(a) Reference Image
(b) Original Image
= input feature 1
1
(c) BHC
= input feature 2
(d) LI
= input feature 3
(e) NMAR1
1
(f) NMAR2
(g) CNN Image
(h) CNN-MAR
= proposed method

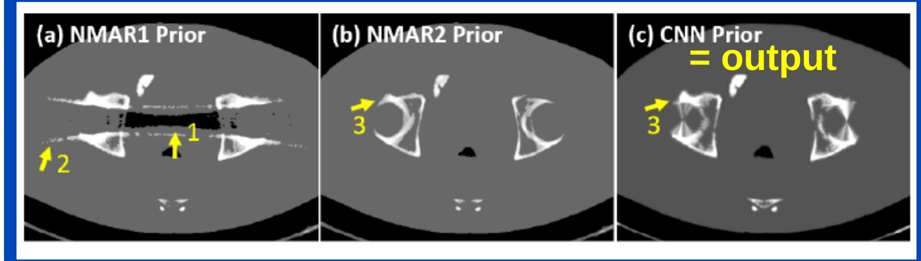
(a) NMAR1 Prior
1
2
(b) NMAR2 Prior
3
(c) CNN Prior
= output
3

Sparse View Restoration Example

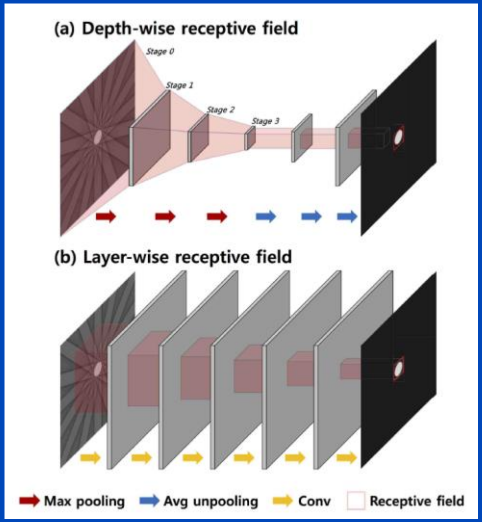

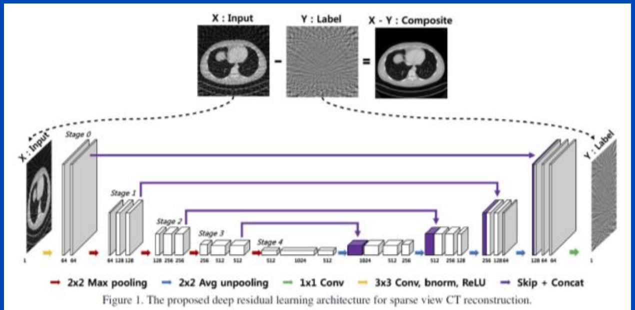

Figure 1. The proposed deep residual learning architecture for sparse view CT reconstruction.

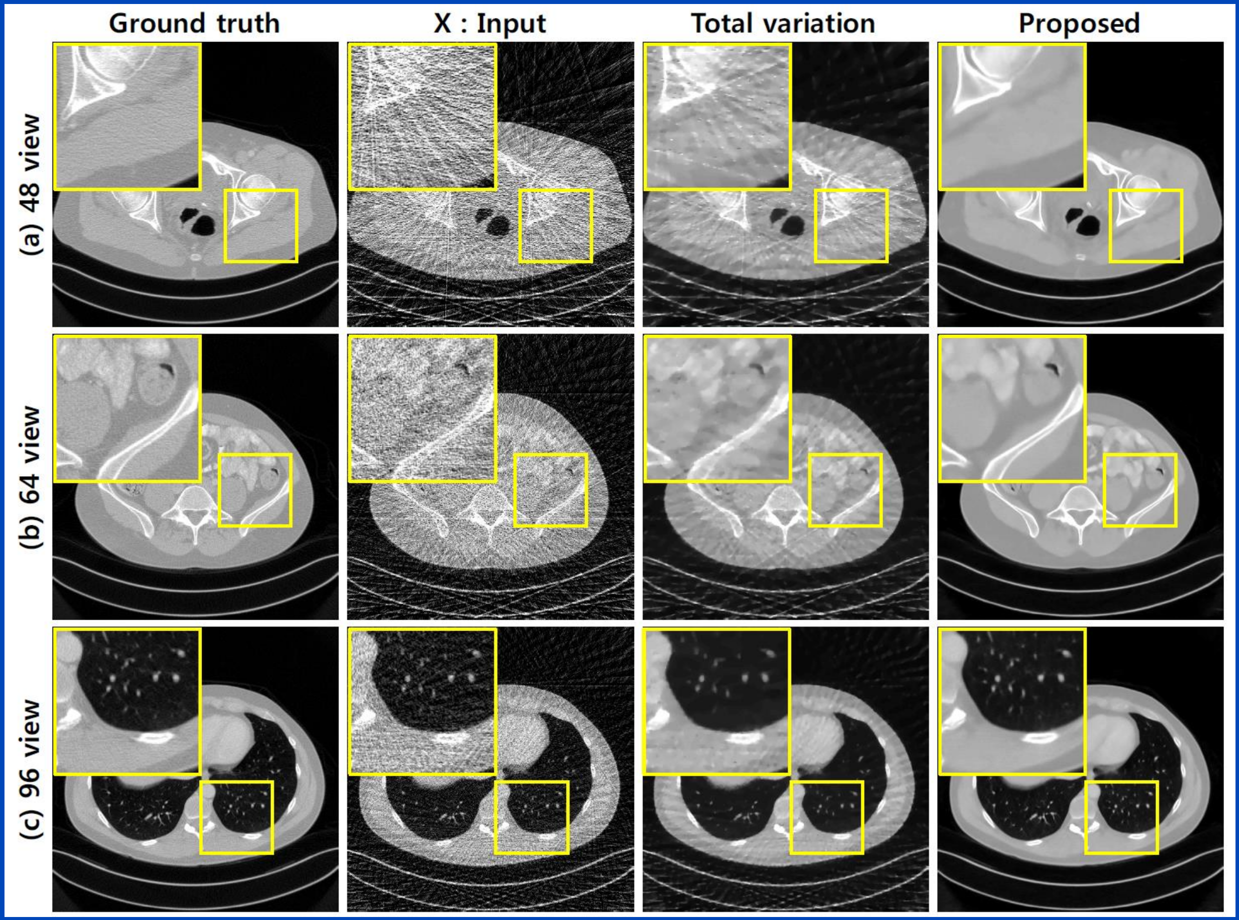

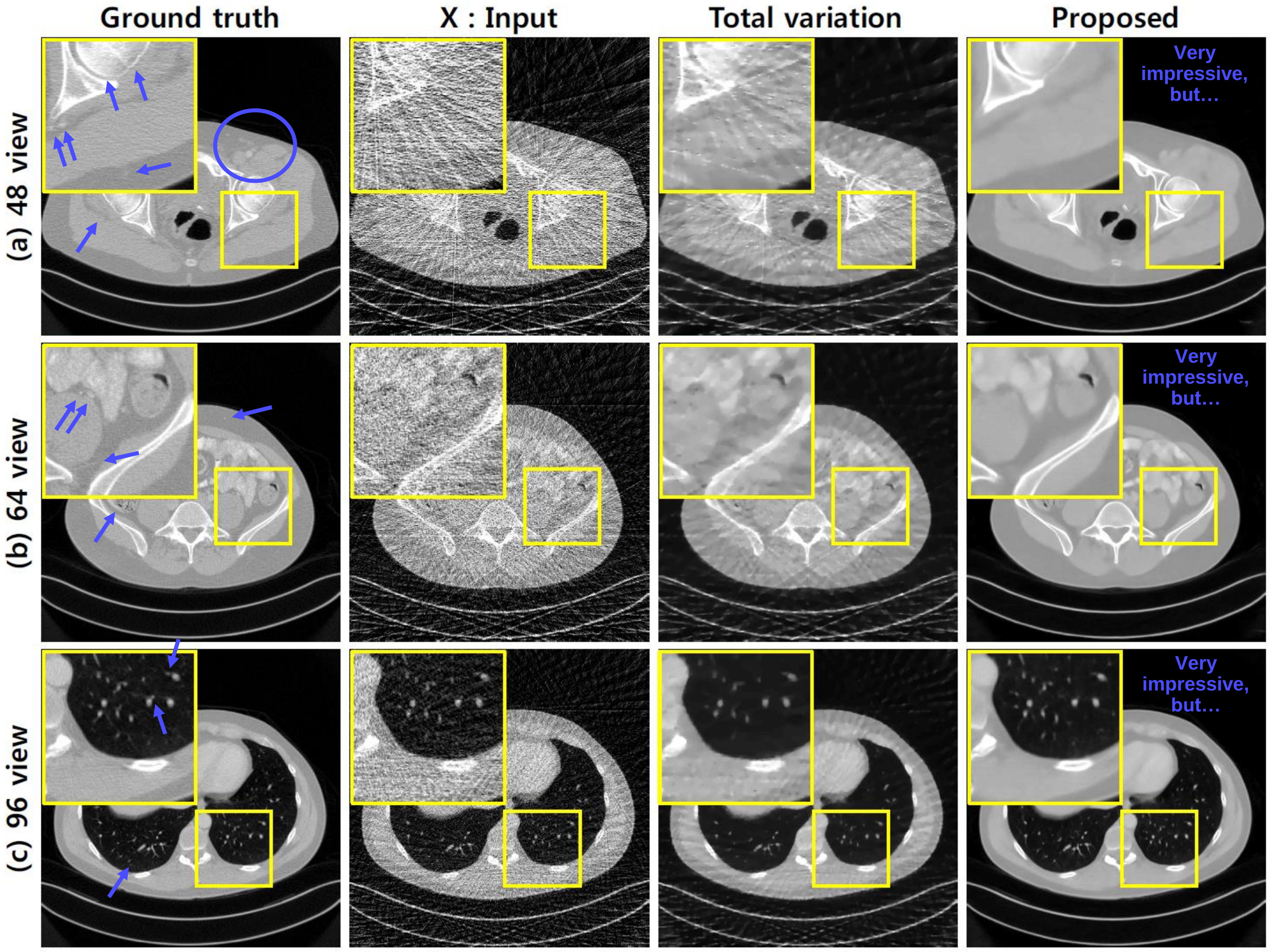

Ground truth
X : Input
Total variation
Proposed
(a) 48 view
(b) 64 view
(c) 96 view
Very impressive, but…
Very impressive, but…
Very impressive, but…

Noise Removal Example

- Task: Reduce noise from low dose CT images.
- A conditional generative adversarial networks (GAN) is used
- Generator *G*:
  - 3D CNN that operates on small cardiac CT sub volumes
  - Seven 3×3×3 convolutional layers yielding a receptive field of 15×15×15 voxels for each destination voxel
  - Depths (features) from 32 to 128
  - Batch norm only in the hidden layers
  - Subtracting skip connection
- Discriminator *D*:
  - Sees either routine dose image or a generator-denoised low dose image
  - Two 3×3×3 layers followed by several 3×3 layers with varying strides
  - Feedback from *D* prevents smoothing.
- Training:
  - Unenhanced (why?) patient data acquired with Philips Briliance iCT 256 at 120 kV.
  - Two scans (why?) per patient, one with 0.2 mSv and one with 0.9 mSv effective dose.

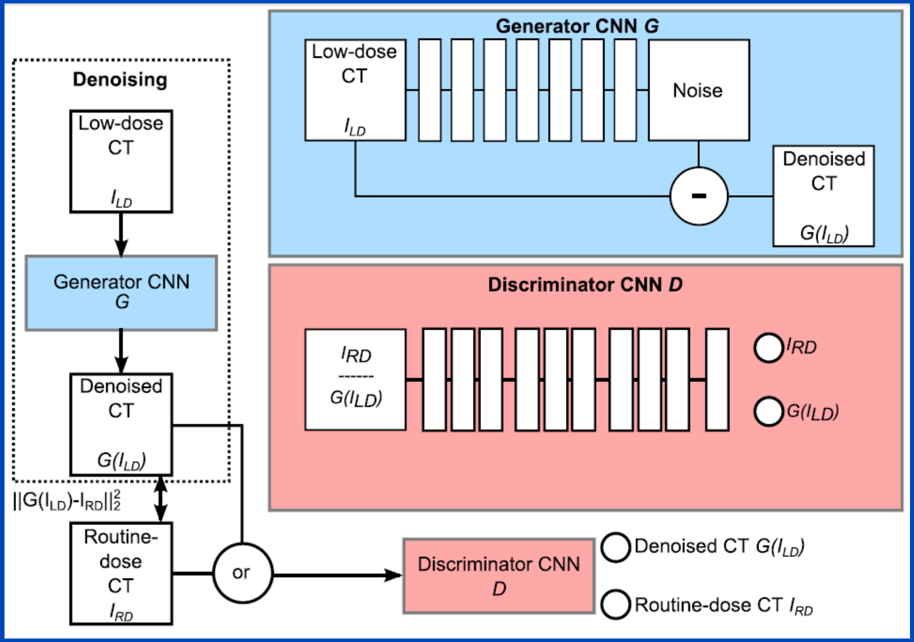

J. Wolterink, T. Leiner, M. Viergever, and I. Išgum. Generative Adversarial Networks for Noise Reduction in Low-Dose CT. IEEE TMI 36(12):2536-2544, Dec. 2017.

Noise Removal Example

Low dose image (0.2 mSv)

Noise Removal Example

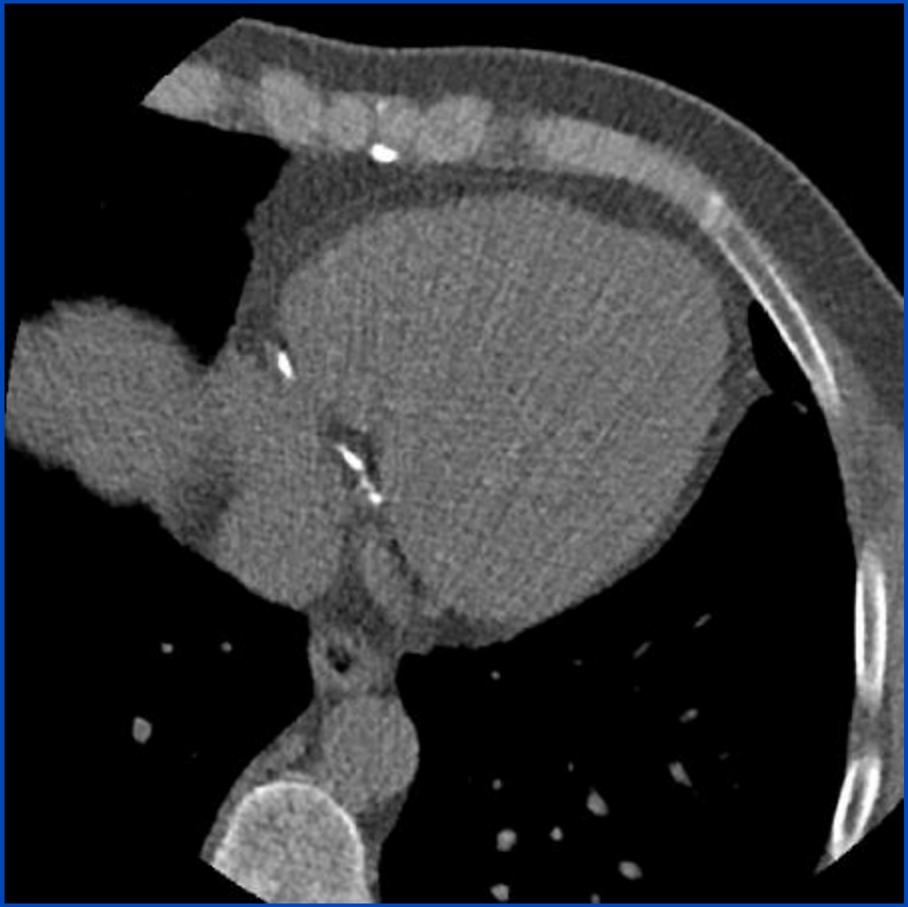

iDose level 3 reconstruction (0.2 mSv)

Noise Removal Example

Denoised low dose image (0.2 mSv)

J. Wolterink, T. Leiner, M. Viergever, and I. Išgum. Generative Adversarial Networks for Noise Reduction in Low-Dose CT. IEEE TMI 36(12):2536-2544, Dec. 2017.

Noise Removal Example

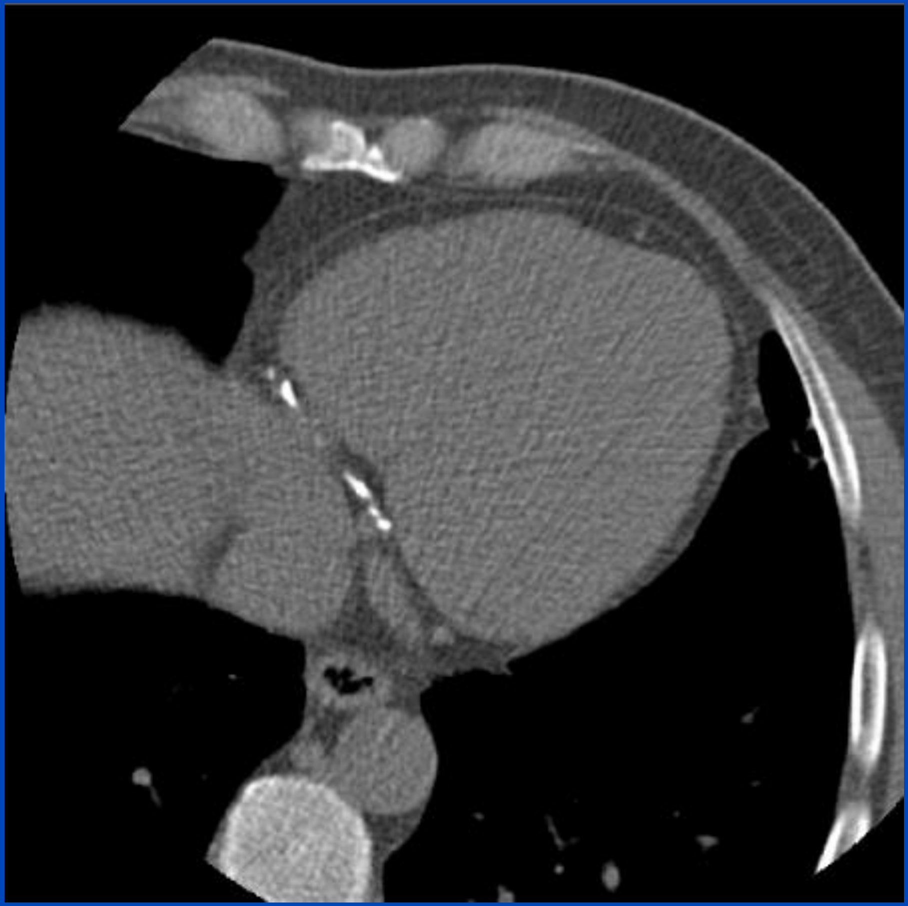

Normal dose image (0.9 mSv)

J. Wolterink, T. Leiner, M. Viergever, and I. Išgum. Generative Adversarial Networks for Noise Reduction in Low-Dose CT. IEEE TMI 36(12):2536-2544, Dec. 2017.

Deep Scatter Estimation

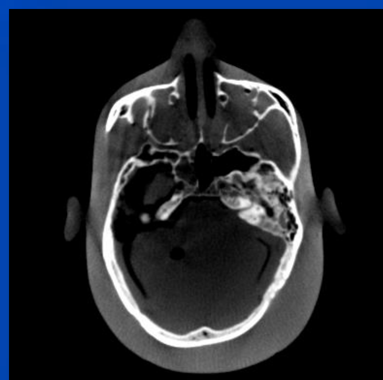

???

In real time?

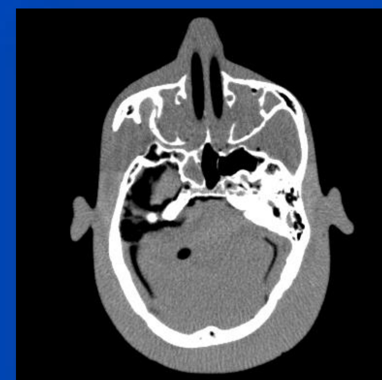

Monte Carlo Scatter Estimation

- Simulation of photon trajectories according to physical interaction probabilities.
- Simulating a large numb… …ories well approximat…

1 to 10 hours per tomographic data set

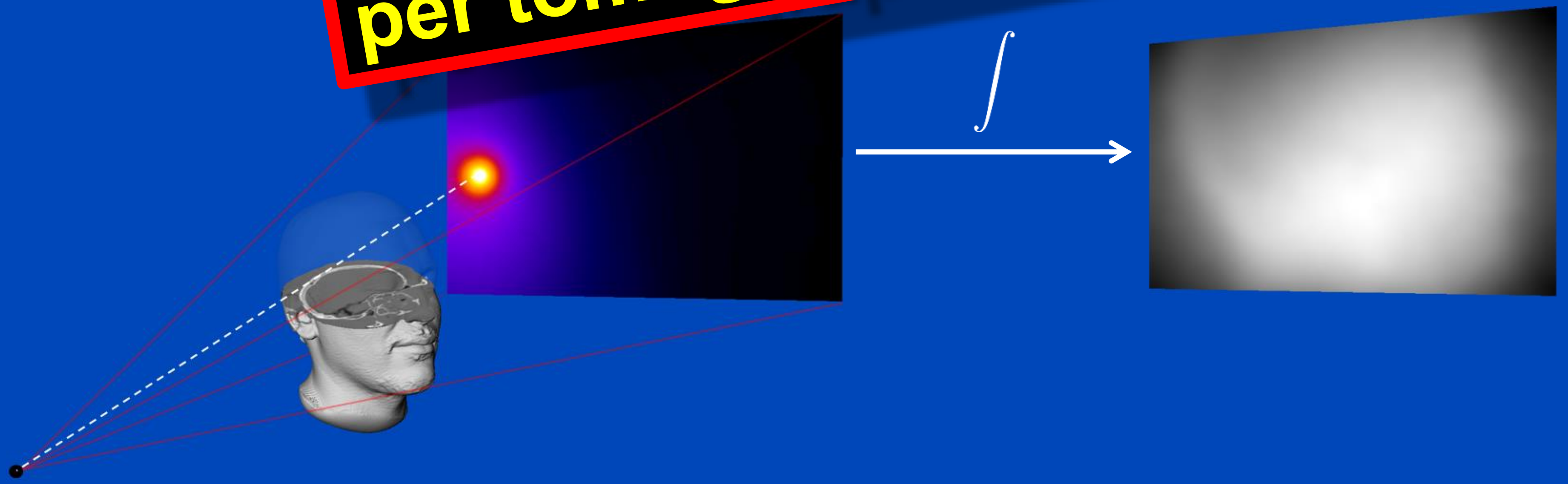

Deep Scatter Estimation

Network architecture & scatter estimation framework

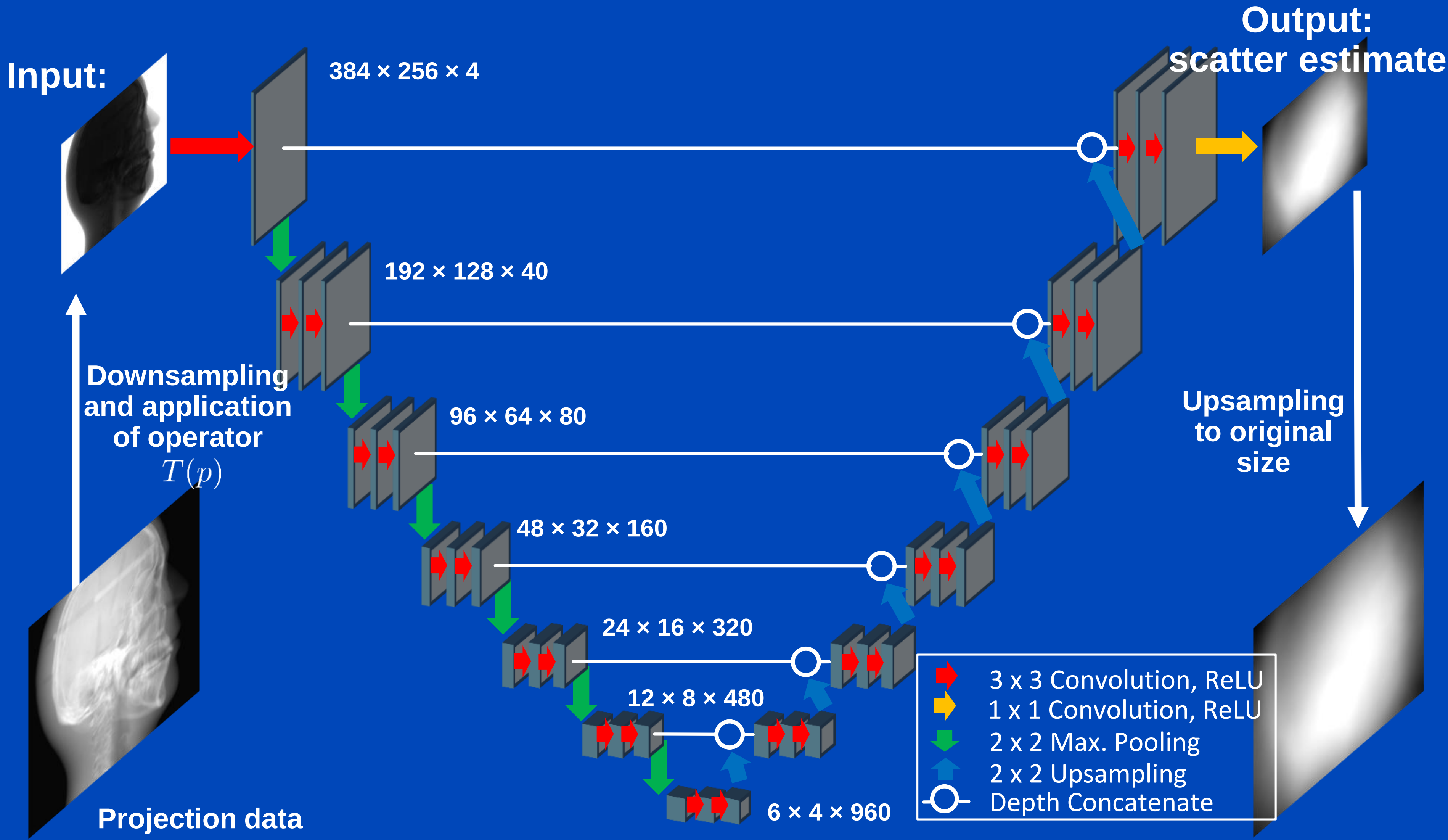

Deep Scatter Estimation (DSE)

Train a deep convolutional neural network (C N) to estimate scatter using a functio d projection data as in

0.1 to 1 minute
per tomographic data set

Input: $T(p)$

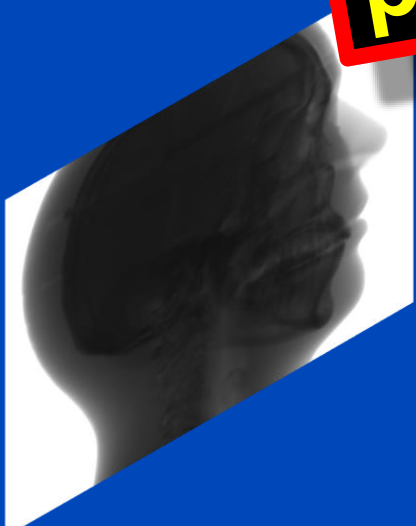

~~Monte Carlo~~

Convolutional neural network

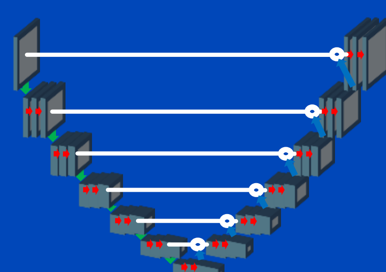

Scatter estimate

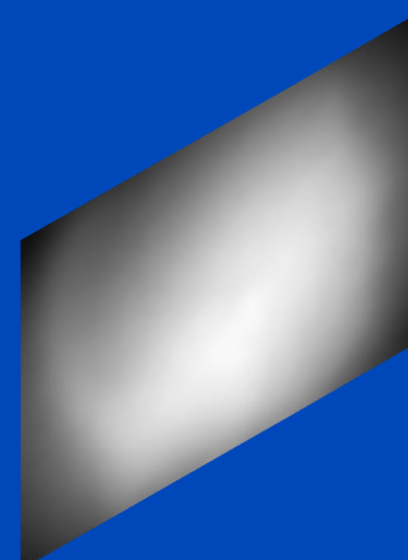

J. Maier, M. Kachelrieß et al. Deep scatter estimation (DSE). SPIE 2017 and Journal of Nondestructive Evaluation 37:57, July 2018.
J. Maier, M. Kachelrieß et al. Robustness of DSE. Med. Phys. 46(1):238-249, January 2019.

Results on Simulated Projection Data

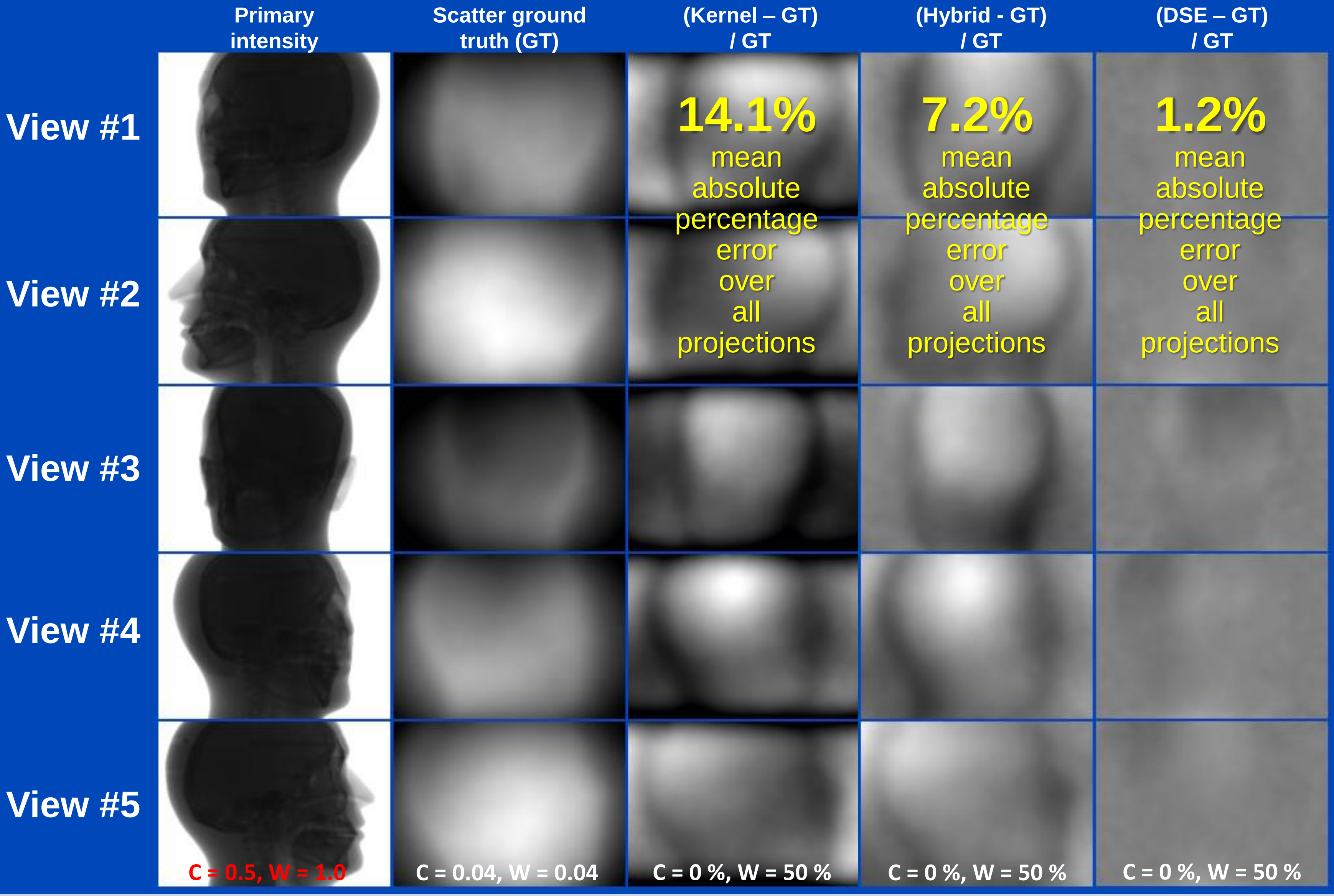

DSE trained to estimate scatter from **primary plus scatter**: High accuracy

dkfz.

Reconstructions of Measured Data

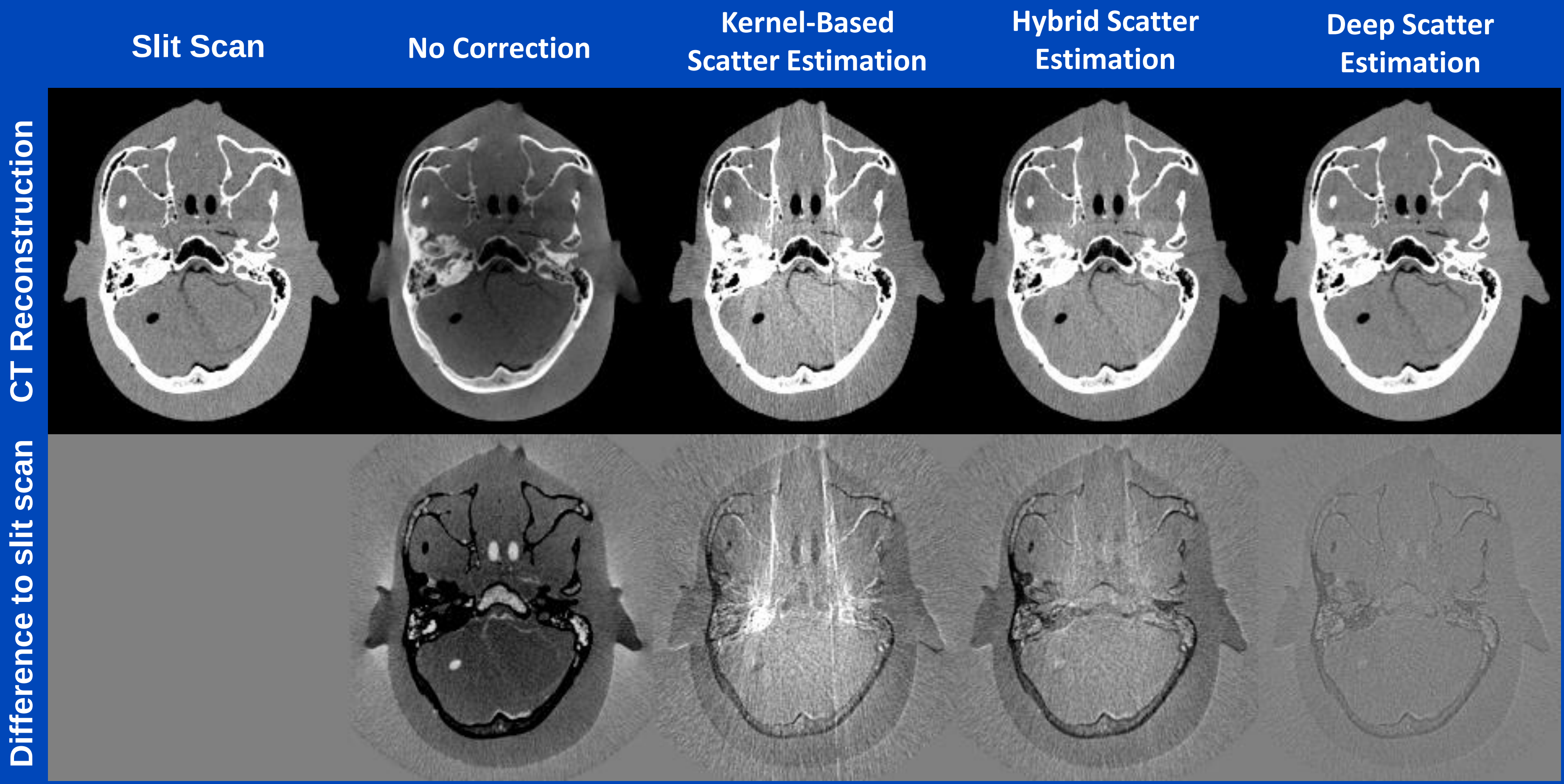

C = 0 HU, W = 1000 HU

J. Maier, M. Kachelrieß et al. Deep scatter estimation (DSE). SPIE 2017 and Journal of Nondestructive Evaluation 37:57, July 2018.
J. Maier, M. Kachelrieß et al. Robustness of DSE. Med. Phys. 46(1):238-249, January 2019.

A simple detruncation was applied to the rawdata before reconstruction. Images were clipped to the FOM before display. *C* = -200 HU, *W* = 1000 HU.

Truncated DSE[1,2]

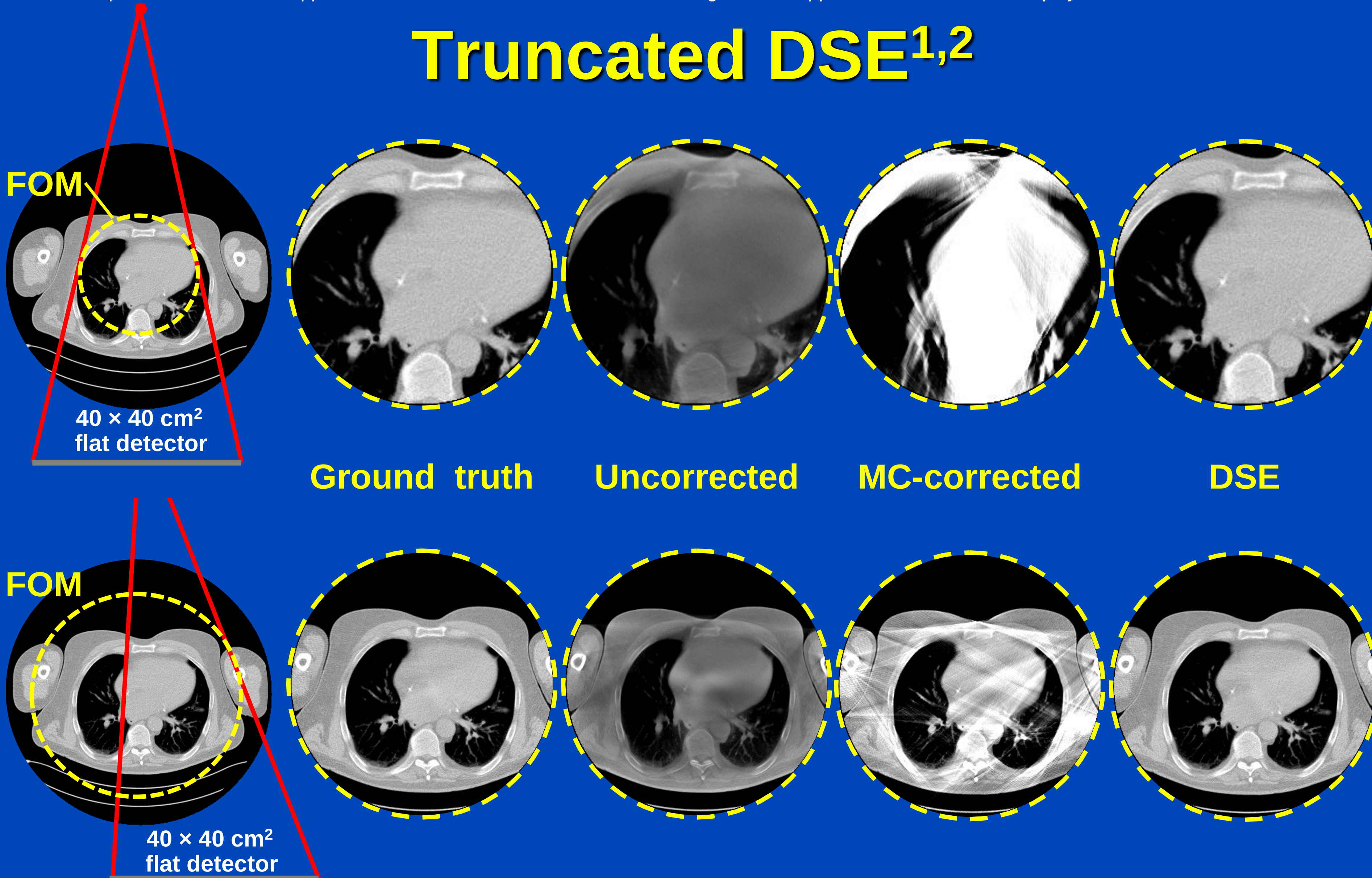

To learn why MC fails at truncated data and what significant efforts are necessary to cope with that situation see [Kachelrieß et al. Effect of detruncation on the accuracy of MC-based scatter estimation in truncated CBCT. Med. Phys. 45(8):3574-3590, August 2018].

[1]J. Maier, M. Kachelrieß et al. Deep scatter estimation (DSE) for truncated cone-beam CT (CBCT). RSNA 2018.
[2]J. Maier, M. Kachelrieß et al. Robustness of DSE. Med. Phys. 46(1):238-249, January 2019.

Results

KSE	Head	Thorax	Abdomen
Head	14.5	26.8	32.5
Thorax	16.2	18.5	19.4
Abdomen	16.8	22.1	17.8
All data	14.9	20.5	19.3

DSE	Head	Thorax	Abdomen
Head	1.2	21.1	32.7
Thorax	8.8	1.5	9.1
Abdomen	11.9	10.9	1.3
All data	1.8	1.4	1.4

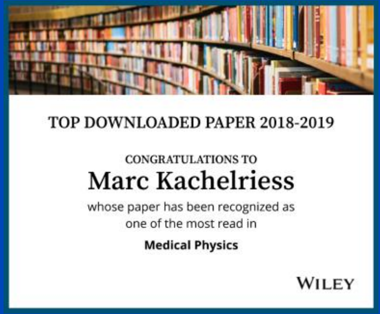

Values shown are the mean absolute percentage errors (MAPEs) of the testing data.
Note that thorax and head suffer from truncation due to the small size of the 40×30 cm flat detector.

J. Maier, M. Kachelrieß et al. Deep scatter estimation (DSE). SPIE 2017 and Journal of Nondestructive Evaluation 37:57, July 2018.
J. Maier, M. Kachelrieß et al. Robustness of DSE. Med. Phys. 46(1):238-249, January 2019.

Deep Dose Estimation

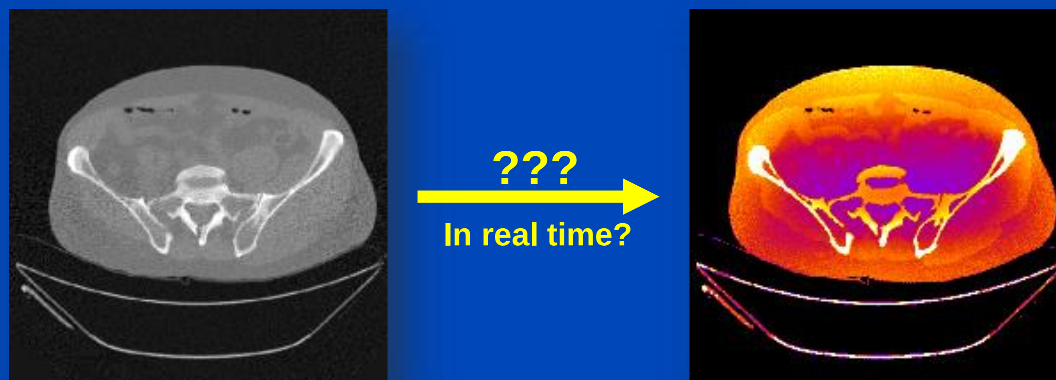

Deep Dose Estimation (DDE)

- **Combine fast and accurate CT dose estimation using a deep convolutional neural network.**
- **Train the network to reproduce MC dose estimates given the CT image and a first-order dose estimate.**

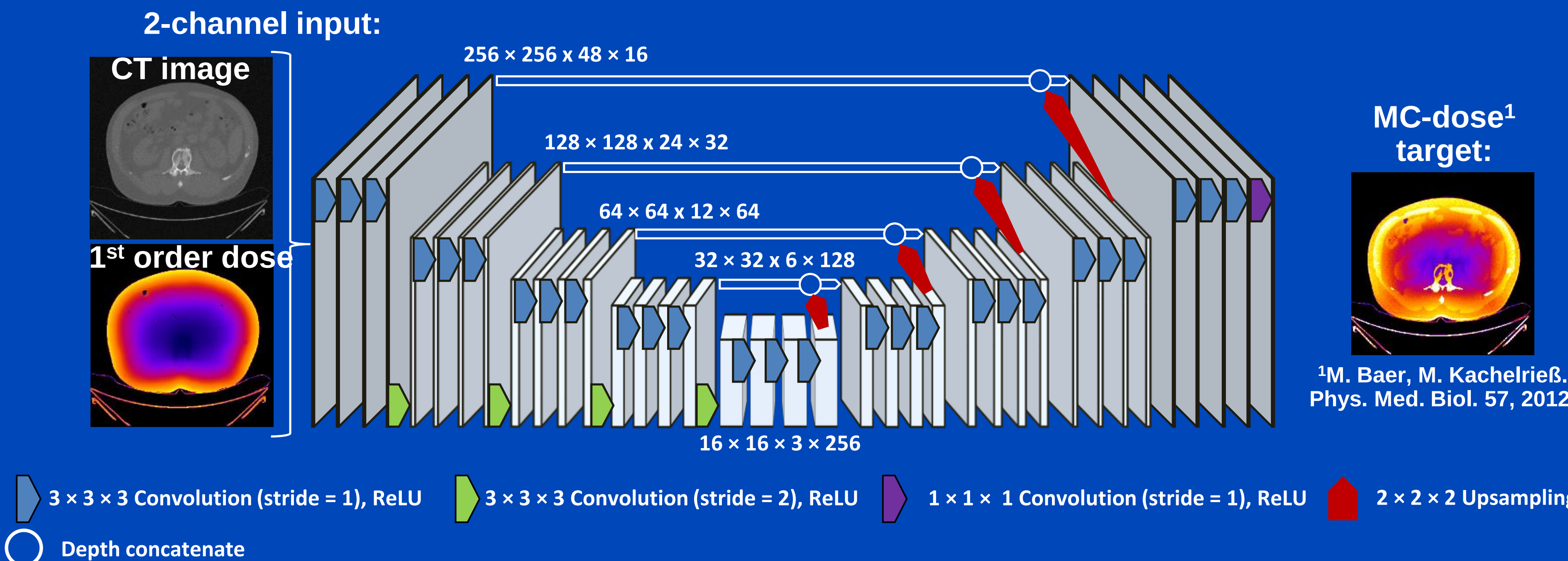

[1]M. Baer, M. Kachelrieß. Phys. Med. Biol. 57, 2012.

J. Maier, E. Eulig, S. Sawall, and M. Kachelrieß. Real-time patient-specific CT dose estimation using a deep convolutional neural network, Proc. IEEE MIC 2018 and ECR Book of Abstracts 2019. *Best Paper within Machine Learning at ECR 2019!*

dkfz.

Results

Thorax, tube A, 120 kV, no bowtie

CT image

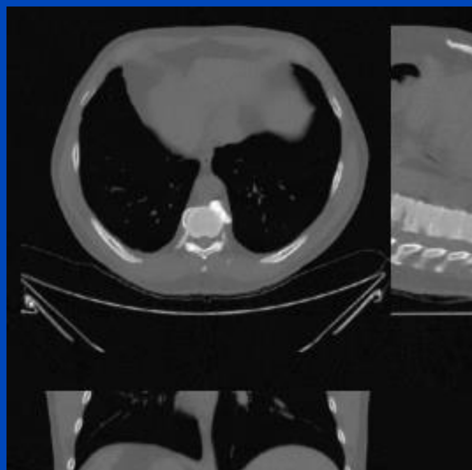

First order dose

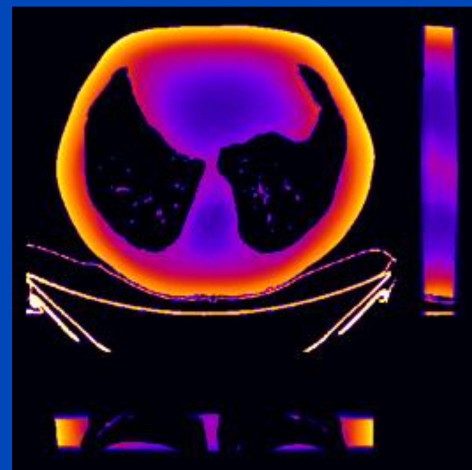

	MC	DDE
48 slices	1 h	0.25 s
whole body	20 h	5 s

MC uses 16 CPU kernels
DDE uses one Nvidia Quadro P600 GPU

DDE training took 74 h for 300 epochs, 1440 samples, 48 slices per sample

MC ground truth

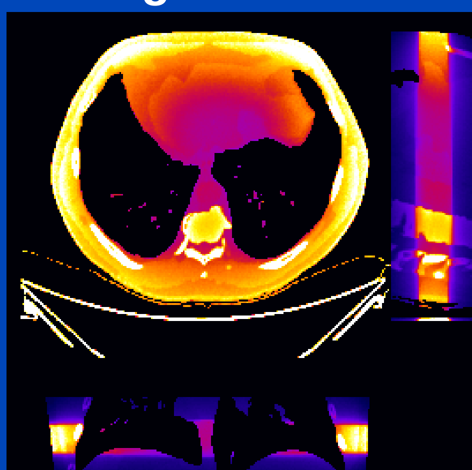

DDE

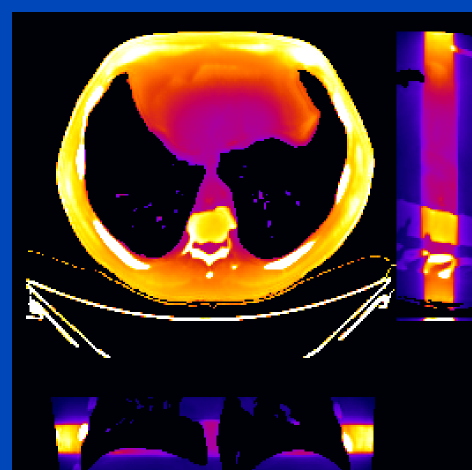

Relative error

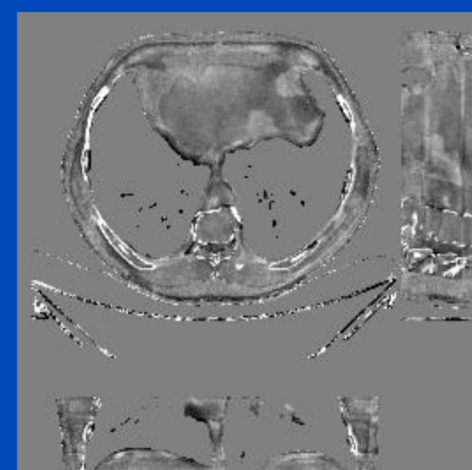

C = 0%
W = 40%

J. Maier, E. Eulig, S. Sawall, and M. Kachelrieß. Real-time patient-specific CT dose estimation using a deep convolutional neural network, Proc. IEEE MIC 2018 and ECR Book of Abstracts 2019. *Best Paper within Machine Learning at ECR 2019!*

Deep Cardiac Motion Compensation

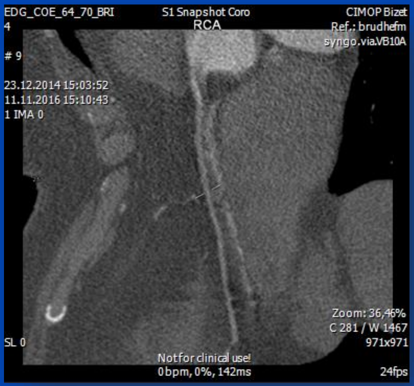

???

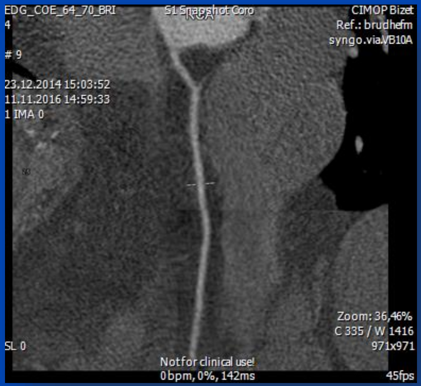

Motion Compensation for Cardiac CT

Input: CT image with motion artifacts

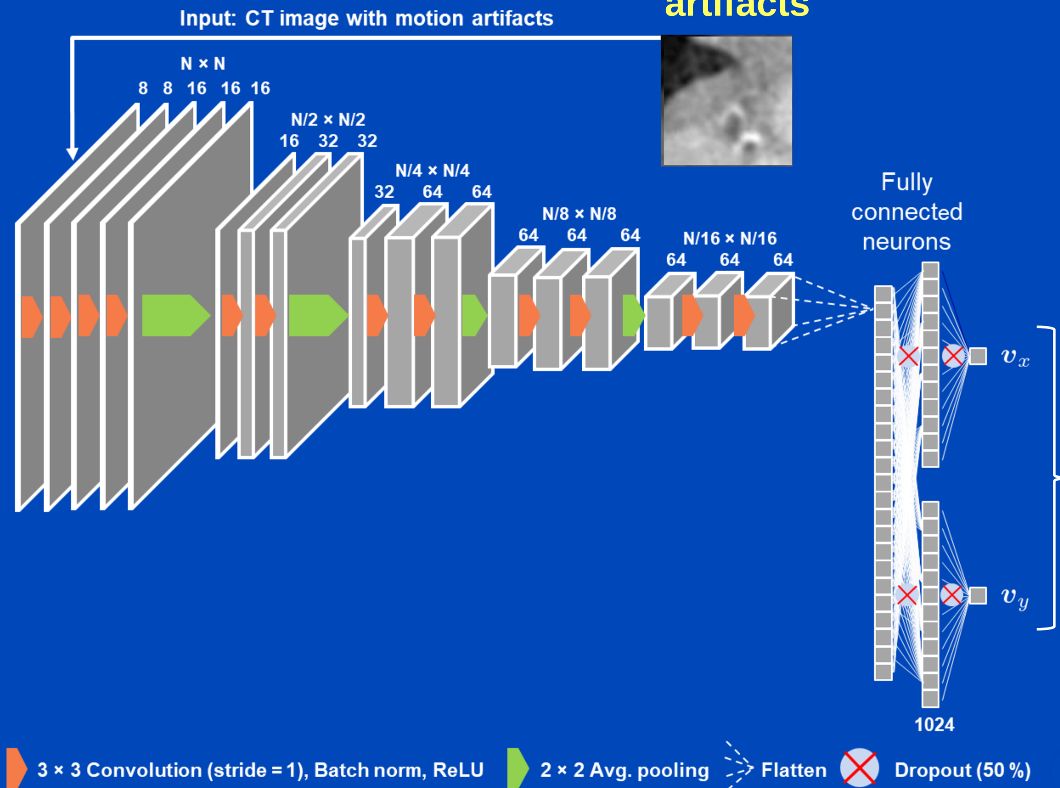

Output: motion direction (to be used by MoCo recon)

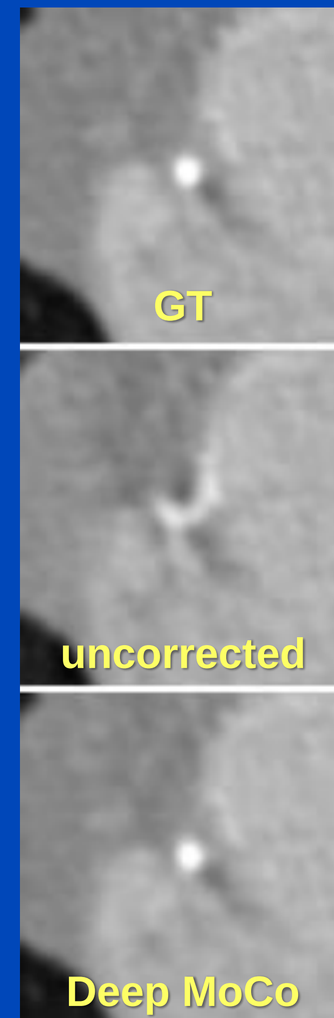

J. Maier, S. Lebedev, E. Eulig, S. Sawall, E. Fournié, K. Stierstorfer, and M. Kachelrieß .Coronary artery motion compensation for short-scan cardiac CT using a spatial transformer network. Conference Program of the 6th International CT-Meeting, August 2020.

Deep PAMoCo

Network architecture

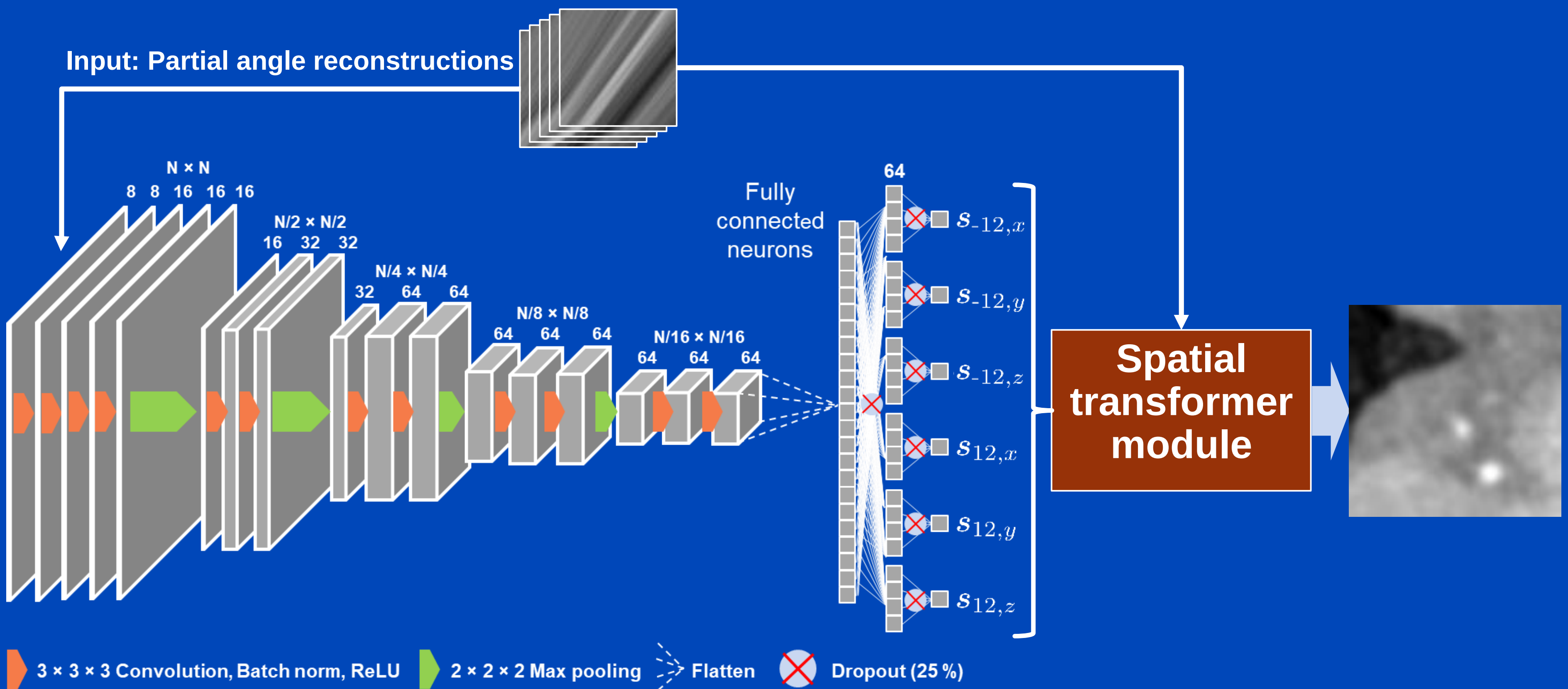

J. Maier, S. Lebedev, E. Eulig, S. Sawall, E. Fournié, K. Stierstorfer, and M. Kachelrieß .Coronary artery motion compensation for short-scan cardiac CT using a spatial transformer network. Conference Program of the 6th International CT-Meeting, August 2020.

Results

Measurements, patient 1

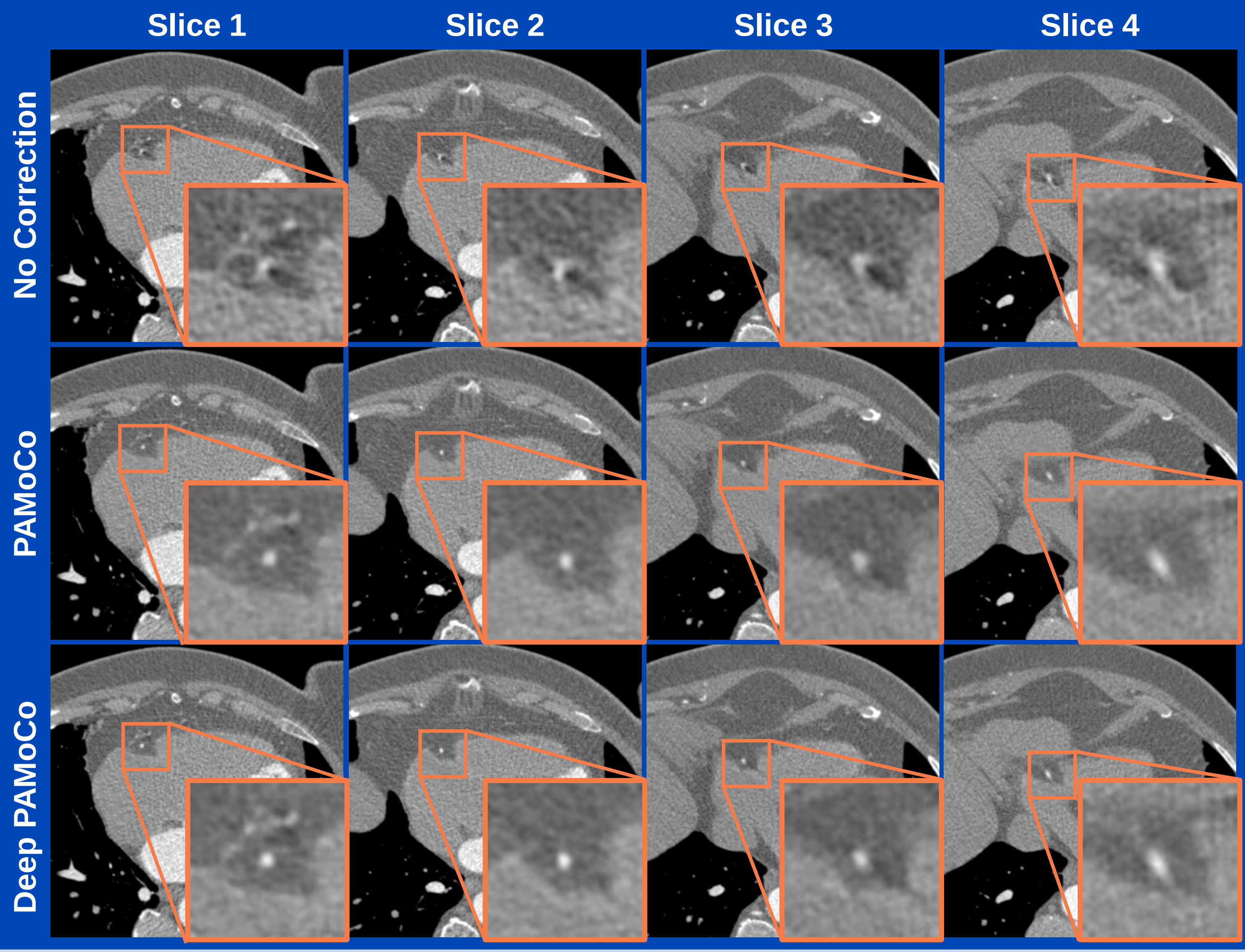

C = 1000 HU
W = 1000 HU

J. Maier, S. Lebedev, E. Eulig, S. Sawall, E. Fournié, K. Stierstorfer, and M. Kachelrieß .Coronary artery motion compensation for short-scan cardiac CT using a spatial transformer network. Conference Program of the 6th International CT-Meeting, August 2020.

Results

Measurements, patient 2

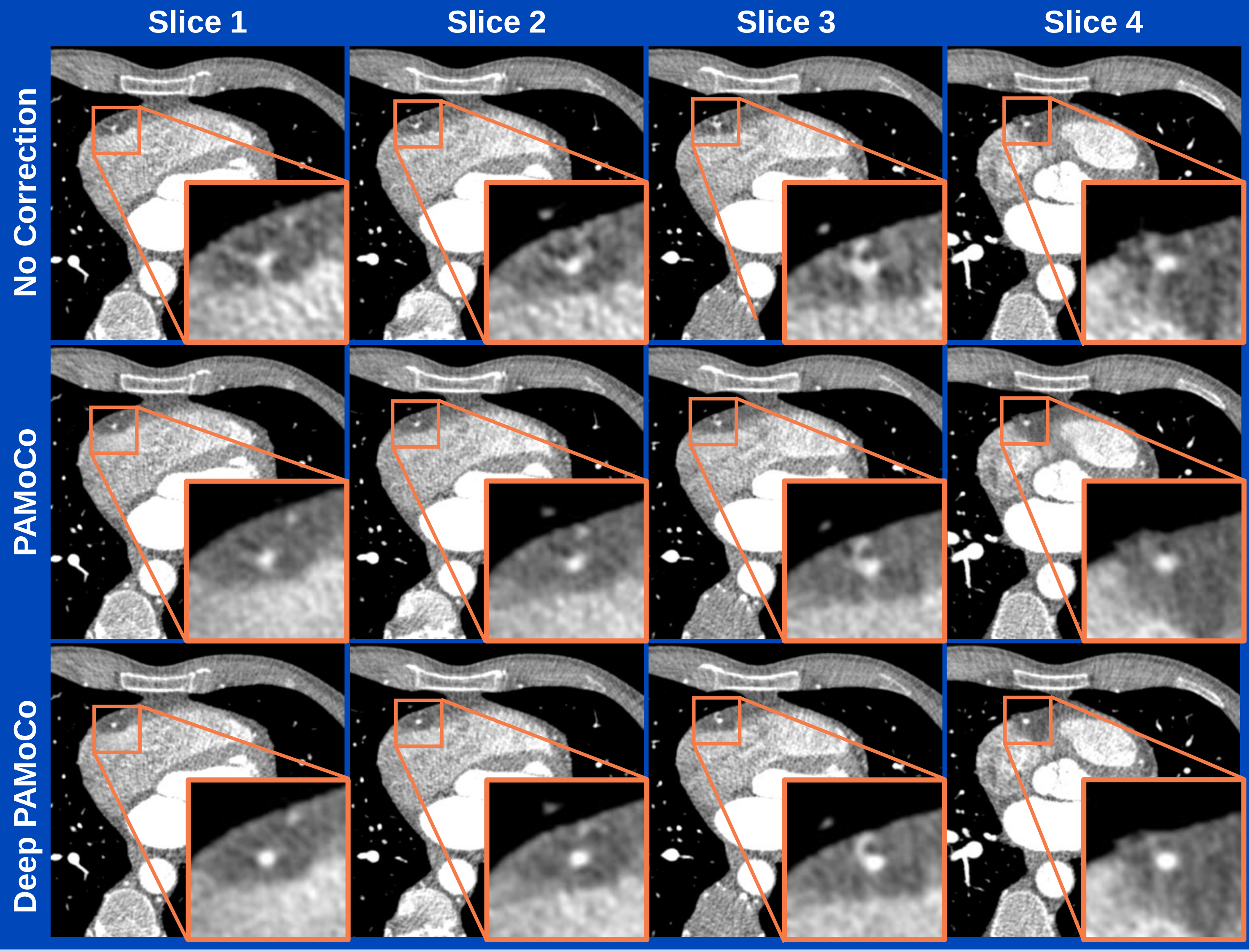

C = 1000 HU
W = 1000 HU

J. Maier, S. Lebedev, E. Eulig, S. Sawall, E. Fournié, K. Stierstorfer, and M. Kachelrieß .Coronary artery motion compensation for short-scan cardiac CT using a spatial transformer network. Conference Program of the 6th International CT-Meeting, August 2020.

Results

Measurements, patient 3

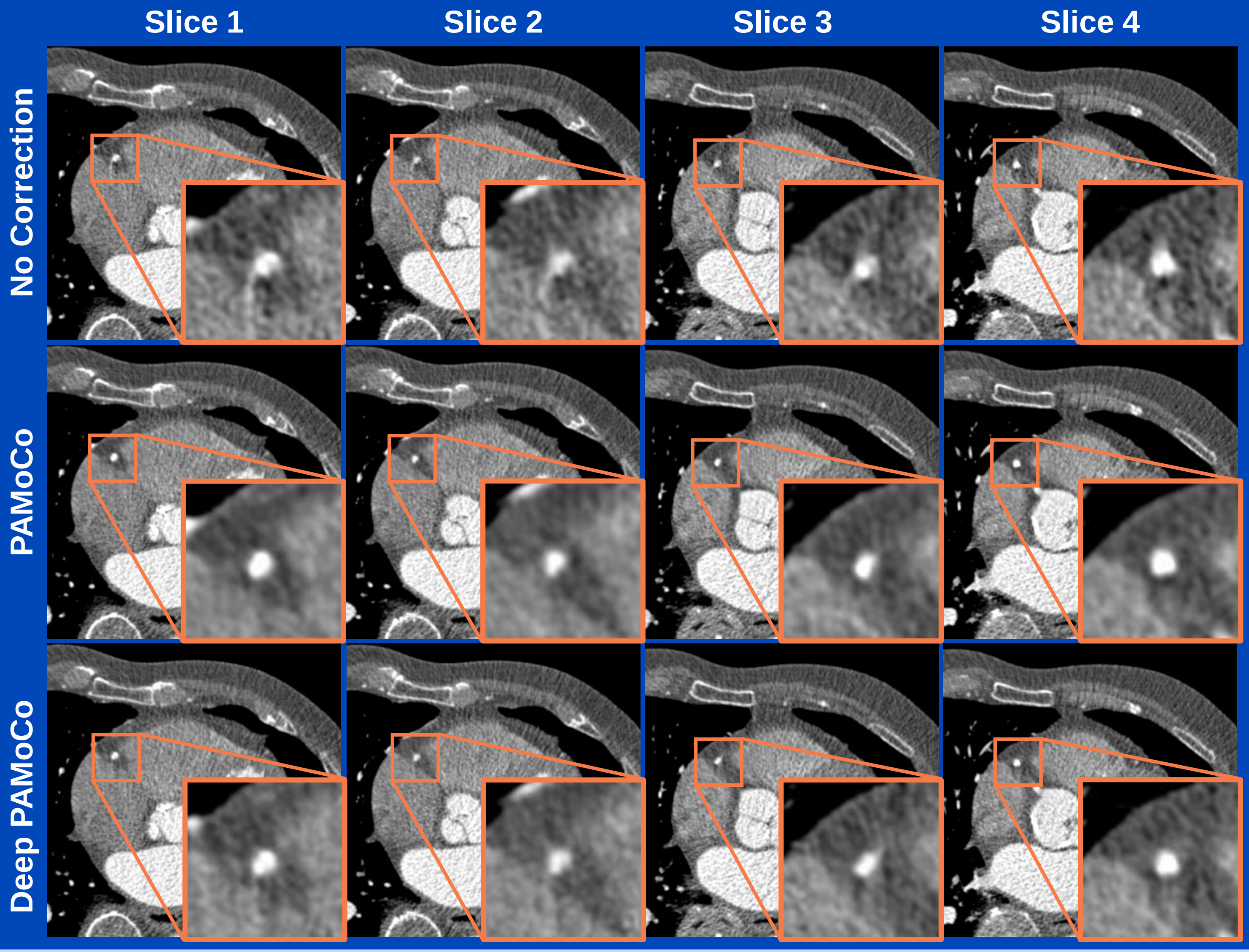

C = 1100 HU
W = 1000 HU

J. Maier, S. Lebedev, E. Eulig, S. Sawall, E. Fournié, K. Stierstorfer, and M. Kachelrieß .Coronary artery motion compensation for short-scan cardiac CT using a spatial transformer network. Conference Program of the 6th International CT-Meeting, August 2020.


Thank You!
Job opportunities through DKFZ's international PhD or Postdoctoral Fellowship programs (www.dkfz.de), or directly through Marc Kachelriess (marc.kachelriess@dkfz.de).
Parts of the reconstruction software were provided by RayConStruct® GmbH, Nürnberg, Germany.